**NDOR Research Project Number SPR-P1(09) P321**

# Comprehensive Evaluation of Fracture Critical Bridges

FINAL REPORT


Huy Pham
Saeed Doust, Ph.D.
Aaron Yakel, Ph.D.
Atorod Azizinamini, Ph.D., P.E.

**Department of Civil and Environmental Engineering**
**Florida International University**
**Miami, Florida**

10555 W. Flagler Street, EC 3600
Miami, FL 33174

Sponsored By
**Nebraska Department of Roads**

February, 2014

| 1. Report No.<br>SPR-P1(09) P321 | 2. Government Accession No. | 3. Recipient's Catalog No. |
|---|---|---|
| 4. Title and Subtitle<br>Comprehensive Evaluation of Fracture Critical Bridges | | 5. Report Date<br>February 2014 |
| | | 6. Performing Organization Code |
| 7. Author(s)<br>Huy Pham<br>Saeed Doust, Ph.D.<br>Aaron Yakel, Ph.D.<br>Atorod Azizinamini, Ph.D., P.E. | | 8. Performing Organization Report No. |
| 9. Performing Organization Name and Address<br>Florida International University, Miami<br>University Park, Room P.C. 539<br>Miami, FL 33199-0000<br>USA | | 10. Work Unit No. (TRAIS) |
| | | 11. Contract or Grant No. |
| 12. Sponsoring Agency Name and Address<br>Nebraska Department of Roads | | 13. Type of Report and Period Covered<br>Final Report |
| | | 14. Sponsoring Agency Code |
| 15. Supplementary Notes | | |


16. Abstract

Two-girder steel bridges are classified as fracture critical bridges based on the definition given in the AASHTO LRFD Bridge Design Specifications. In a fracture critical bridge a failure of a tension member leads to collapse of the bridge. However, a number of such bridges with a partial or full-depth crack in one girder have been reported. The main objective of this research project is to understand the behavior of two-girder steel bridges and evaluate their redundancy level in the event that one member is fractured. This can be achieved by investigating and identifying the factors that control whether a two-girder steel bridge will survive a girder fracture without collapse. Once identified, these factors may be used in the evaluation of existing in-service bridges to reclassify their redundancy level as "non-fracture critical" and decide whether a mandatory hands-on inspection is necessary every two years.

In this research, laboratory testing of full-scale two-girder steel bridges and detailed finite element analyses were carried out. Data from the experimental testing was used to verify and calibrate the non-linear finite element model of these testing specimens. It was observed for the specimens tested that redundancy was dependent upon the level of damage. Fracture of the tension flange alone did not result in immediate collapse and the strength of the intact system could be attained. However, when the initial fracture involved at least half of the web, a reduced capacity was observed and the crack rapidly propagated leading to collapse.


| 17. Key Words<br>fracture critical, two girder steel bridge, redundancy, evaluation, finite element analysis | 18. Distribution Statement<br>No restrictions. | | |
|---|---|---|---|
| 19. Security Classif. (of this report)<br>Unclassified | 20. Security Classif. (of this page)<br>Unclassified | 21. No. of Pages<br>131 | 22. Price |

# Disclaimer

The opinions, findings, and conclusions expressed in this publication are those of the authors and not necessarily those of the Nebraska Department of Roads.

# Acknowledgements

Funding for this investigation was provided by the Nebraska Department of Roads. The authors would like to express their appreciation for this support and for the valuable, suggestions and comments.

# Executive Summary

The American Association of State Highways and Transportation Officials (AASHTO) define a fracture critical member (2010) as a "component in tension whose failure is expected to result in the collapse of the bridge or the inability of the bridge to perform its function". A bridge that has at least one fracture critical member is designated as a fracture critical bridge. Although design and construction of fracture critical bridges is not currently prohibited, these bridges must be designed and fabricated with special requirements and, a hands-on full inspection is required every two years. These requirements burden bridge owners and transportation agencies with huge initial and annual expenses.

Currently, the State of Nebraska has about 1400 bridges that are designated as bridges with fracture critical members or components based on the above definition. Almost 500 of these bridges are two-girder steel bridge systems. Anecdotal evidence suggests that such steel two-girder bridges may not always be fracture critical. If the number of steel two-girder bridges classified as non-redundant can be reduced, a significant savings in resources may be realized for the State.

The primary objective of this research was to understand the behavior of two-girder steel bridges and to quantify their redundancy level. This can be achieved by investigating and identifying the factors which control whether a two-girder will survive a girder fracture without collapse. Once identified, these factors may be used in the evaluation of existing in-service bridges to reclassify their redundancy level as "non-fracture critical" and decide whether a mandatory hands-on inspection is necessary every two years. These factors may also be used in the design of new bridges so that future steel two-girder bridges are no longer classified as fracture-critical.

To this end, a series of scale model tests were conducted. The model contained two main longitudinal supporting girders with transverse floor beams. Loading was applied at midspan and offset from the centerline. In the first model, the bridge had rolled girders and two separate tests were performed. The first test was to evaluate the lateral torsional buckling capacity of the intact bridge. The bridge in its undamaged condition was loaded up to the point at which the lateral and torsional displacement of girders was observed to begin accelerating, or incipient buckling. This occurred at 92 kips of load corresponding to 1.36 inches of vertical displacement in the bottom flange. Strain gauge data showed that a majority of the specimen did not yield except for the top flange of the girder (near the loading point) at mid-span.

In the second test, the bottom flange of the girder closer to the loading point was cut at the mid-span section to simulate fracture. Under load, the behavior of the specimen was linear up to 51 kips of load, when its stiffness began to decrease. The maximum load carrying capacity of this cracked bridge was reached at 54 kips with 1.37 inches of vertical displacement. After reaching the maximum capacity the crack propagated up through the web which led to a drop in

capacity of the specimen. The test was stopped when the load capacity had dropped to 21 kips with a 6.8 inch displacement.

Non-linear finite element analysis was used to evaluate the redundancy of the test specimen following the procedures given by NCHRP report 406. The redundancy analysis for the first model bridge showed the bridge was redundant for the cases of undamaged and bottom flange cracked. Nevertheless, when a quarter of the web was cracked, the bridge did not satisfy the functional limit state. And when a half of the web was cracked the bridge did not satisfy both functional limit state and damage limit state.

In the second model, a bridge with a built-up girder was used to provide a taller specimen. This provided the maximum ratio found in practice for the height of the girder to height of the floor beams. In this experiment, the ratio was approximately 4.0. There were a total of five tests performed in on the second model. In the first test, the uncracked bridge system carried a maximum load of 106 kips with a maximum vertical displacement of 1.7 inches. After unloading, the girder closer to the loading point (Girder A) experienced a permanent vertical deformation of approximately 0.45 inch at mid-span.

In the second test, the built-up girder system was cut at the bottom flange of the girder near the loading points and then strengthened using two high-strength rods parallel to the bottom flange. This specimen was able to carry approximately 108 kips of load with 1.4 inch of displacement before starting a plateau in the load-deflection curve. This load was a little more than the load carried by the intact bridge, 106 kips. The permanent vertical displacement observed in this second test was approximately 0.32 inch, which occurred in the loaded girder.

In the third test, the strengthening rods were removed and the specimen with the cracked bottom flange was loaded again. The maximum load-carrying capacity of this specimen was observed to be approximately 100 kips.

In the fourth test, the crack in the bottom flange was extended up the web to a depth of 2.5 inch. The specimen was loaded up to 80 kips then unloaded. The load-displacement curve shows the specimen response was still linearly elastic.

In the last test, the crack was extended further in the web up to 10.5 inches. The maximum load carrying capacity of this specimen dropped down to 48 kips. At this point, the initial crack started propagating further into the web. Due to this crack propagation, the capacity of the bridge decreased. At the time the test was stopped, the bridge specimen had 6 inches displacement under 33 kips of load.

The second bridge model 2 showed a higher level of redundancy than the first due to a larger cross section of girders. Even when the web was cracked up to half of its depth, the bridge was still proved redundant. Once the crack was extended up to three quarters of the web, the bridge wasn’t redundant anymore since it didn’t satisfy functional and damage limit states.

In this research, a new equation to estimate the lateral torsional buckling capacity of two-girder bridges was proposed. This equation presents moment capacity as a linear function of the floor beam spacing and varies between the maximum moment capacity of $M_P$ and the minimum buckling moment capacity of $C_{bu}M_o$. The equation was validated by means of finite element analysis and was also compared with Yura's equation and the traditional equation based on AASHTO LRFD Specification. The comparison showed that the proposed equation provided better agreement with the finite element analysis results than the other two methods.

The primary conclusions that can be drawn from this research are:

- Depending on the level of damage, certain two-girder steel bridge systems can be considered redundant.
- In specimen # 2 (that had larger ratio of girder height to floor beam height), the strength of the specimen with a fracture of the bottom flange only was similar to the strength of the undamaged specimen and the crack did not propagate under increasing load.
- As bottom flange in one girder was cracked, the capacity of specimen 1 reduced significantly while the capacity reduction in specimen 2 was minimal. It implies that larger ratio of girder height to floor beam height in specimen 2 helps to improve the redundancy of the system once the crack occurs.
- As the artificial fracture (cut) extended into the web, the resulting strength of the specimens reduced. However, crack propagation was minimal when the maximum load carrying capacity of the specimen was reached. It was not until the cut in the web was extended to mid-depth that crack propagation occurred once the maximum load was reached.
- Additional work is required to develop fracture mechanic or fatigue based procedures to relate traffic volume to inspection cycle.

# Table of Contents

# List of Figures

# List of Tables

# Chapter 1 Introduction

Sudden collapse of bridges such as the Silver Point Bridge (1967) and the I-35W Mississippi River Bridge (2007) prove that fracture of a single member cause the collapse of an entire bridge. In bridge engineering parlance, these members are known as fracture critical members although the precise definition may vary. The American Association of State Highways and Transportation Officials (AASHTO) define a fracture critical member (2010) as a "component in tension whose failure is expected to result in the collapse of the bridge or the inability of the bridge to perform its function". A bridge that has at least one fracture critical member is designated as a fracture critical bridge. Although design and construction of fracture critical bridges is not currently prohibited, these bridges must be designed and fabricated with special requirements and, a hands-on full inspection is required every two years. These requirements burden bridge owners and transportation agencies with huge initial and annual expenses.

Currently, the State of Nebraska has about 1400 bridges that are designated as bridges with fracture critical members or components based on the above definition. Almost 500 of these bridges are two-girder steel bridge systems. However, a number of such bridges with cracks in one girder, even though the full depth, have been reported. Two examples are the US-52 Bridge over The Mississippi River near Savanna, IL and the I-79 Neville Island Bridge in Pittsburg, PA. Both bridges were in-service with the fractured girder and did not collapse. This anecdotal evidence suggests such steel two-girder bridges may not always be fracture critical. If the number of steel two-girder bridges classified as non-redundant can be reduced, a significant savings in resources may be realized for the State.

## 1.1 Background

In the past years, several research projects on fracture critical bridges have been conducted by bridge researchers for different sponsoring agencies. National Cooperative Highway Research Program (NCHRP) Report 406 is one of the first. In that report, an attempt was made to quantify the redundancy of a bridge structure. For that purpose, four load factors and three reserve ratios based on the load factors are defined. Limiting values for each reserve ratio are intended to ensure redundancy. The results of other studies are also available for researchers in this field. NCHRP Synthesis 354 provides a guide for "Inspection and management of bridges with fracture critical members" (2005). Michel Ghosn et al. (2010) studied redundancy and robustness of highway bridge superstructures and substructures.

On the subject of fracture critical members, a memo was issued by The Federal Highway Administration (FHWA) in order to clarify the policy of FHWA for design, fabrication and

inspection of fracture critical bridges. There are also two major research projects on redundancy of twin box-girder bridges conducted by HNTB/MTP for WisDOT and University of Texas-Austin for TxDOT. Additional information on these three resources are provided.

**FHWA Memo**

In June 2012, FHWA issued a memorandum on clarification of requirements for fracture critical members. The objective of the memo is described as follows:

"The purpose of this memo is to provide clarification of the FHWA policy for the classification of Fracture Critical Members. For design and fabrication, only Load Path Redundancy may be considered. For in-service inspection protocol, Structural Redundancy demonstrated by refined analysis is now formally recognized and may also be considered. Internal member redundancy is currently not recognized in the classification of Fracture Critical Members for either design and fabrication or in-service inspection. Finally, this memo introduces a new member classification, a System Redundant Member (SRM), which is a non-load-path-redundant member that gains its redundancy by system behavior."

In the memo, the FHWA policy on specification of proper material and testing for design and fabrication and also proper in-service inspection protocol are clarified. In addition, it is mentioned that the analysis requirements of AASHTO LRFD section 6.6.2 is supported which requires the bridge owner and the bridge engineer agreement on the level of complexity of the bridge analysis. It means the type on elements, fracture modeling technique, method of dynamic simulation, location of fracture and all other characteristics of a computer modeling should be mutually agreed.

In addition, it is stated in the memo that "a member that requires fabrication according to the AWS FCP, but need not be considered an FCM for in-service inspection" is defined as a System Redundant Members (SRM). In this case, it is requested that SRMs be designated on the design plans to be fabricated according to AWS Chapter 12.

**HNTB/MTP Research Project (2005)**

In 2005, Milwaukee Transportation Partners published a report on "Redundancy of Box Girder Steel Bridges" based on a study on the Marquette Interchange HPS twin box girder bridges. The intent of that project was to demonstrate that the selected twin box girder bridges are redundant in their as-designed condition or to make recommendations to render them redundant.

Marquette Interchange includes eight directional ramps to be constructed using twin box-girder system. It was decided that these bridges be designed and fabricated in accordance to fracture critical requirements and the major target was to eliminate the two-year inspection need. Therefore, two of the ramp bridges were modeled using elaborate nonlinear finite element models. The other six bridges of the interchange were modeled using simplified grillage models with beam elements. So in those models, all main girders, slab strips and diaphragms were

modeled using beam elements in a 2D planar grid. The results of the 2D models were calibrated by means of the results of the two 3D models to make them more reliable. The considered damage for each bridge was a total steel section fracture of one of the two box girders at 0.4 times of the end span. A stepwise pushover analysis was used to monitor the responses of all of the bridge elements through the incremental loading process.

The results of both 2D and 3D analyses show that these bridges were able to carry the live loads greater than the minimum required loads. In addition, the dynamic effects due to sudden failure of one of the box girders on global stability of the bridge were evaluated which was beyond the requirements of NCHRP Report 406. A simplified approach was selected to attack this problem. Although, the analyses showed that this dynamic effect controls the failure, the two girder bridges proved to have enough capacity to accommodate such sudden failures.

This project demonstrated that twin box girder bridges in their as-designed condition have sufficient reserved capacity to be classified as non-fracture critical and no additional requirement should be added to the current design methods. The redundancy of this type of bridges comes from the alternate load path embedded in these structures such as continuity of girders, concrete deck 3D action and participation of cross frames and diaphragms to carry the loads of damaged girder.

**Texas Research Project (2006-2010)**

Texas Department of Transportation (TxDOT) and Federal Highway Administration (FHWA) co-sponsored a large scale experimental study at the Ferguson Structural Engineering Laboratory (FSEL) in the University of Texas-Austin. In this research project, Karl Frank et al. conducted a valuable full scale experiment and presented analytical and finite element solutions to evaluate the load carrying capacity of a composite twin steel box-girder bridge. The outcome of the research was analytical and numerical solutions to find the "redundant capacity" of twin box-girder bridges. This FESL project that had major experimental and computational resources continued for four years (2006-2010). Different aspects of this project included analytical structural analysis presented through hand calculations, numerical structural analysis conducted through finite element modeling, laboratory experiments to evaluate the capacity of specific bridge elements, and a full scale test on a reconstructed twin box-girder bridge.

In the analytical part of this study, the capacity of the bridge was estimated using the yield line theory. In this method, a failure pattern (yield line) is assumed for the bridge and then by equating the internal work done by the internal forces and the external work done by the external forces, the maximum capacity of the structure is found. This method was successfully applied to the tested bridge and a lower bound was resulted for the load capacity of the bridge.

The laboratory tests were focused on the pullout capacity of the shear connectors of the bridge girders which connect the girders to the concrete deck. In this project it is identified that the shear connectors' capacity plays a key role in the redundancy of such bridges as they are a weak point in the load carrying capacity path. These tests were conducted on shear studs in static and

dynamic states and revealed information on the effect of stud length, spacing and positioning and also the effect of a haunch on the capacity of the girder-to-deck connection.

The full scale bridge test of this research project revealed the intrinsic redundant behavior of twin box girder bridges, despite the test was conducted in the worst case scenario from the redundancy point of view. The tested bridge was a simple-span one and therefore it had no redundancy due to continuity of its superstructure. In addition, all external diaphragms of this bridge were removed. Besides, the railings of the bridge were constructed with expansion joints. This limits the effectiveness of the contribution of the railing to the load carrying capacity of the bridge. And finally the bridge had a horizontal curvature and the fractured girder was the outside girder which has the maximum internal forces. Therefore, it is observed that the situation of a real-life bridge cannot be worse than this bridge from redundancy standpoint. Figure 1-1 shows a picture of this test bridge before conducting the tests.

**Figure 1-1. FSEL Twin Box-Girder Bridge [Source: FHWA Report No.: FHWA/TX-10/9-5498-1]**

Three different tests have been done on this bridge. In the first test, the bottom flange of the exterior girder was rapidly cut by an explosive to simulate a sudden fracture while an equivalent HS-20 load was positioned above the fractured girder and in the worst possible location. Figure 1-2 illustrates the bridge during the explosion and Figure 1-3 shows the bottom flange cut after the explosion. The response of the bridge during and after this test was satisfactory and its maximum deflection was less than one inch.

**Figure 1-2. FSEL First Bridge Fracture Test [Source: FHWA Report No.: FHWA/TX-10/9-5498-1]**

**Figure 1-3. Bottom Flange Cut after the Explosion [Source: FHWA Report No.: FHWA/TX-10/9-5498-1]**

In the second test, the bridge was supported by means of a scissor jack while about 83% of the webs of the cracked girder were cut manually and then the scissor jack was removed suddenly using an explosive acting on the jack. This way the sudden nature of the crack was simulated. Figure 1-4 shows the supporting scissor jack before, during and after the explosion. Again, the bridge showed a well performance with a maximum deflection of seven inches.

**Figure 1-4. FSEL Second Bridge Fracture Test [Source: FHWA Report No.: FHWA/TX-10/9-5498-1]**

The third test was a static test to measure the load capacity of the damaged bridge. In this test, the load on the bridge was increased incrementally until the bridge was not able to carry more

loads. In this test, the bridge carried 363 kips of load which, considering the extent of the damage, was a remarkable capacity. Figure 1-5 shows the incremental loading of the bridge and also the bridge in its collapsed mode.

**Figure 1-5. FSEL Third Bridge Fracture Test [Source: FHWA Report No.: FHWA/TX-10/9-5498-1]**

The capacity tested bridge is also evaluated by means of numerical simulation. In this approach, a sophisticated finite element model of the bridge is developed using Abaqus/Standard finite element program. In the simulations, the nonlinear material properties of steel and concrete, contact properties of railing joint and also the stud connection failure were taken into account. The results of the numerical simulation showed a good agreement with the collected data. In addition, the finite element models were able to capture the observed failures during the second and third test.

Based on the performed experiment and computer simulations, major failure in this type of bridges include:

- pull-out failure of shear studs (which is tension failure of the concrete surrounding the studs) resulting in hunch separation
- crushing of railing concrete in compression

A number of theses and reports were published by Bernard (2006), Hovell (2007), Neuman (2009) and others based on the results of this experimental work, each of them investigating different aspects of the tested bridge behavior.

## 1.2 Objective

The primary objective of this research is to understand the behavior of two-girder steel bridges and to quantify their redundancy level. This can be achieved by investigating and identifying the factors which control whether a two-girder will survive a girder fracture without collapse. Once identified, these factors may be used in the evaluation of existing in-service bridges to reclassify their redundancy level as “non-fracture critical” and decide whether a mandatory hands-on inspection is necessary every two years. These factors may also be used in

the design of new bridges so that future steel two-girder bridges are no longer classified as fracture-critical.

## 1.3 Scope of Work Performed and Report Organization

The following is the full list of tasks contained in the project.

1. Review of the past and ongoing works: Major studies related to fracture critical members and redundancy evaluation were reviewed including NCHRP 406 Report, NCHRP Synthesis 354, the project for WisDOT done by HNTB/MTP consultant companies and the TxDOT project done by University of Texas, Austin. The last two projects are summarized in Section 1.1.
2. Review of Nebraska bridges with Fracture Critical members: Based on the State of Nebraska bridge inventory, the state has a total of 1400 fracture critical highway bridges. The majority is two-girder steel bridge systems, with almost 500 bridges. Therefore two-girder steel bridge system is chosen as the object of this research.
3. Identifying the elements of the two-girder bridge systems that need calculation checks: The commentary section of the 6.6.2 of the AASHTO LRFD Bridge Design Specifications provides general guidelines that can be used to re-classify some of the bridges that are designated as fracture critical to "redundant systems".
4. Conducting experimental tests for establishing performance and capacity of critical elements and bridge structures: Experimental results later will be used to verify the accuracy of the nonlinear FE models in Task 5.

Developing systematic step by step procedures for demonstrating the redundancy of two-girder bridge systems: In this task, detailed finite element models with non-linear material and geometrical capabilities for the above experimental testing are developed. The results from finite element analysis are used to evaluate the redundancy of the structure.In this report, the review and categorization of two-girder steel bridges in the state of Nebraska are provided in Chapter 2. The design details, instrumentation plans and laboratory test results of the steel two-girder bridges are presented in Chapter 4. The 3-D nonlinear finite element analyses are presented in Chapter 3. Based on the results from experiments and finite element analyses, a new equation to estimate the lateral torsional buckling capacity of two-girder steel bridges is recommended. This recommended equation and its verification are presented in Chapter 5. The redundancy analyses for tested bridges are carried out using the method recommended in NCHRP Report 406 and the results are presented in Chapter 6. Lastly, the conclusions are provided in Chapter 7.

# Chapter 2 Survey of Existing Structures

Based on a survey on about 1500 Fracture-Critical bridges, 500 of those bridges were found to be two-girder bridges. This shows the importance of two-girder bridges from a population point of view.

Seven different basic classes of two-girder bridge types can be found.

Figure 2-1 through Figure 2-6 illustrate these structural systems of two-girder bridges.

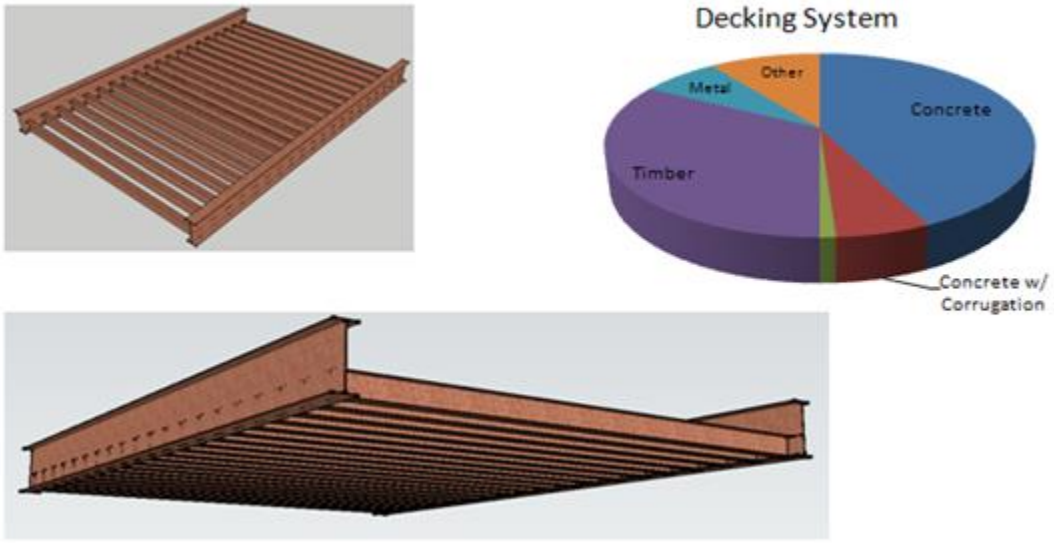


**Figure 2-1. Two-girder Bridge Type 1, 144 Bridges, 46%**

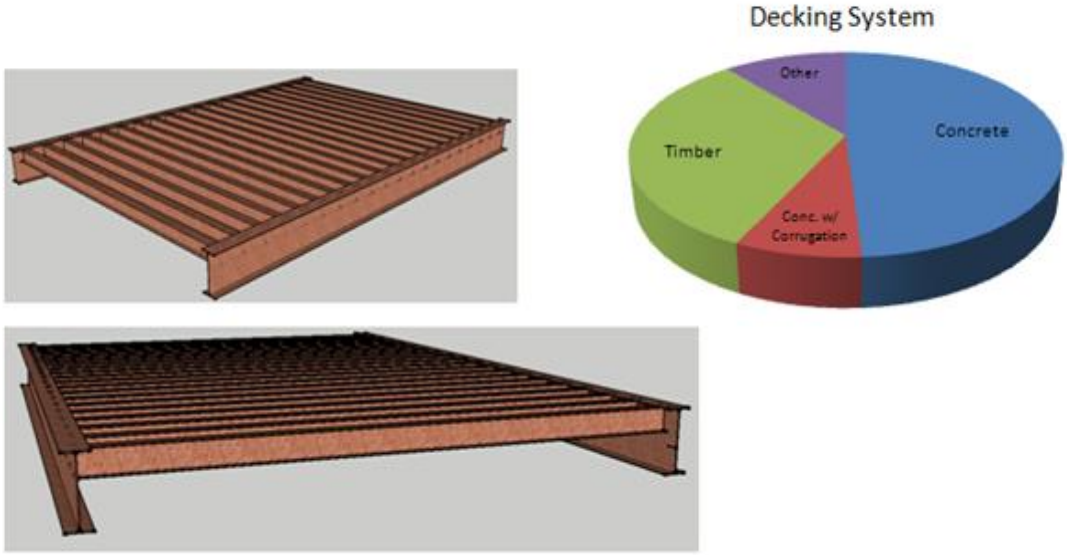


**Figure 2-2. Two-girder Bridge Type 2, 37 Bridges, 12%**

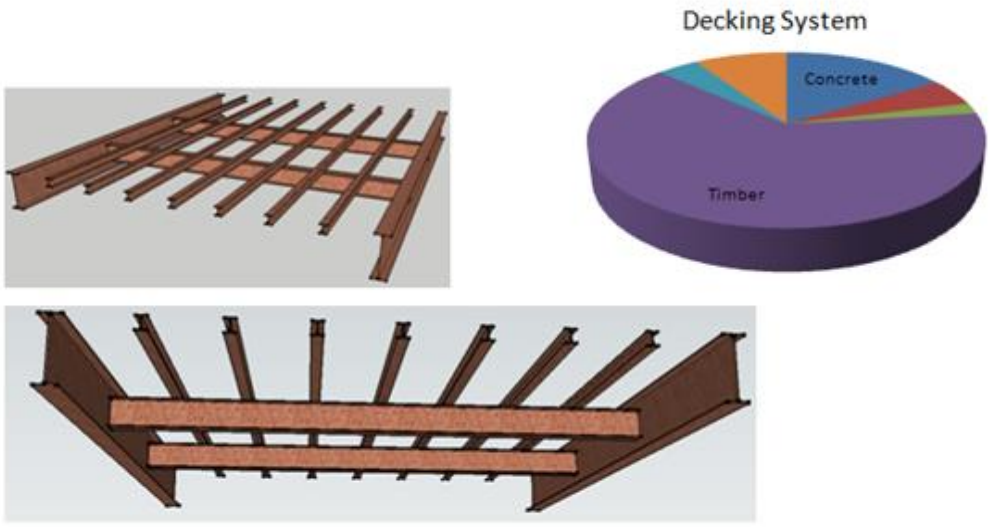


**Two-girder Bridge Type 3, 102 Bridges, 32%**

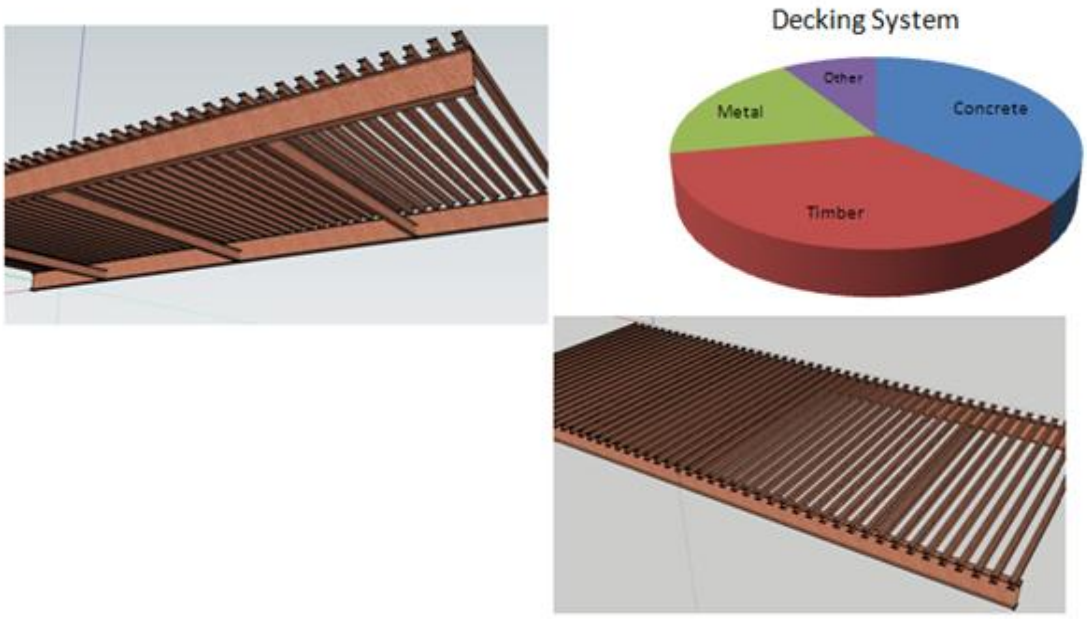


**Figure 2-3. Two-girder Bridge Type 4, 11 Bridges, 3%**

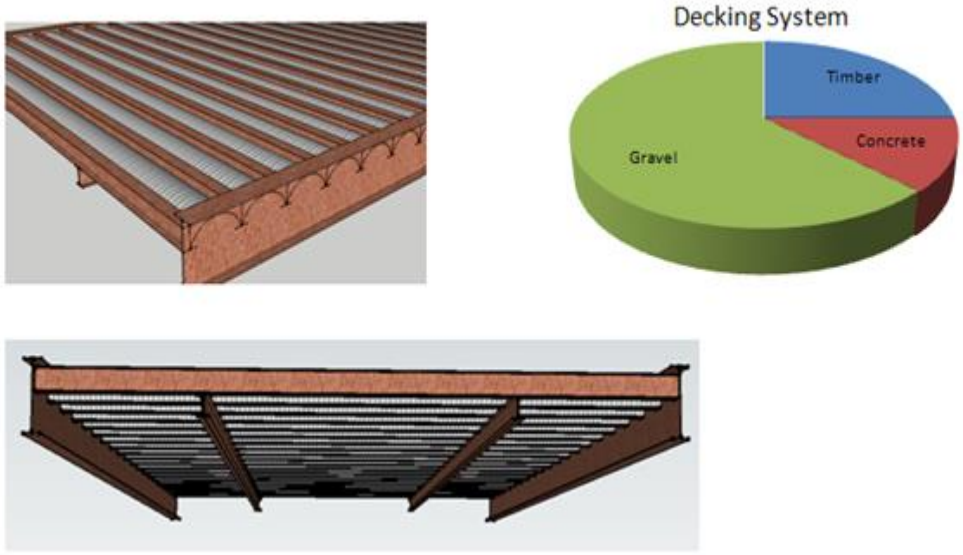


**Figure 2-4. Two-girder Bridge Type 5, 8 Bridges, 2.5%**

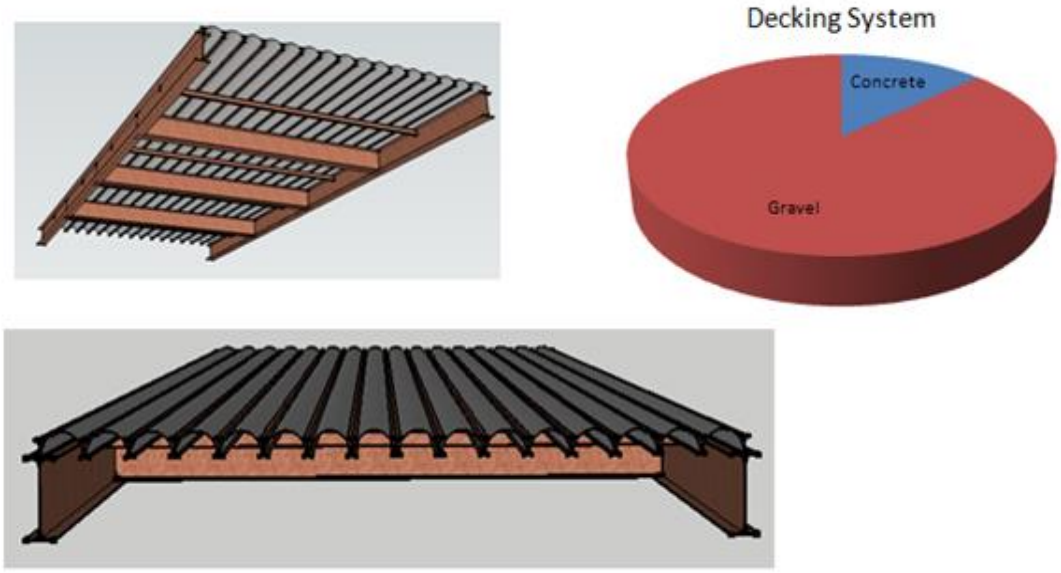


**Figure 2-5. Two-girder Bridge Type 6, 8 Bridges, 2.5%**

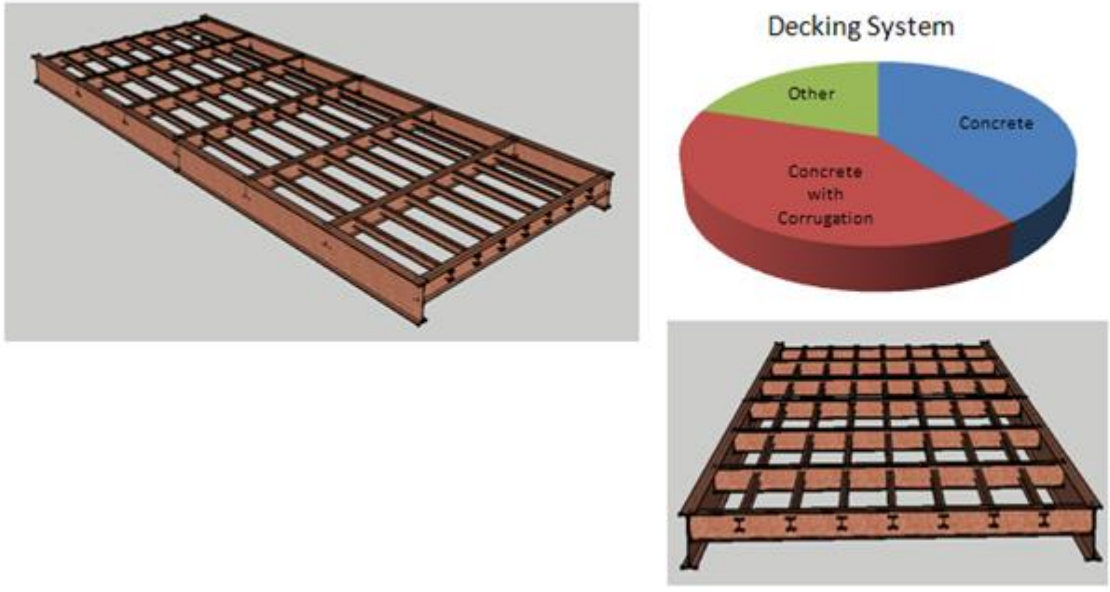


**Figure 2-6. Two-girder Bridge Type 7, 5 Bridges, 2%**

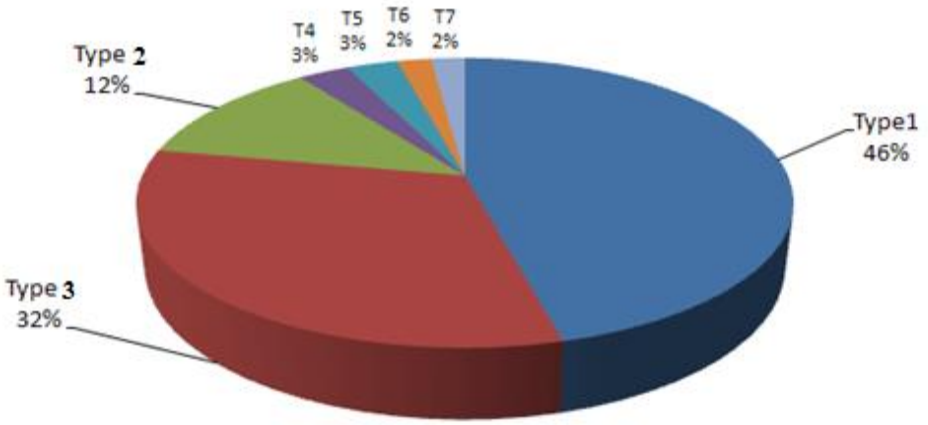


**Figure 2-7. Distribution of Different Types**

Figure 2-7 shows the percentage of each type from the total number of two-girder bridges. It is observed that bridge Type 1 has the largest population consisting of about 46 percent of all two-girder bridges. Type 2 bridges, which are similar to the Type 1, make up about 12 percent, and Type 3 bridges constitute about 32 percent of the population. The other four types of bridges make up the remaining 10 percent.

Based on these findings, the remainder of this report concentrates on Type 1 structures.

# Chapter 3 Finite Element Analysis of Two-Girder Bridges

In this chapter, the load carrying capacity of two-girder bridges was estimated using nonlinear finite element analysis techniques. For this purpose, the finite element package Abaqus 6.9.1 was used. First, the results from finite element analysis were used to aid to the selection of experiments needed to perform. Secondly the results from the testing were used for further calibration and verification of the finite element model. The finite element model could then be used to evaluate the redundancy under various conditions, such as different levels of initial damage. In the finite element modeling of the bridges, material and geometric nonlinearities were taken into account. The details of the numerical models are described in the following sections.

## 3.1 Finite Element Models

Three single span two-girder bridges with the span length equal to 60 feet are modeled. W30x191 sections are used for the main girders of these bridges. The floor beams of bridges Type 1 and Type 2 are made up of W10x19 sections, which have about one third of the main girders height. For bridge type 3, W27x84 sections are used for floor beams. The floor beams are connected to the girders by means of 3x3x1/2 angles with a length of 6 inches. The main girders are 18’-2” apart which results in a length of 18’-1” for the floor beams to provide a half inch distance between the ends of the floor beams and the vertical center lines of the girders. Figure 3-1 shows the dimensions of the elements used in the analysis.

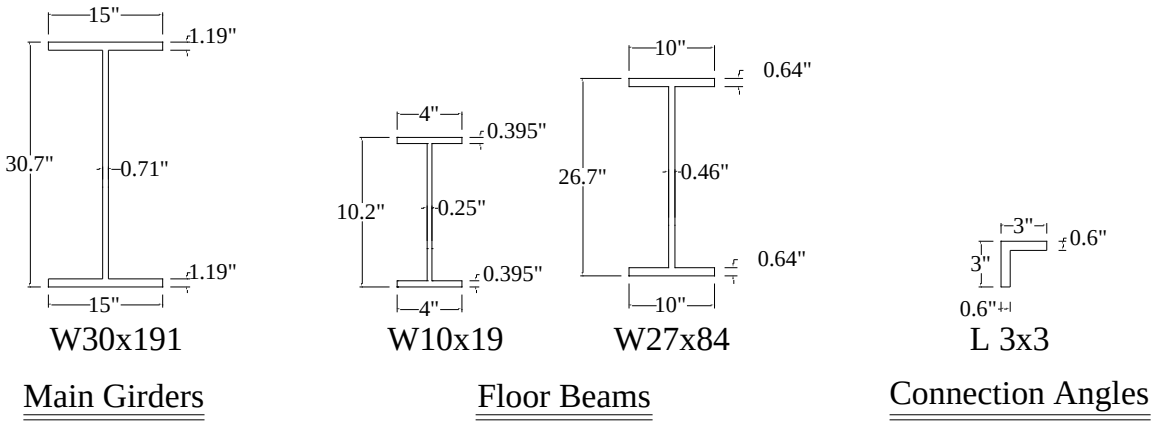


**Figure 3-1. Dimensions of the elements used**

Figure 3-2 shows the general picture of the modeled bridges.

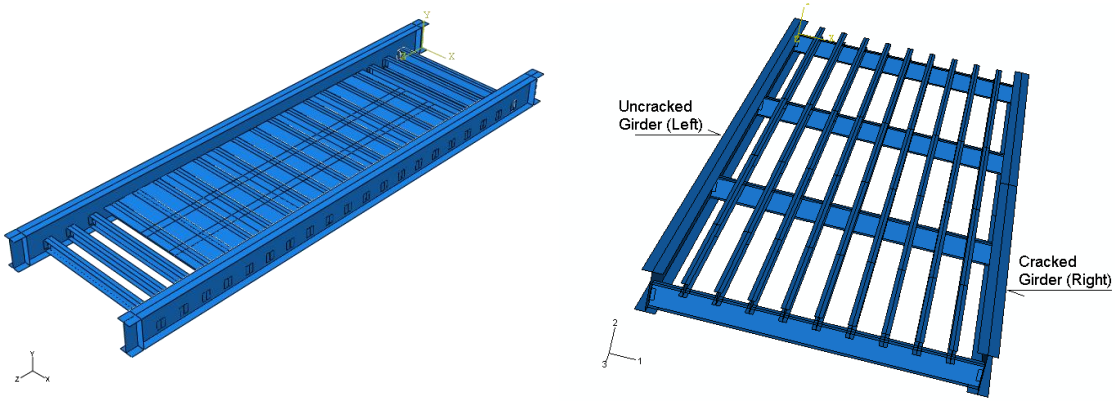


**Figure 3-2. General Picture of the Modeled Bridges (Type 1 Left and Type 3 Right)**

### 3.1.1 Loading Configuration

The loads are applied to the bridges in two steps. In the first step, the self-weight of components is applied to the models. Then, when the stresses are in the self-weight condition, the point loads are applied. In order to simulate the eccentric loading and have the critical condition in only one of the girders, the point loads are placed closer to one girder (denoted as Girder A) compared to the other (denoted as Girder B). Figure 3-3 shows the eccentric loading configuration.

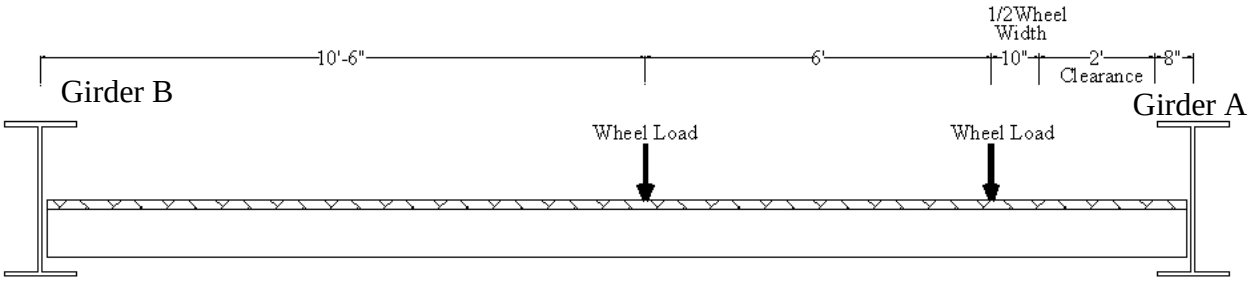


**Figure 3-3. Loading Configuration**

### 3.1.2 Material Properties

The steel components (girders, floor beams and angles) have a bilinear stress-strain behavior with a Young's modulus of 29000 ksi for stresses up to 53 ksi and a Young's modulus of 75 ksi for stresses between 53 ksi and 70 ksi. This material ruptures at the stress level of 70 ksi. The unit weight of steel is 490 lb/ft3 and its Poisson's ratio is 0.3. Figure 3-10 shows the stress-strain relationship for the steel material. The considered timber material for deck has a Young's modulus of 1500 ksi, a unit weight of 50 lb/ft3 and a Poisson's ratio of 0.2.

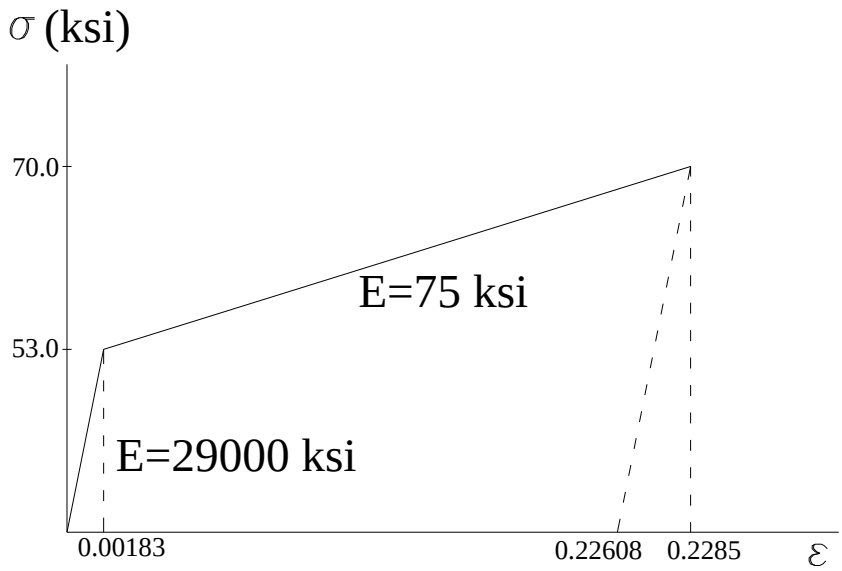


**Figure 3-4. Stress-Strain relationship of Steel Components**

### 3.1.3 Connections

In the models, the floor beams are connected to the girders by means of angles to provide flexibility similar to the actual connections. Figure 3-5 illustrates the typical floor beam to girder connection.

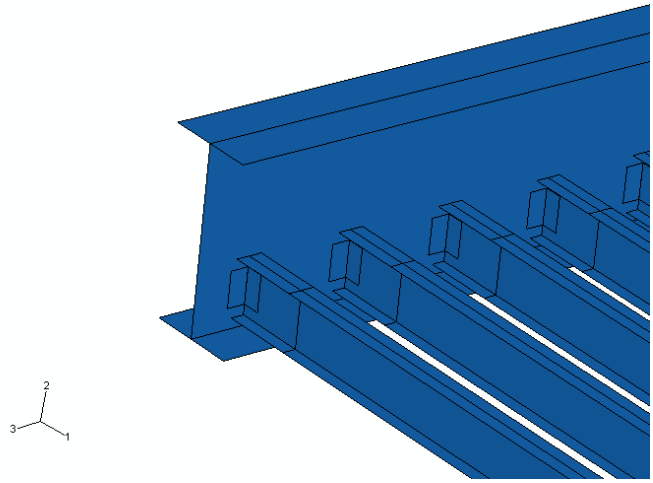

**Figure 3-5. Typical Floor Beam to Girder Connection**

### 3.1.4 Cracking Patterns

Each bridge is analyzed in three different states. In the first state, the bridge girders are uncracked. The second state has the bottom flange of the girder closer to the loading (Girder A) fully cracked. And the last state is the case where the lower half of the girder A is cracked. Figure 3-6 and Figure 3-7 illustrate these two cracking patterns.

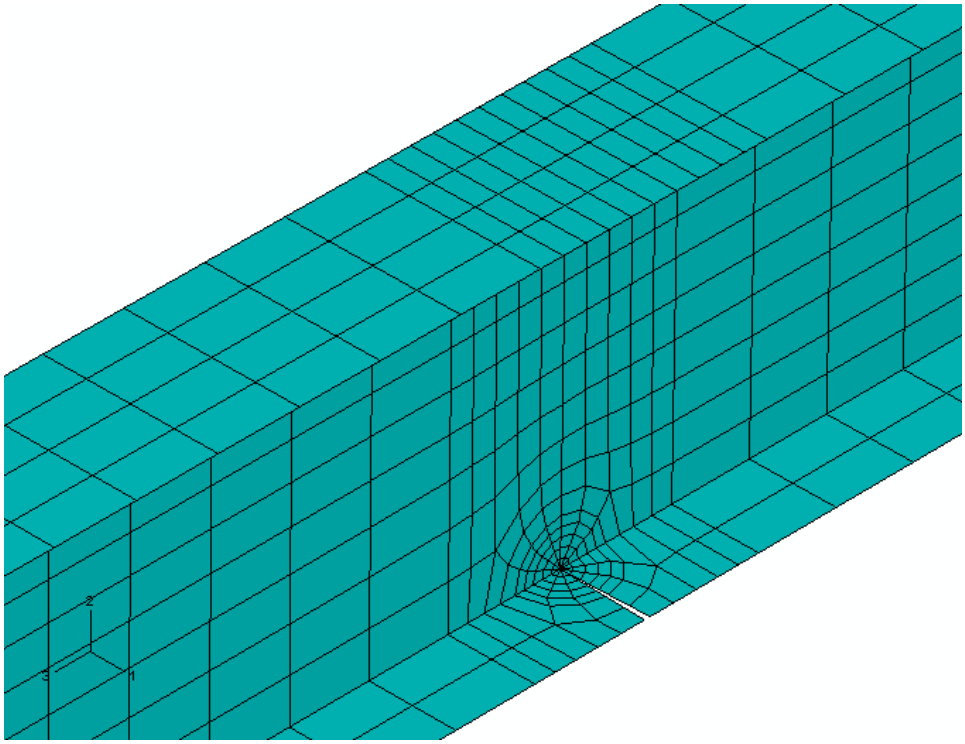

**Figure 3-6. Bottom Flange Cracking Pattern**

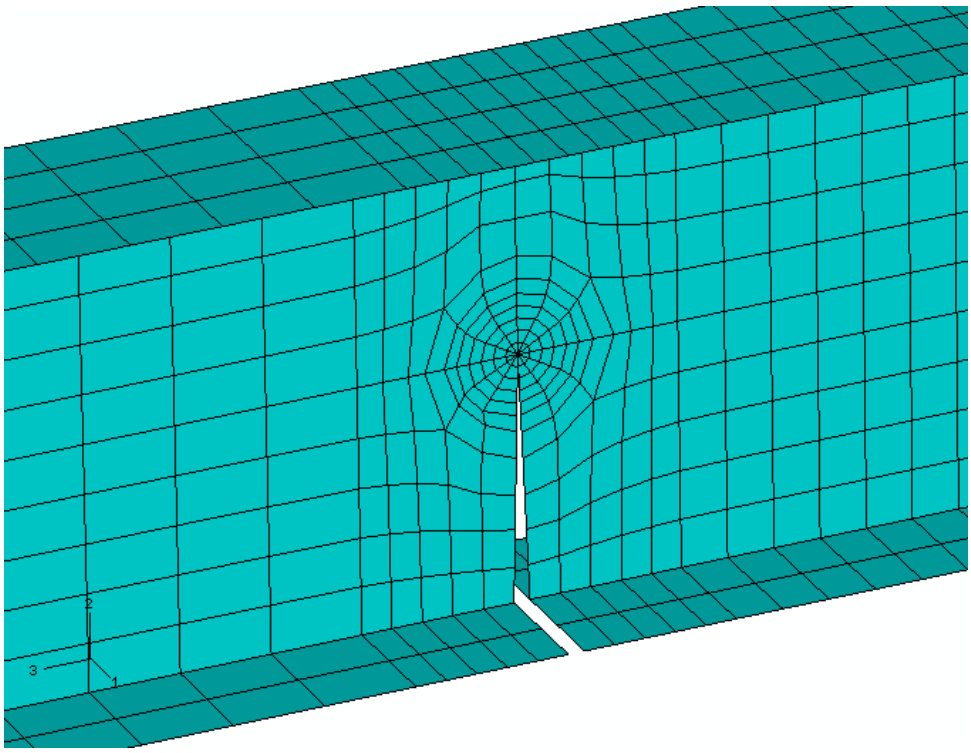


**Figure 3-7. Girder Lower Half Cracking Pattern**

The following subsections show the results of the finite element analyses conducted on these bridges.

## 3.2 Analysis of Two-girder Bridge Type 1

Figure 3-8 shows the two-girder bridge Type 1 and its load deflection curves. The bridge was analyzed in its uncracked mode and also the two cracking patterns described earlier. The load capacity of the bridge is denoted by the number of the HS-20 trucks that the bridge could carry. The uncracked bridge was able to carry about 3.35 times HS-20 loads in its uncracked state. When it had the bottom flange of one of the girders cracked, the load decreased to about 2.85 trucks. And when the bridge was modeled with half the depth of one of its girders cracked, the load capacity of the bridge dropped to approximately 0.6 times the weight of a HS-20 truck. The deflections of both cracked and uncracked girders of the bridges are shown in Figure 3-8.

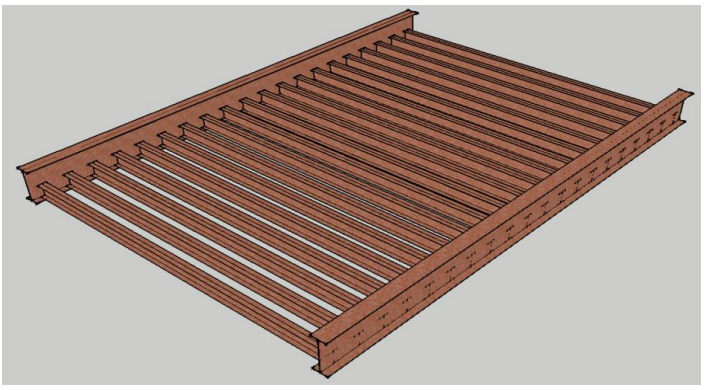

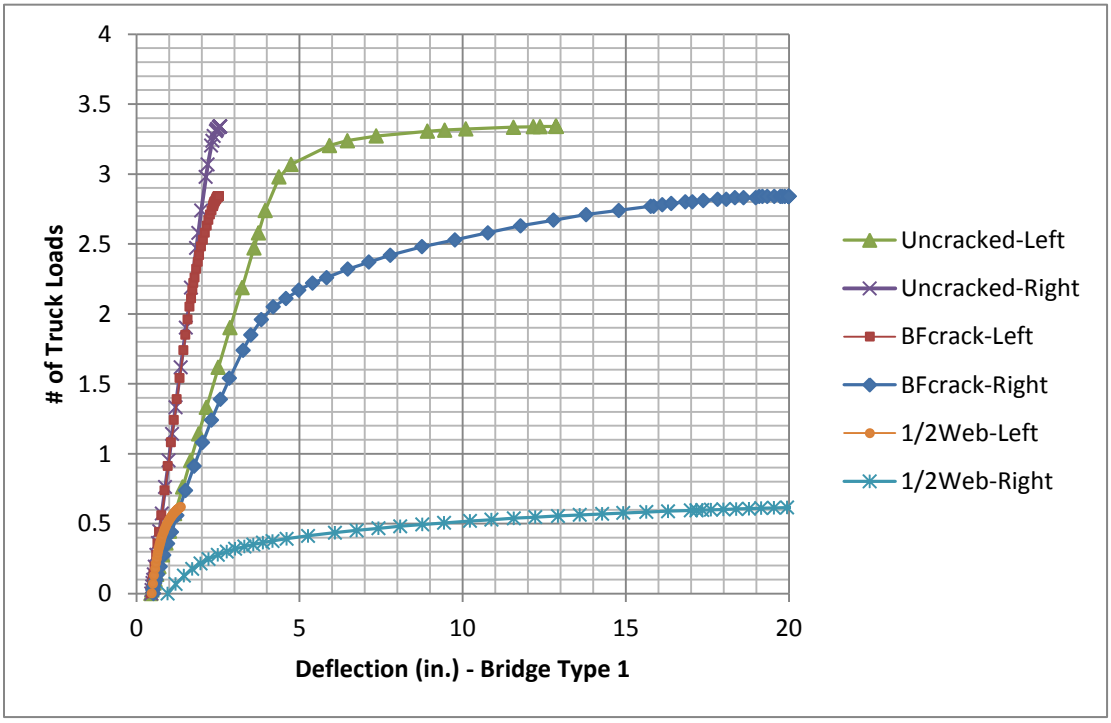


**Figure 3-8. Two-girder Bridge Type 1 and its Load-Deflection Curve**

## 3.3 Analysis of Two-girder Bridge Type 2

The two-girder bridge Type 2 and its load deflection curves are illustrated in Figure 3-9. The bridge was analyzed in its uncracked mode and also the two described cracking patterns. The uncracked bridge was able to carry about 3.60 times HS-20 loads in its uncracked state. When it had the bottom flange of one of the girders cracked, the load reduced to about 2.90 times of HS-20 truck load. When the bridge had one half of the depth of one of its girders cracked, the load capacity of the bridge dropped to approximately 0.60 times of HS-20 load. The deflections of both cracked and uncracked girders of the bridges are shown in Figure 3-9.

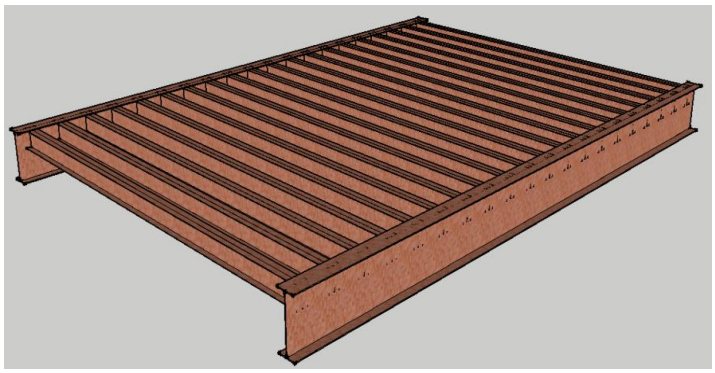

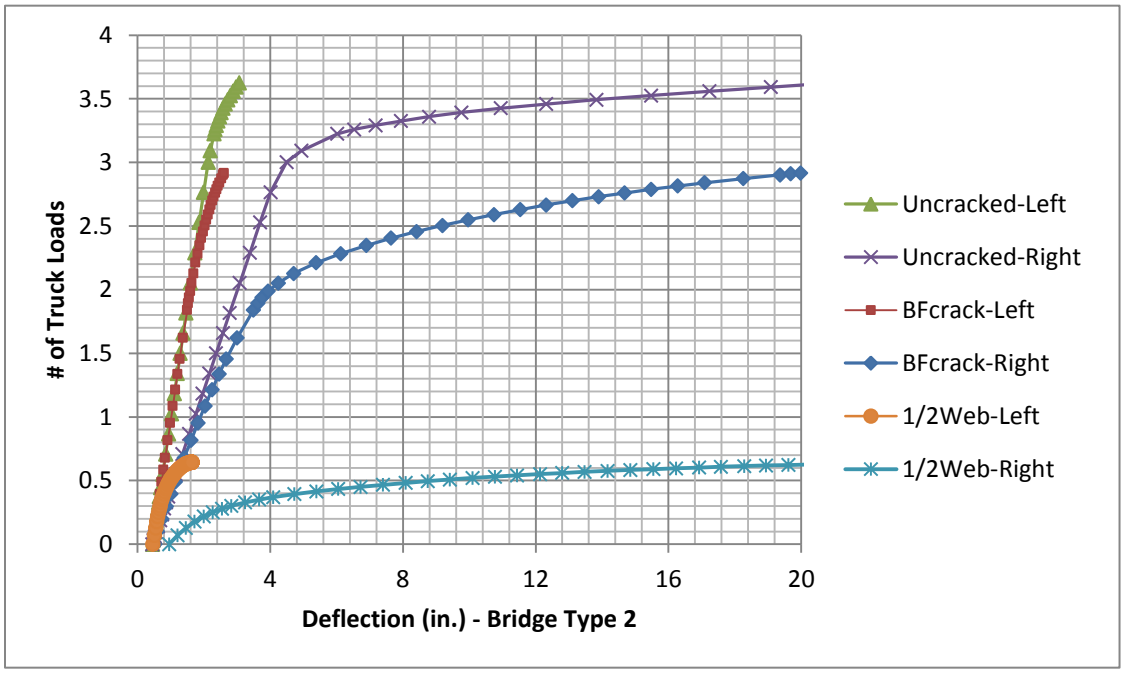


**Figure 3-9. Two-girder Bridge Type 2 and its Load-Deflection Curve**

## 3.4 Analysis of Two-girder Bridge Type 3

Figure 3-10 displays the two-girder bridge Type 3 and its load deflection curves. The bridge was analyzed in its uncracked mode and also the two cracking patterns. The uncracked bridge was able to carry about 3.5 times of HS-20 load in its uncracked mode. When the bottom flange of one of the girders was cracked, the load decreased to about 2.9 trucks load. And when the bridge was modeled with half depth of one of its girders cracked, the capacity of the bridge reduced to approximately 1.1 times of the weight of HS-20 truck. The deflections of both cracked and uncracked girders of the bridges are shown in Figure 3-10.

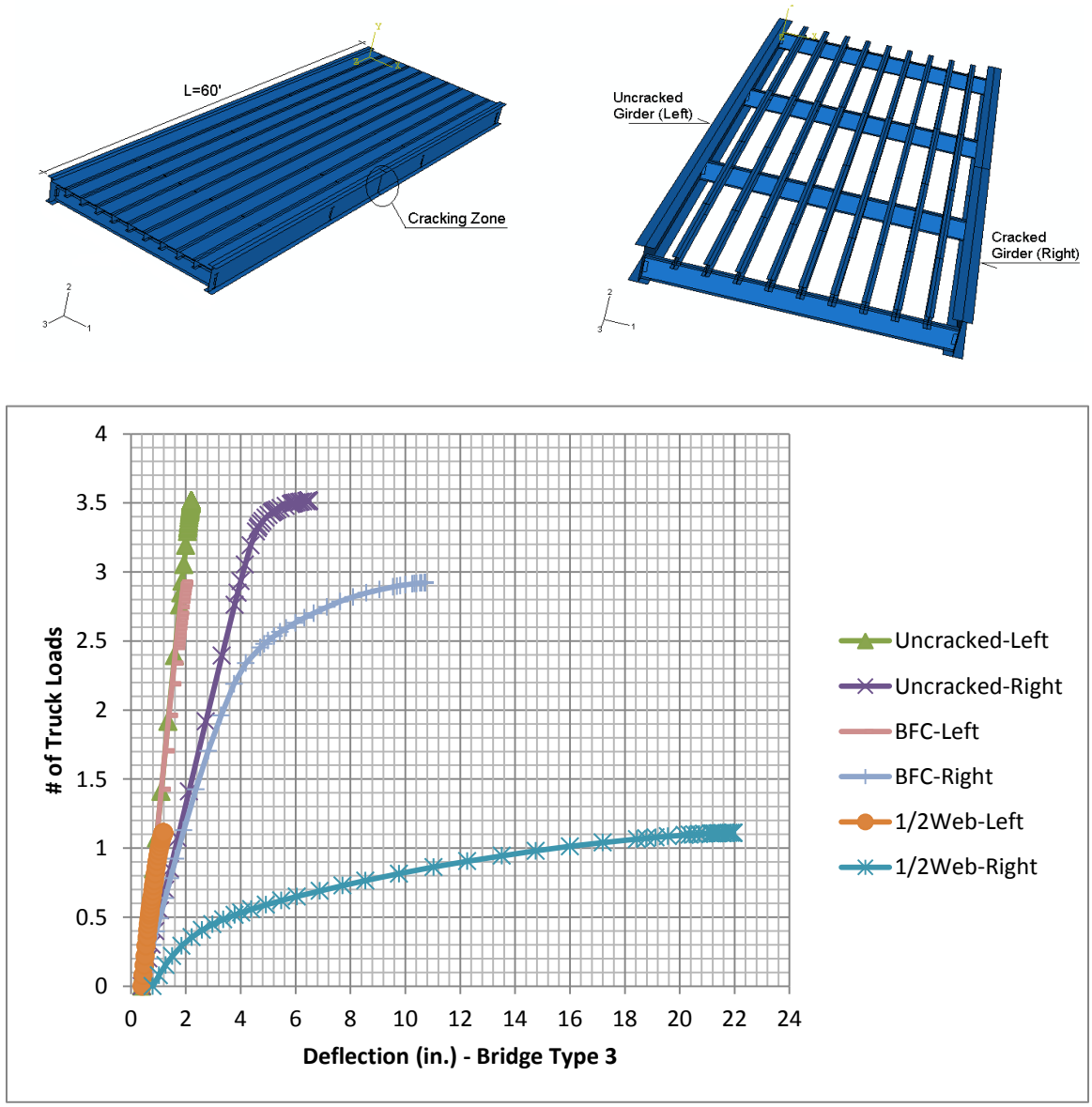


**Figure 3-10. Two-girder Bridge Type 3 and its Load-Deflection Curve**

The capacity of each bridge type under different cracking levels are summarized in Table 3-1. In this table, the Type 2 and Type 3 bridge models showed higher load-carrying capacity than Type 1 model. In the Type 2 model, the floor beams attached to the upper portion of the webs of the main girders and provided lateral restraint for the webs, which in turn increased lateral torsional buckling capacity of the structure as compared with Type 1, where the floor beams were attached to lower portion of the webs. However, when the web of the girder closer to the loading (Girder A) was cracked by half of its depth, the capacity of Type 2 bridge model was just slightly larger than that of Type 1.

The Type 3 Bridge, with stringers provided on the top of floor beams, showed similar capacities as the Type 2 bridge model for both the uncracked and bottom flange cracked cases.

Nevertheless, when one half of the web was cracked, the capacity of Type 3 bridge was 82% larger than that of Type 1 and 73% larger than that of Type 2. It was because some of the loads were carried directly by stringers then transferred to the floor beams at ends and then to the supports. The role of stringer with respect to redundancy of the structure can be seen clearly in Type 3 bridge as the web of one of the main girders was cracked by half.

**Table 3-1. Capacity of each bridge type expressed in term of number of HS-20 trucks.**

| Damage Levels | Type 1 | Type 2 | Type 3 |
|---|---|---|---|
| Uncracked | 3.34 | 3.56 | 3.51 |
| Bottom Flange Cracked | 2.84 | 2.9 | 2.92 |
| One Half Web Cracked | 0.61 | 0.64 | 1.11 |

# Chapter 4 Experimental Evaluation

In order to verify the results of finite element analyses of Chapter 2 and allow refinement of the modeling, several experiments on two large-scale two-girder bridges were conducted in the structures laboratory of the University of Nebraska-Lincoln. The two bridges had the same span length equal to 22 feet with different girder heights. The main parameter that differentiates these two experiments is the ratio of girder height to floor beam height. The reason for choosing this parameter as the key variable for the two tests is that the capacity of two girder bridges is mainly governed by the lateral torsional capacity of their girders and the only supports throughout the length of the girders are the floor beams. Therefore, the height of the floor beams, which dictates the rotational stiffness of the girder, is chosen as the major parameter for the experimental tests. A summary of the tests performed in this study is provided in Table 4-1. Since all tests performed use unsymmetrical loading, for the convenience and consistency the girder that is closer to the loading points was denoted as Girder A while the girder that is away from the loading points was denoted as Girder B.

**Table 4-1: Summary of Performed Tests.**

| Specimen | Test | Condition | Note |
|---|---|---|---|
| Specimen 1-Small ratio of girder height to floor beam height – lower bound (Experiment #1) | 1-A | Unsymmetrical loading, Uncracked System | The specimen is loaded to the point the top flange start to move out of plane laterally |
| | 1-B | Unsymmetrical loading, the bottom flange of the girder near loading point (Girder A) is cracked | The specimen is loaded until its load-carrying capacity drops significantly (nearly collapse) |
| Specimen 2- Large ratio of girder height to floor beam height – upper bound (Experiment #2) | 2-A | Unsymmetrical loading, Uncracked | The specimen is loaded up to its lateral torsional buckling capacity |
| | 2-B | Unsymmetrical loading, the bottom flange of the new girder near loading point (Girder A) is cracked but strengthen by two high strength rods | The cracked girder in the previous Test, Test 2-A is replaced by new one. The specimen is loaded until the plateau in load-deflection curve is observed. |
| | 2-C | Unsymmetrical loading, the bottom flange of the girder near loading point is cracked but the strengthening rods are now removed | The specimen is loaded until the plateau in load-deflection curve is observed. |
| | 2-D | Unsymmetrical loading, the web is cut 2.5 inches in addition to the crack in the bottom flange of Girder A | The specimen is loaded until the plateau in load-deflection curve is observed. |
| | 2-E | Unsymmetrical loading, the web is cut 10 inches in addition to the crack in the bottom flange of Girder A | The specimen is loaded until its load-carrying capacity drops significantly (nearly collapse) |

The geometry of the test bridges, the loading configuration, instrumentation, the test results for the lateral torsional capacity evaluation and the test results for the capacity of the bridge with predetermined cracking patterns are presented and discussed in the following sections.

## 4.1 Experiment #1

The geometrical and structural characteristics of the first experiment and the results of the test are explained in the following subsections. To have a better understanding of the experiment geometry and results, six pictures of different stages of fabrication are shown in Figure 4-1 through Figure 4-6.

**Figure 4-1. Floor Beams (Cut with the specified length)**

**Figure 4-2. Drilling Girder Web for Connecting the Floor Beams**

**Figure 4-3. Girders and Floor Beams Ready for Assembly**

**Figure 4-4. Assembled Two-Girder Bridge on Laboratory Floor**

**Figure 4-5. Two-Girder Bridge Setup**

**Figure 4-6. Two-Girder Bridge Ready for Loading and Data Acquisition System**

### 4.1.1 Bridge Geometry and Loading Configuration

The geometric characteristics of the test bridge are explained in this section. In this experiment, the main girders have a total length of 22 feet. The span length of the single span bridge is 21 feet so the girders extend 6 inches beyond the supports in the longitudinal direction. The girders have W16x40 sections and the floor beams have W6x9 section. Figure 4-7 shows a photo of the specimen and the connection. The main girders are 73 inches apart that allows for a half inch gap between the ends of the 6-foot long floor beams and the web of the girders. The ratio of girder height to floor beam height is approximately 2.3. The floor beams are connected to the web of the girders by means of L3x3x3/8 angles. The angles are 6 inches long. Each leg of the angles is attached to the webs of the floor beams or main girders by two ½ inch A325 high strength bolts. Four spreader beams were used to simulate 4-wheel vehicle loading for the test as illustrated in Figure 4-11. The distance between the front and back wheels was chosen to be 6 feet. The loading points (vehicle loading) are placed closer to one girder, Girder A(the one that later will be fractured) than the other. The final loading locations in both longitudinal and transverse views are illustrated in Figure 4-8 and Figure 4-9.

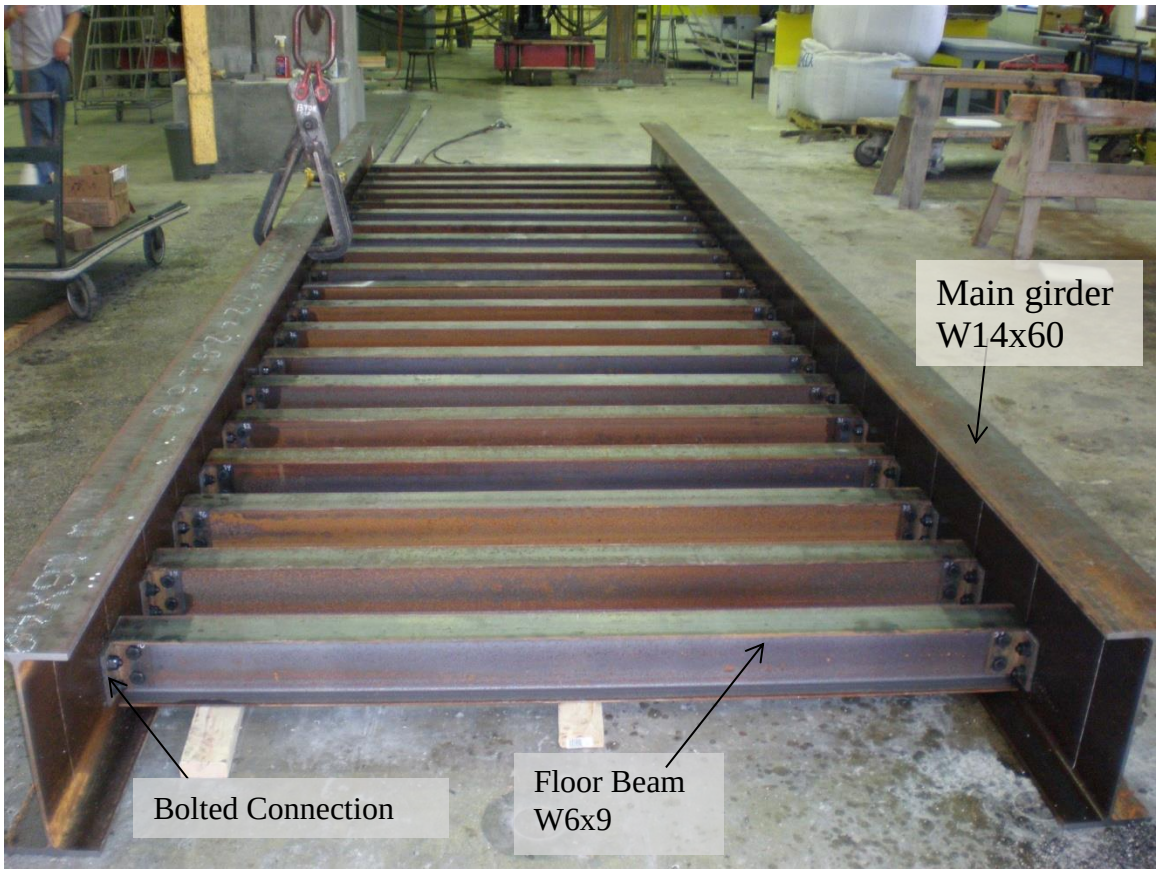


**Figure 4-7. Complete Two-Girder Bridge Specimen.**

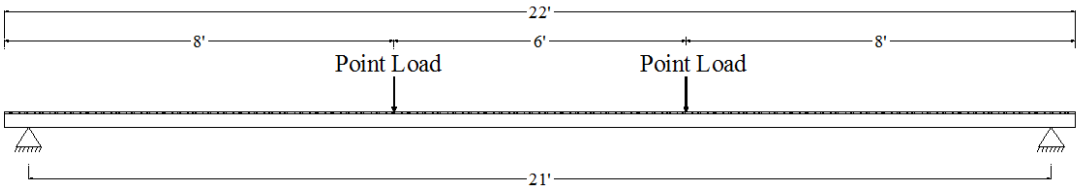


**Figure 4-8. Longitudinal View of Loading Points in Experiment 1.**

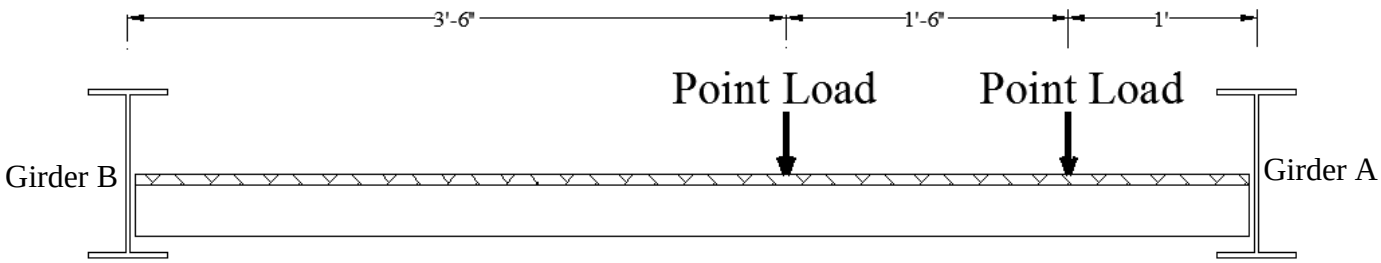


**Figure 4-9. Transverse view of Loading Points in Experiment 1.**

### 4.1.2 Instrumentation

Several strain gages and potentiometers were installed on this test bridge. The following subsections describe the position and type of the instruments:

#### *4.1.2.1 Main Girder Strain Gages*

There were seven strain gages installed on each main girder. The gages can be seen in Figure 4-10. Each girder has three strain gages installed below the bottom flange, one at each quarter points of the length. One strain gage was installed on the web of the girders, which is located at mid-height of the web at the mid-span cross section. And there is one strain gage attached to the top of the top flange, which is in the middle of the width of the top flange at the first quarter point of girder length. Two other strain gages were installed on the top flange at the mid-span section each of the one inch away from the edges of the top flange.

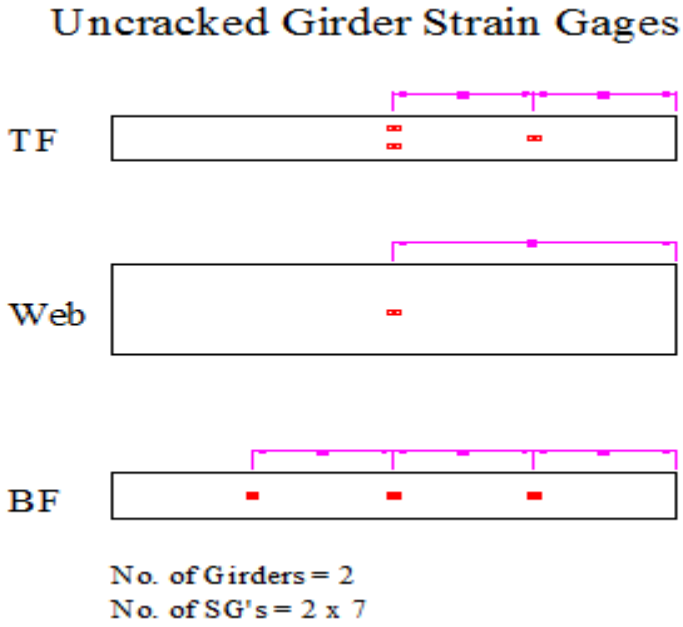


**Figure 4-10. Strain Gauges in Main Girders.**

#### 4.1.2.2 Floor Beams Strain Gages

The length of spreader beams that apply the point loads is about 3ft-9in, such that four floor beams under the spreader beams are engaged, as shown in Figure 4-11. Therefore, to capture the response of the floor beams, all four of those beams were instrumented. The strain gauges on each floor beam are shown in Figure 4-12. One strain gage was attached under the bottom flange of these four floor beams at 2ft-6in from their loaded end. For the top flanges of the floor beams, since the timber deck sits on the top flanges, to avoid damaging the strain gages during the loading, the top flanges were instrumented on their lower face. Two strain gauges were attached to each side of the top flange. One strain gage was installed at the mid-height of the web of one of the floor beams. This strain gage, which was very close to the neutral axis of the W6x9 section, was used for interpolation purposes and to monitor for changes in neutral axis location.

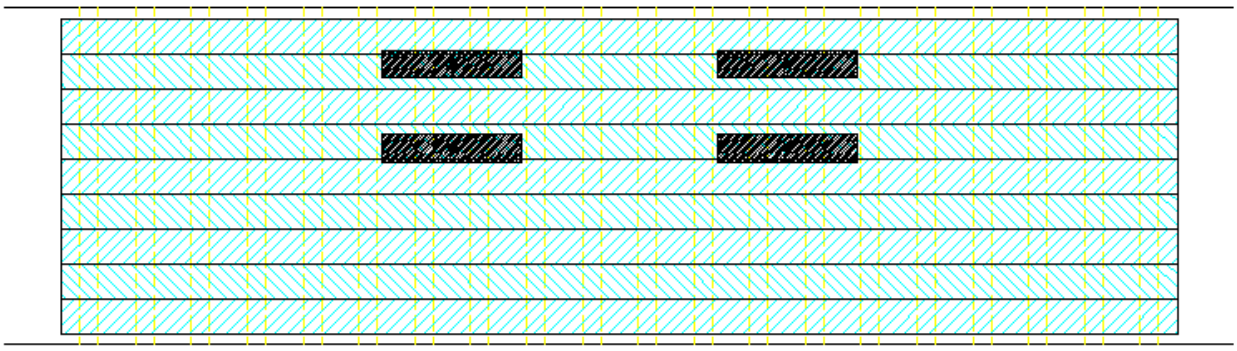

**Figure 4-11. Spreader Beams (Black Rectangular).**

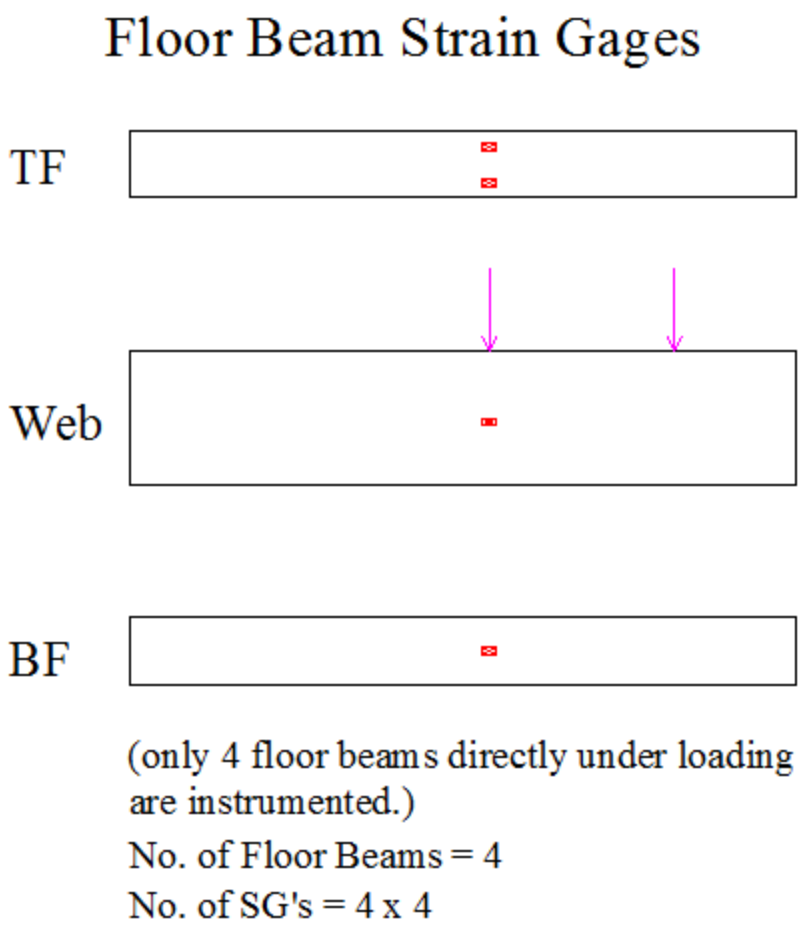


**Figure 4-12. Strain Gauges in Floor Beams.**

#### *4.1.2.3 Connection Angle Strain Gages*

The L3x3x1/2 angles that connect the floor beams to the girders were attached to the webs of floor beams and webs of girders by means of two ½ inch high strength bolts. Two strain gages were installed right beside the bolts to measure the strains of the angles during the loading. The gage can be seen in Figure 4-13. The angle that was chosen for this measurement was the angle connecting one of the floor beams adjacent to loading rods.

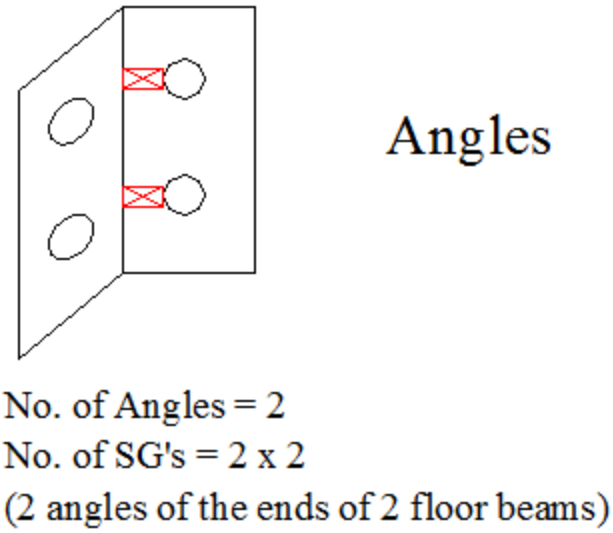


**Figure 4-13. Strain Gauges in Connection Angle.**

#### *4.1.2.4 Potentiometers*

For the two different tests performed on the test bridge, two different configurations for the position of the potentiometers were used. The positions of the potentiometers are described in the following sections:

##### 4.1.2.4.1 LTB Test

For the first part of the test, which was the lateral torsional buckling capacity evaluation of the bridge, six potentiometers were provided; the positions of which are shown in Figure 4-14. The girder away from the loading points (Girder B) had one potentiometer located at its mid-span. The other girder has three potentiometers, one at each quarter point along the length of the girder. Two other potentiometers were located 30 inches away from the end of the two floor beams beside the loading rods.

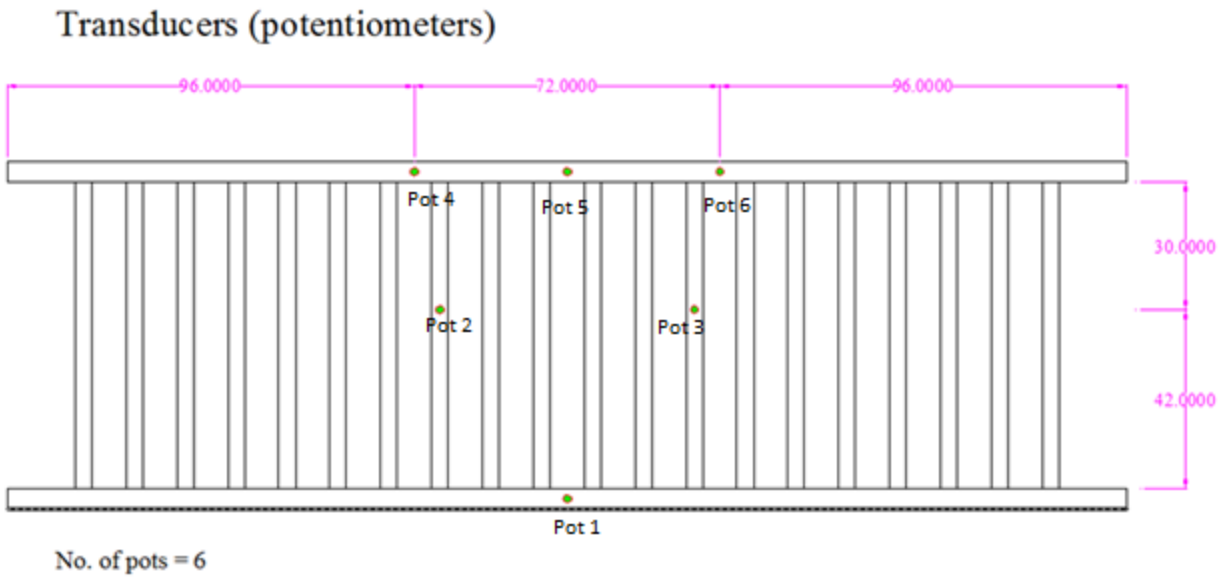


**Figure 4-14. Location of Potentiometers.**

#### 4.1.2.4.2 Fracture Test

The potentiometers in the fracture test are those of the LTB test plus three additional. All of the three added potentiometers are located at the mid-span of the cracked girder and measure the lateral movement. Two of them were attached to the two sides of the bottom flange, right beside the cracked section and one potentiometer was attached to the outer edge of the top flange of this girder.

### 4.1.3 Test 1-A - Partial LTB Capacity Evaluation

In this experiment, it was decided to perform a partial LTB capacity evaluation on the bridge and stop loading when the strains of the bridge elements, especially the girder close to the loading points, start to increase drastically. This point was the point that the girder top flange started to move out of plane laterally. Then, the bridge was unloaded and it was setup for the cracking test. In this section the results obtained from the partial LTB test are presented.

Figure 4-15 shows the vertical displacements obtained from the potentiometers during the loading. It was observed that the deflection of the girder further away from loading (Girder B) had a maximum of about 0.56 inch, which was the lowest maximum deflection recorded during the test. The deflection of the floor beams, which were measured by POT-2 and POT-3 were similar and have a maximum of about 1.23 inch. The other three potentiometers were attached to the mid-span section of the girder close to the loading. POT-4 and POT-6 were attached to the edges of the bottom flange of the girder near the loading point and are almost similar, with a maximum of 1.36 inch. But POT-5, which was attached to the outer edge of the top flange, had the largest deflection among the potentiometers approximately 1.49 inches. It also showed that the girder started to rotate about its bottom flange, which was why a larger displacement was observed in the top flange of the girder.

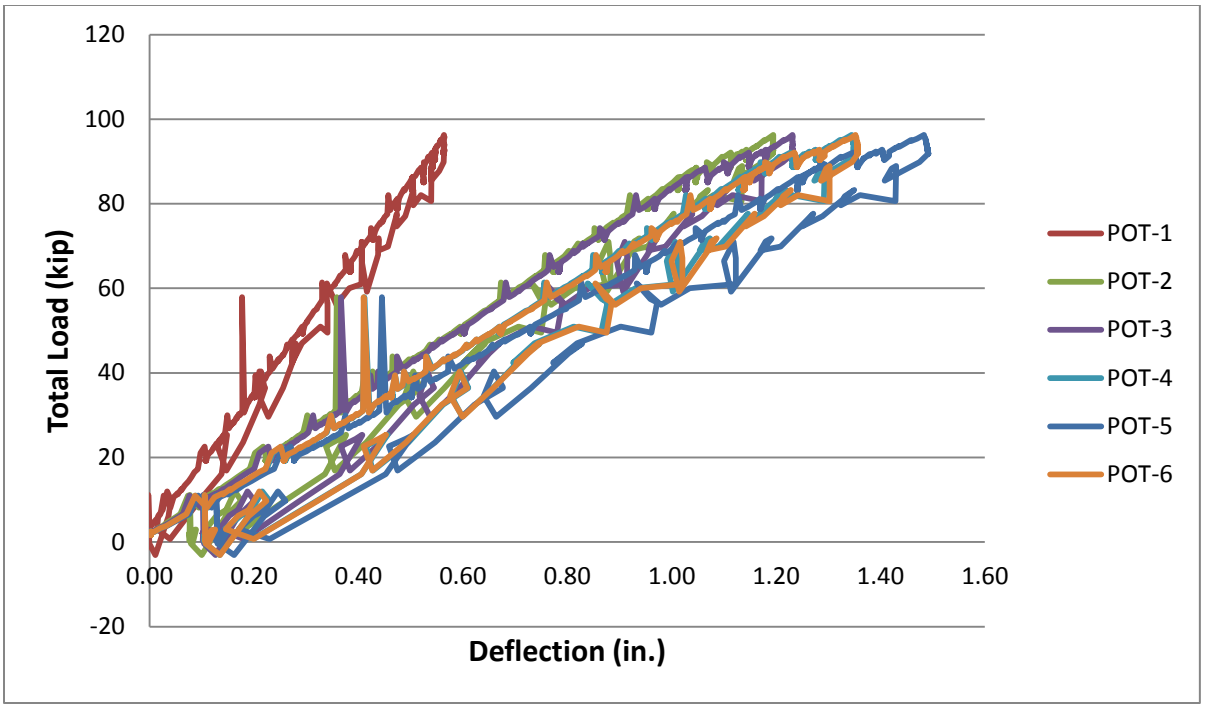


**Figure 4-15. Load-Deflection Curves- Partial LTB Test**

The data obtained from strain gages are divided into two groups. The first group consists of the strain gages attached to floor beams, angles and the girder away from point of loading (Girder B). These strain gages showed values of strain between -1113 me and +1228 me which were less than the yielding strain of 1700 me for Grade50 steel material. The results from this group of gages followed from linear elastic predictions and were not shown. The more important data were acquired from strain gages of the main girder close to loading (Girder A). As shown in Figure 4-16, the strains in bottom flange of the girder at quarter length sections, named G1B1 and G1B3 showed positive values less than 1058 me. These tensile strains were less than the yielding strain of the steel material and restored to zero after unloading the test bridge. The strain gage of the bottom flange at mid-span section, G1B2, and strain gage of the quarter length of top flange, G1T1, showed similar but opposite responses with maximum values of +1444 me and -1028 me, respectively. However, the two strain gages attached to top flange of the girder at mid-span section had larger values of strain. The one attached to the inside edge of the top flange, G1T3, had a strain of +1678 me which was at the yielding threshold and the other one, G1T2, located at the outer edge of the top flange, had a strain of +1941 me which is greater than the yielding strain. It was observed in Figure 4-16 that the strains from these gages did not restore to zero after unloading the bridge.

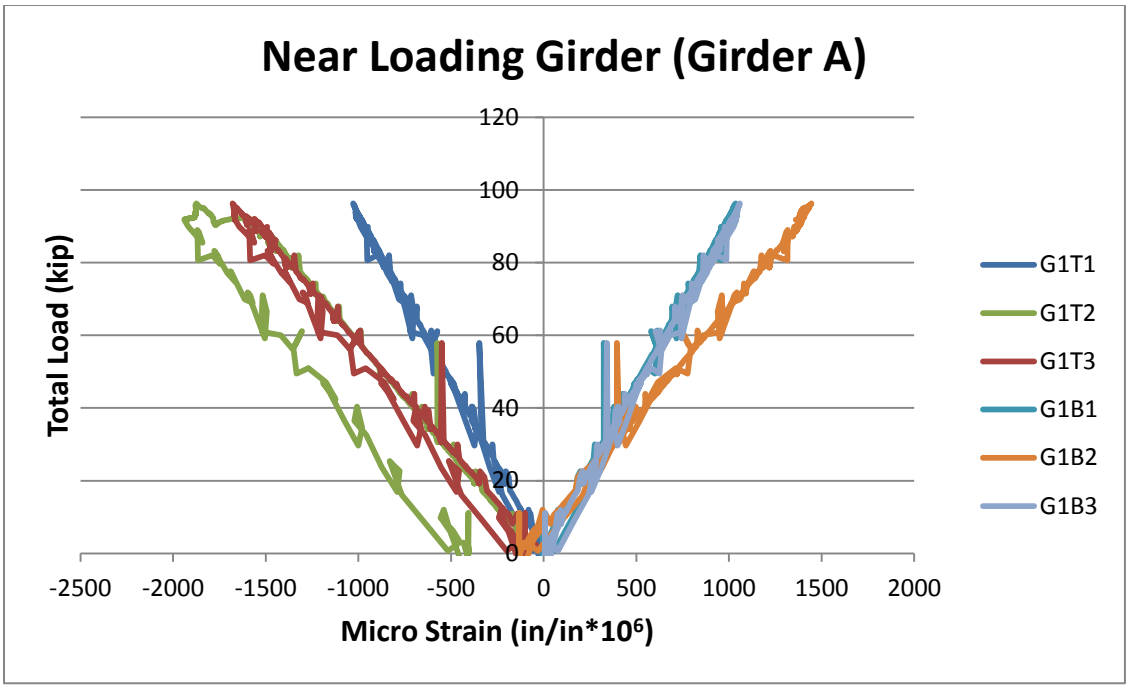


**Figure 4-16. Main Girder Strains (με) vs. Applied Load (kip)- Partial LTB Test**

### 4.1.4 Test 1-B - Loading of Pre-cracked Bridge

This section presents the results of the loading of the pre-cracked bridge. In this stage, the bottom flange of one of the girders of the bridge (the girder closer to loading, Girder A) was cracked for the whole width at the mid-span section of the girder. Then, the bridge was loaded gradually with the hydraulic rams. Figure 4-17 shows that load-deflection curve of the cracked girder during the test. The load in the graph is the total load applied to the two-girder bridge and the deflection is the recorded deflection at the mid-span of the cracked girder. These deflections were recorded by the potentiometer connected to the girder immediately adjacent to the crack plane.

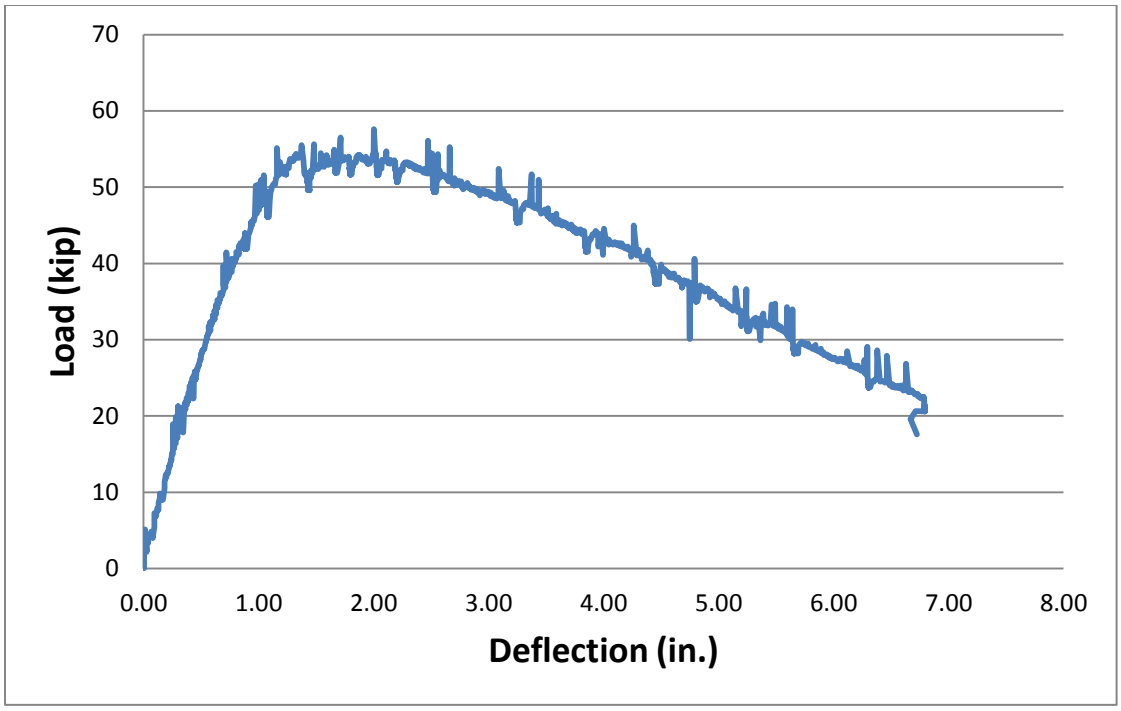


**Figure 4-17. Load vs. Mid-Span Deflection of the Cracked Girder**

In Figure 4-18, the load-deflection curve obtained from the experiment is compared to two analytical load-deflection curves obtained from Finite Element Analysis. The red curve is the load-deflection of the bridge with bottom flange crack and the green curve is for the bridge with bottom flange and half of the web cracked. It is observed that the test bridge response is very close to the curve of the bottom flange cracked bridge up to the point that the crack in the test bridge starts to propagate, which corresponds to a load of 51 kips with a deflection of 1.15 inches. Beyond that point, the deflections in the test bridge begin to increase noticeably with a minimal increase in the load. This relates to the lower moment of inertia and stiffness of the girder section at the cracked plane because of the propagation of the crack. The maximum load that the bridge was able to carry at this stage was equal to 54 kips corresponding to a deflection of 1.37 inches. More propagation of the crack yielded more deflection with lower load capacity. The test was stopped when the deflection of the bridge reached 6.80 inches with 21 kips of load on the bridge. The curve of the half web cracked bridge resulted from the finite element analysis intersects with the test bridge load-deflection curve at a point with 5.69 inches of deflection and 28.51 kips of load. That point is very close to the point that the girder crack reached half of the web height during the experiment. The drop in capacity of bridge versus the crack length is illustrated in Figure 4-19. It shows once the bottom flange crack propagated, a linear relationship was observed between reduction in capacity and growth in crack length.

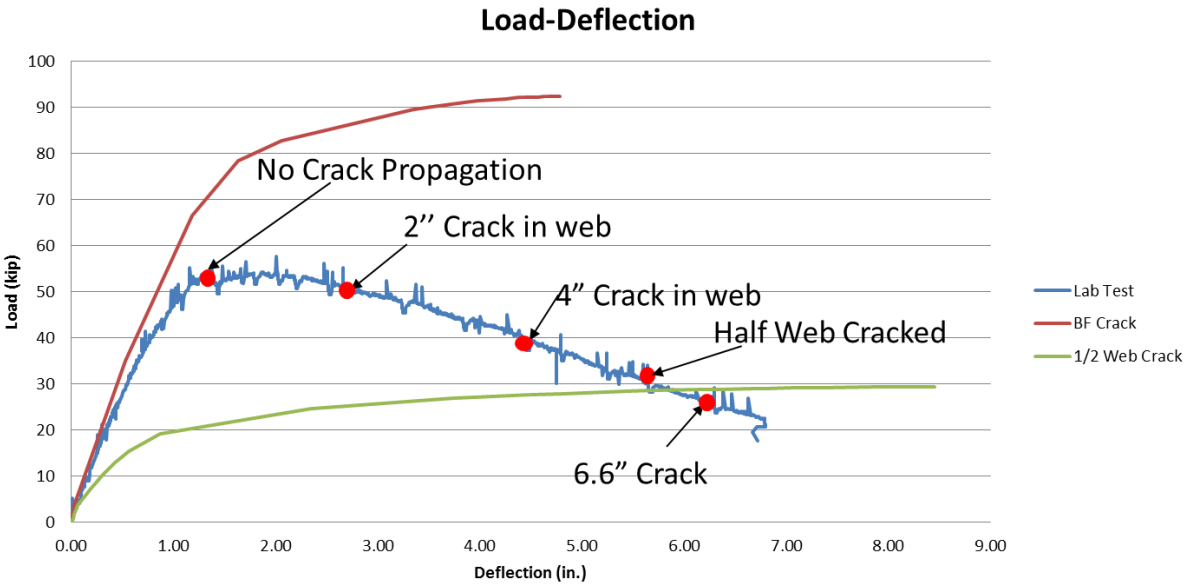


**Figure 4-18. Comparison of Experimental and Analytical Load-Deflection Curves**

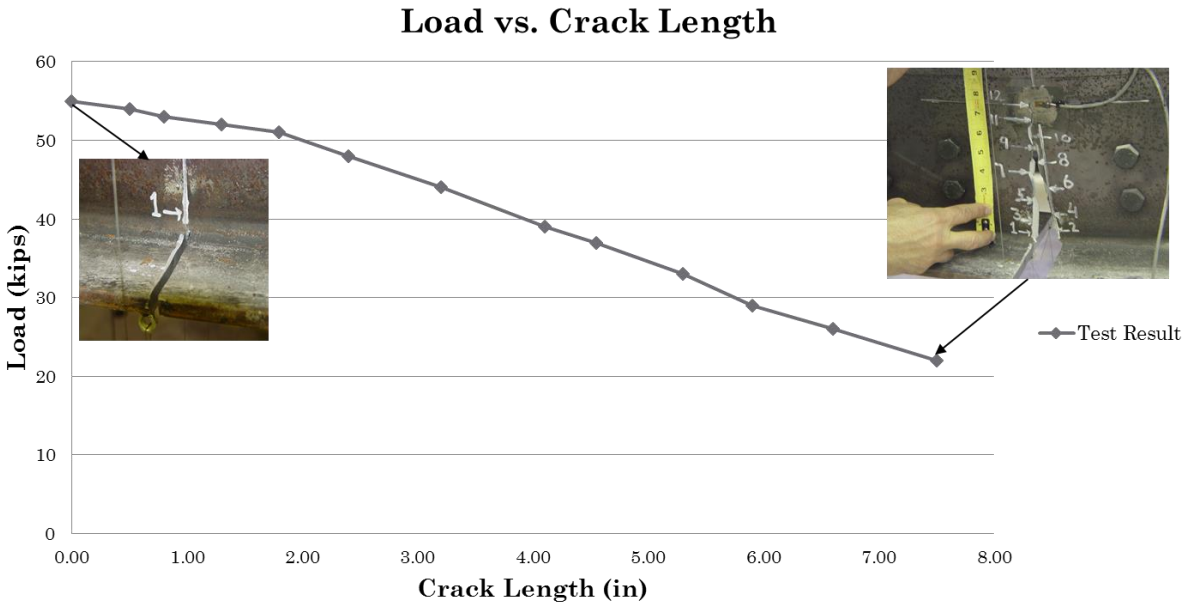


**Figure 4-19. Change in Capacity vs. Growth of Crack**

Figure 4-20 shows the deflections recorded by all potentiometers installed for the test. Pot1 was connected to the uncracked girder, which was the only recorded deflection that was not affected by the large deflection of the cracked girder. Pot2 and Pot3 are the potentiometers attached to the floor beams. Although the floor beams do not experience any large strains, because of the large deformation of the cracked girder, they were exposed to a rigid body

rotation which caused the large deflections of about 2.82 inches at the points of potentiometers attachment. Pot4 and Pot6 were connected to the quarter points of the cracked girder length. It was observed that the experiment was symmetric about the mid-span plane of the bridge and the deflections at these two locations were exactly the same. Pot5, Pot7, Pot8 and Pot9 are the four potentiometers that are connected to the two sides of the crack plane of the cracked girder. Pot9, Pot5, and Pot8 were attached to the inner edge, mid- point and outer edge of the bottom flange at the cracked section, respectively. Pot7 was attached to the outer edge of the top flange at this section and showed more deflection due to addition of the vertical deflection and the vertical component of the torsional displacement of the top flange. For that reason, the deflection recorded at Pot7 was the maximum among the deflections recoded during this experiment.

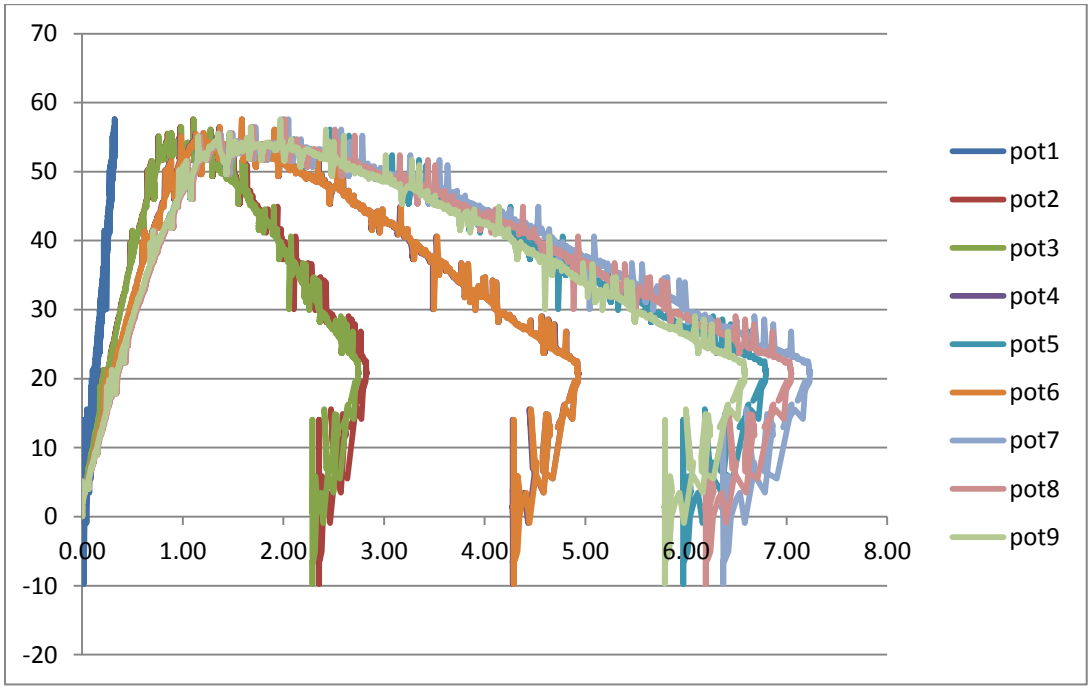


**Figure 4-20. Load vs. Deflection of the Cracked Bridge- POT's 1 thru 9**

### 4.1.5 Summary of Experiment #1

In the partial LTB capacity test, the undamaged specimen was loaded up to the point at which the lateral and torsional displacement of girders occurred. This behavior was captured at 92 kips of load corresponding to 1.36 inch vertical displacement in bottom flange and 1.49 inch vertical displacement in top flange. Strain gauge data showed that a majority of the specimen did not yield except for the top flange of the girder (near the loading point) at the mid-span section.

In the second test, the bottom flange of the girder closer to the loading point, Girder A was cracked at the mid-span section. The behavior of specimen was linear up to 51 kips of load when the stiffness began to decrease. The maximum load carrying capacity of this cracked bridge was reached at 54 kips with 1.37 inch in displacement. After reaching the maximum capacity, the

crack propagated up through the web, which led to a drop in capacity of the specimen. The test was stopped when the load capacity dropped down to 21 kips with a 6.8 inch displacement.

In general, FEA results showed a reasonable agreement with the test results up to 51 kips at which the crack began propagating up to the web. Plus the FE results showed a reasonable prediction on the capacity of the specimen when crack reached a half depth of the web.

## 4.2 Experiment #2

In the second experiment, a bridge with a built-up girder was chosen. The reason for not using rolled girders was to be able to perform the experiment on the maximum ratio that can be found in practice for the height of the girder to height of the floor beams. Figure 4-21 shows a photo of the two-girder bridge in which the ratio of the heights of the girders and floor beams can be seen. The geometrical configuration of the test bridge, loading position, instrumentation and different stages of loading in this experiment are explained in the following subsections.

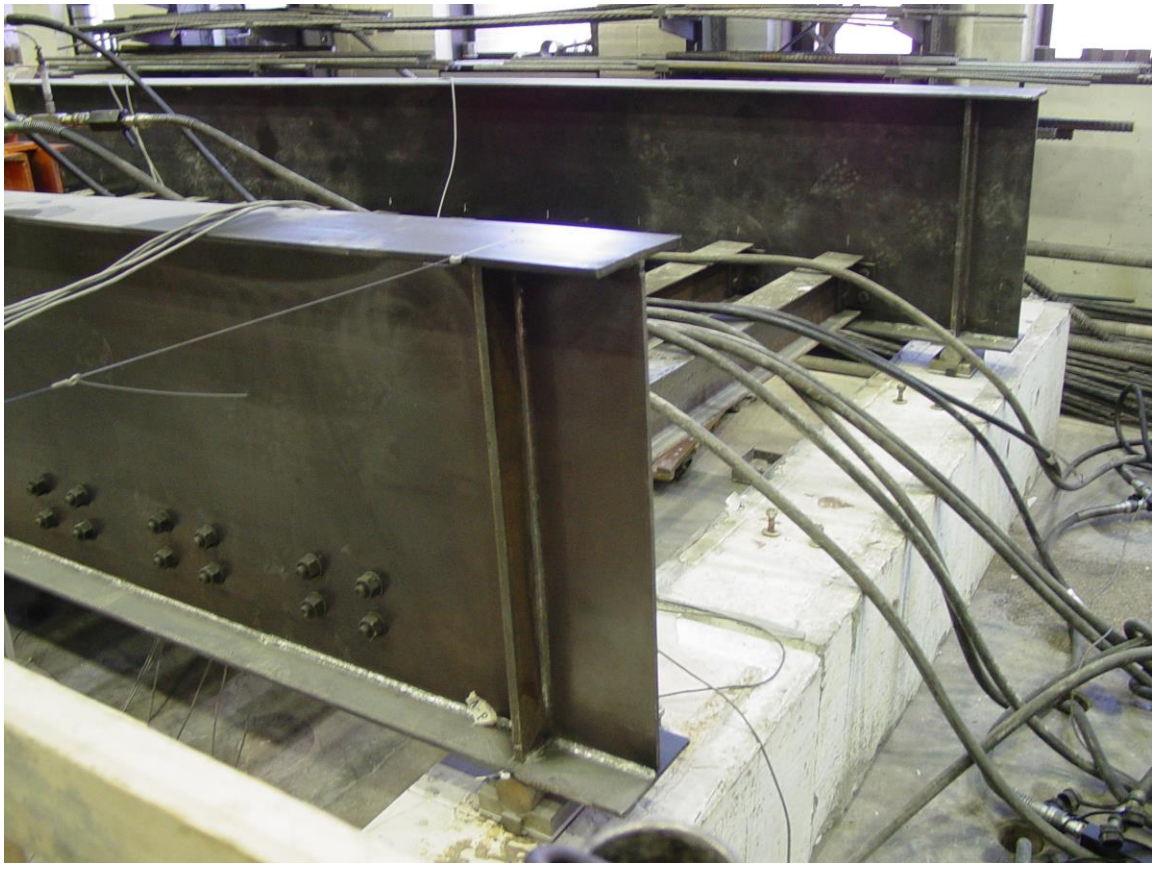

**Figure 4-21. Two-Girder Bridge with Deep Girders**

Figure 4-22 and Figure 4-23 depict the test bridge with deep girders and the data acquisition setup employed in this experiment.

**Figure 4-22. Test Bridge with Deep Girders (Initial Trial Loading Configuration)**

**Figure 4-23. Data Acquisition and Test Bridge Setup (Initial Trial Loading Configuration)**

### 4.2.1 Bridge Geometry and Loading Configuration

The girders were built up of 23 inch webs with a thickness of 5/16 inch and flanges with a width of 6 inches and thickness of 3/8 inch. The flanges of the girders were connected to the web plate with a continuous ¼ inch fillet weld. The ratio of girder height to floor beam height is approximately 4.0. Figure 4-24 shows the elevation view and cross section of the girder used in this experiment.

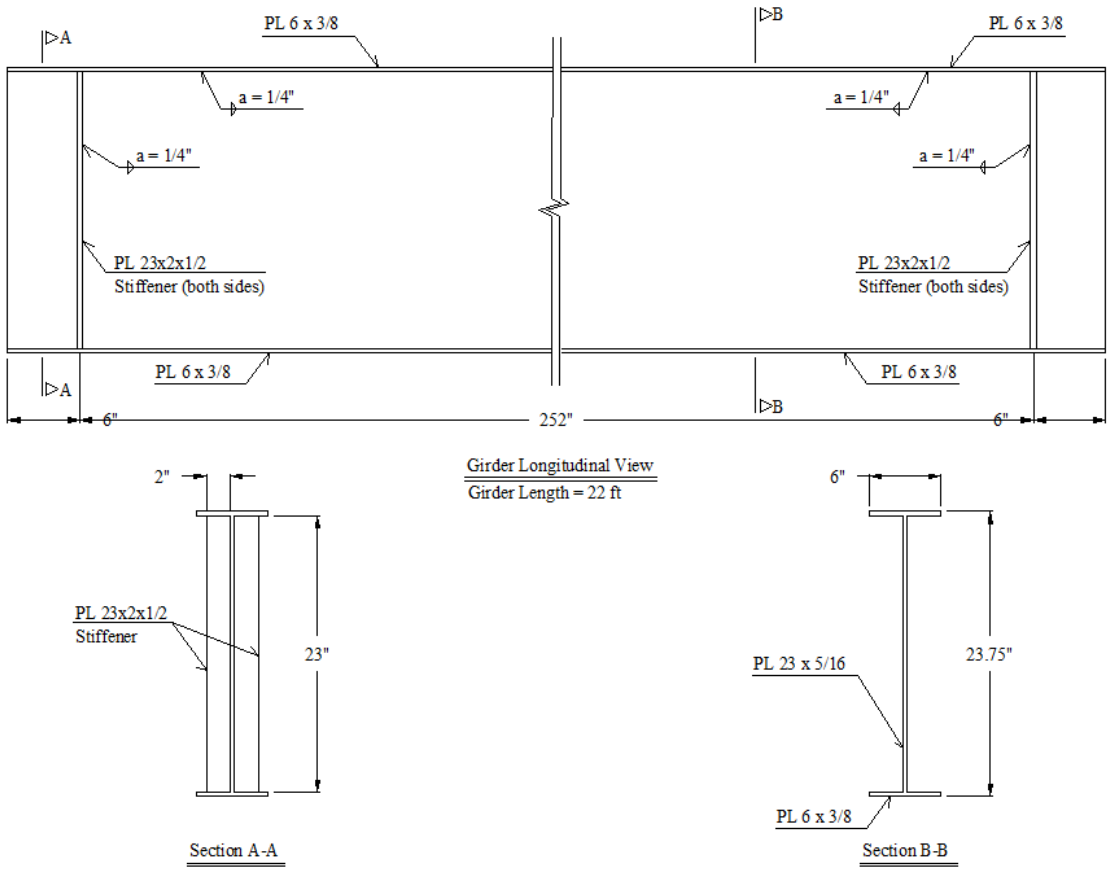


**Figure 4-24. Cross section and Elevation of the Girders with 23.75 in. Height**

The floor beams of the bridge were the same of the floor beams of the first experiment, which were W6x9 hot rolled sections. The top and bottom flanges of the four floor beams directly under the loads were strengthened by means of 48x5x3/8 inch cover plates to avoid yielding of the floor beams under the maximum loads in this test. Figure 4-25 illustrates the cross section of the bridge showing the position of the cover plates. To connect the floor beams to the girder, again the same elements of the first experiment were used, L3x3x3/8 angles and two A325 D=1/2 inch high strength bolts on each leg of the angles.

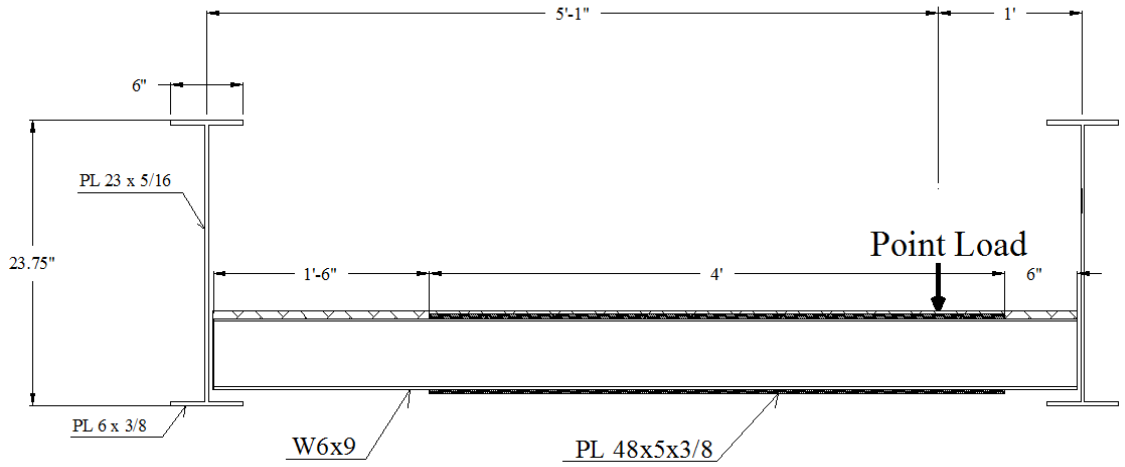


**Figure 4-25. Cross section of Test Bridge with Deep Girders**

As can be seen in Figure 4-25, this bridge was loaded by concentrated forces applied to the floor beams one foot away from one of the girders. Therefore, considering the half inch gap between the ends of the floor beams and the webs of the girders, the distance from the center of the point loads to the center line of the girders is 5 foot, one inch. The loads were applied at two locations along the length of the bridge each of them at a distance of 7 foot, 6 inches from the centerline of the supports. Figure 4-26 shows the longitudinal positioning of the loading points.

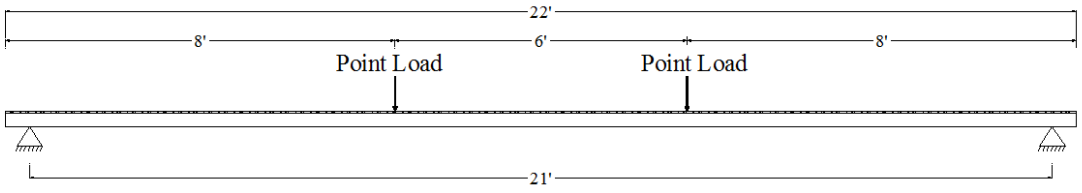


**Figure 4-26. Longitudinal View of Loading Points in Experiment 2.**

### 4.2.2 Instrumentation

In order to capture the behavior and responses of the test bridge during loading, 28 strain gages and 16 potentiometers were installed. The location and type of the instrumentations have been explained in the following subsections.

#### *4.2.2.1 Main Girders Strain Gages*

There are nine strain gages installed on the main girder closer to loading points (Girder A) and seven strain gages installed on the other plate girder (Girder B) as follows:

#### 4.2.2.1.1 Girder far from loading

The girder that is farther from the loading points has three strain gages below its bottom flange each of them at the quarter points of the girder length. It also has one strain gage at the middle of the height of the mid-span section. On the top flange, the girder has three strain gages. One at the quarter point in the middle of the width of the flange and the other two at mid-span section, each of them one inch away from the edges of the top flange. The strain gauge locations on the girder far from loading points are shown in Figure 4-27.

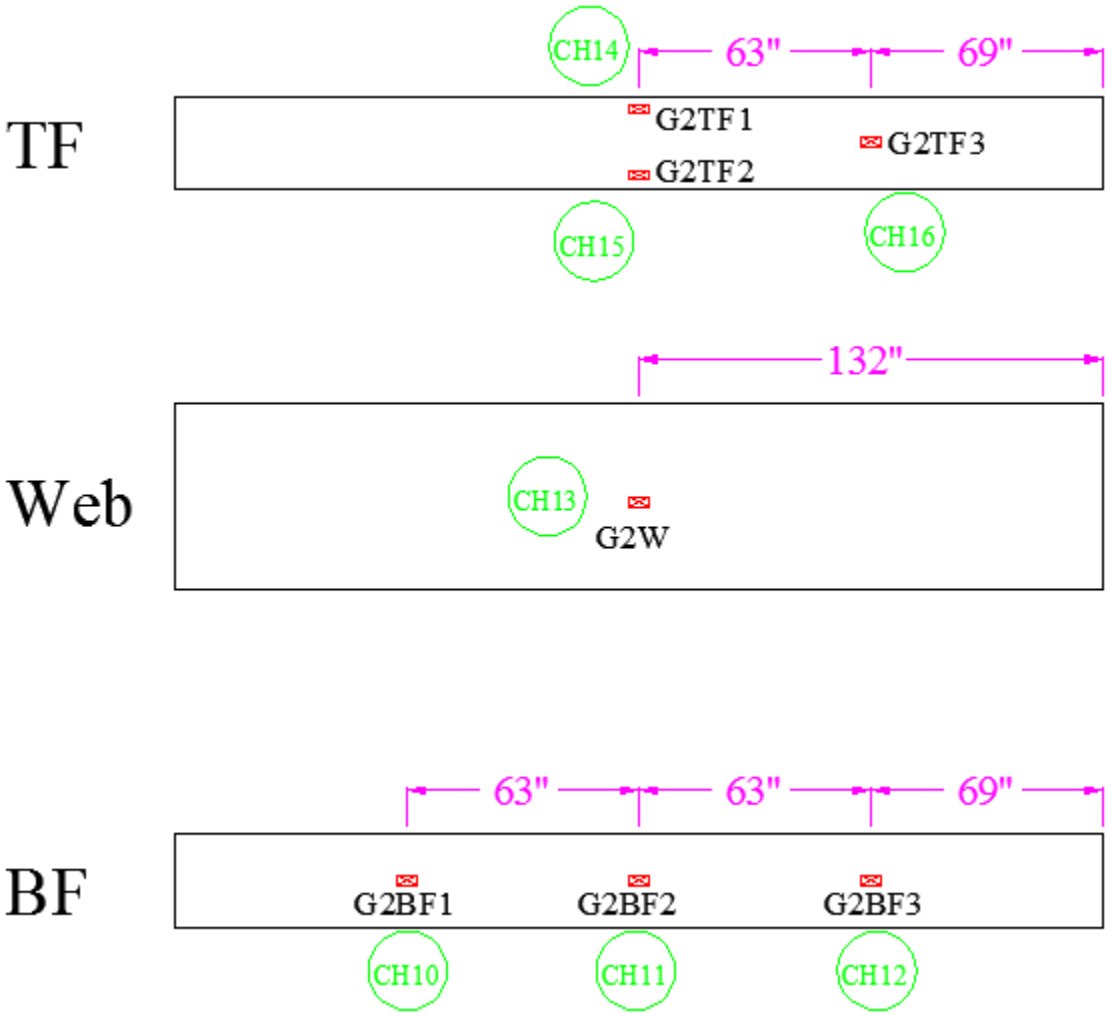


**Figure 4-27. Strain Gauges in Girder far from Loading.**

#### 4.2.2.1.2 Girder close to loading

The strain gages of the girder A has the same strain gage positions plus two more strain gages on the top flange at a section 1'-6" from the mid-span section, as illustrated in Figure 4-28. These two strain gages also have a distance of one inch from the edges of the top flange.

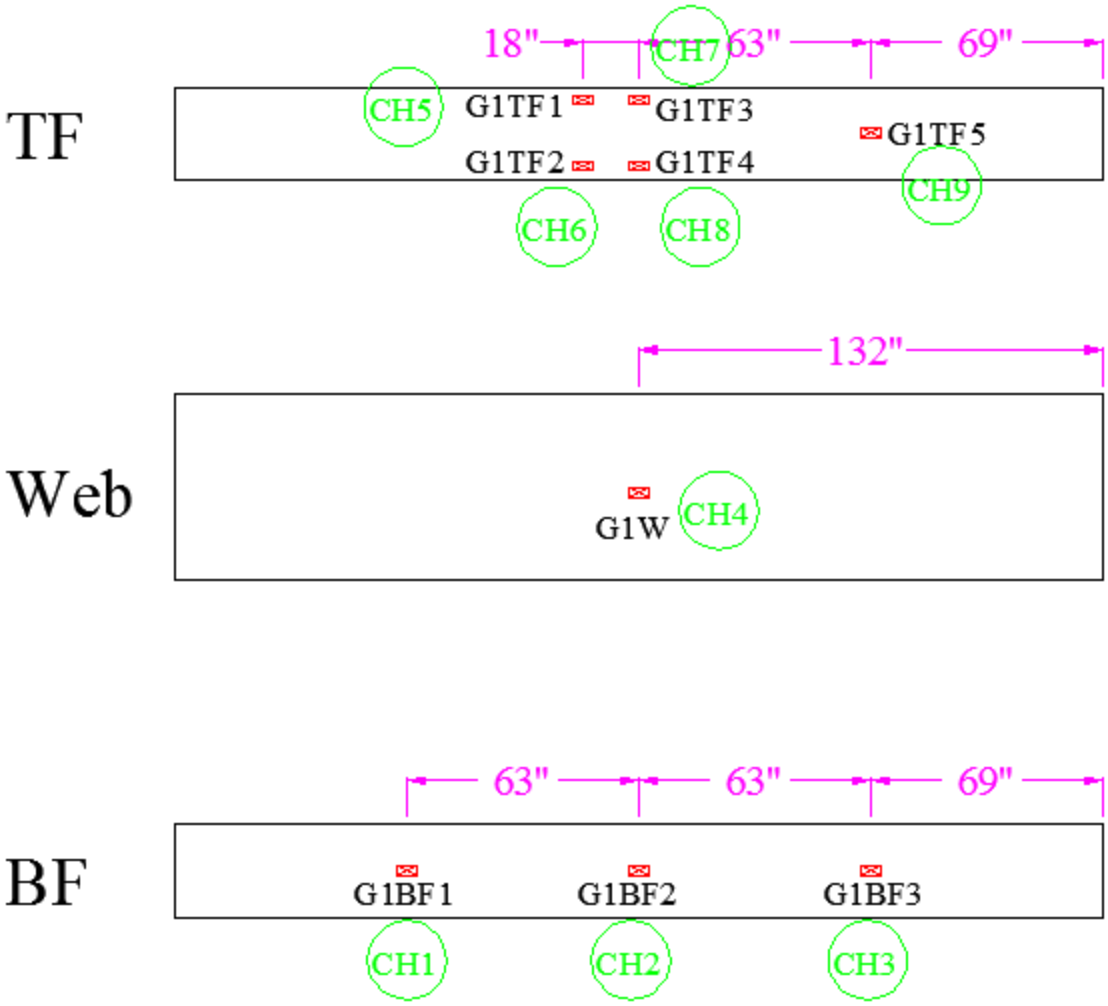


**Figure 4-28. Strain Gauges in Girder Close to Loading.**

#### *4.2.2.2 Floor Beams Strain Gages*

The floor beams that are located directly under the point loads were instrumented with strain gages. Strain gages were installed on the section 2'-6" from the end of the floor beam that is closer to loading. There are three strain gauges installed on each of the four floor beams located under the loading as shown in Figure 4-29. One strain gage is under the bottom flange in the middle of the width of the flange. One strain gage is in the middle of the height of the web. And the third strain gage is located under the top flange in the middle of the projected length of the flange.

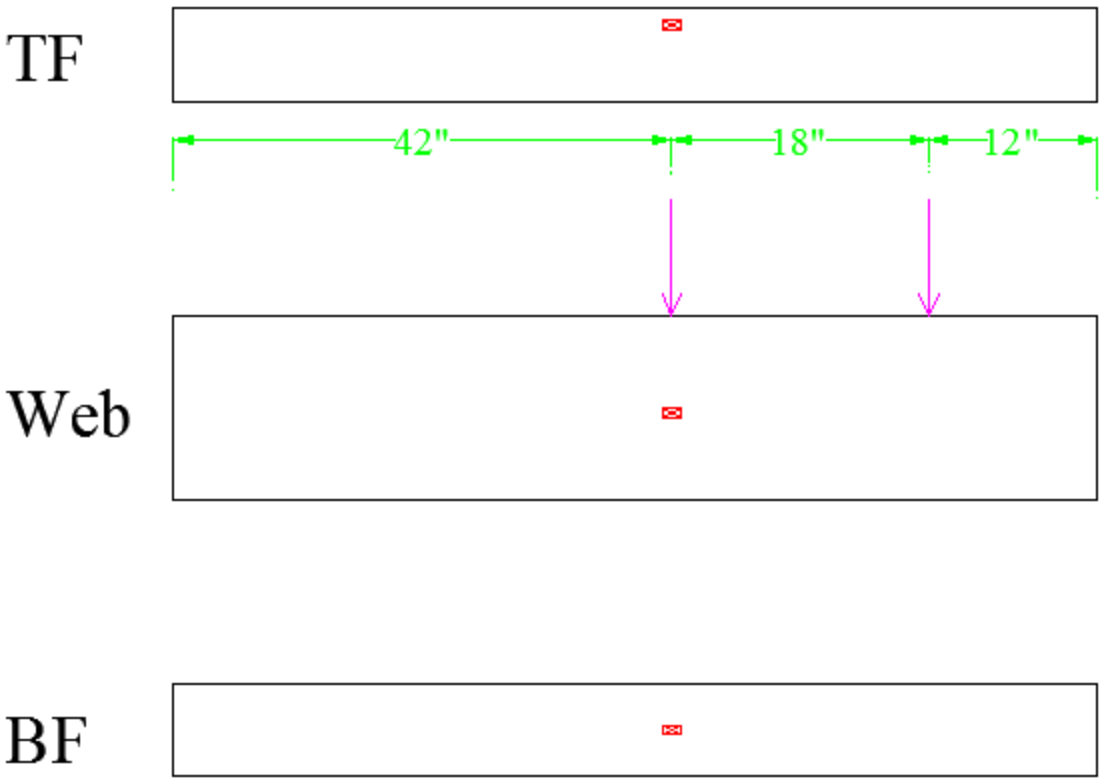


**Figure 4-29. Strain Gauges in Floor Beam.**

#### *4.2.2.3 Potentiometers*

For the two different tests that are arranged to be performed on this test bridge, two different configurations for the position of the potentiometers are planned. The positions of the potentiometers are described in the following sections:

##### 4.2.2.3.1 LTB Test

For the first part of the test which was the lateral torsional buckling capacity evaluation of the bridge, fifteen potentiometers were installed on the test bridge. The girder closer to loading had (Girder A) two vertical potentiometers, one at each quarter point of the length of the girder from its ends. Two more vertical potentiometers were attached to the edges of this girder at the mid-span section. Two other vertical potentiometers were located 30 inches away from the end of the two floor beams close to the loading rods. All vertical potentiometer locations are depicted in Figure 4-30.

Nine horizontal potentiometers are also employed in this test, which are shown Figure 4-31. Five of them are used to measure the displacements of quarter points plus the two ends of the top flange of the girder close to loading. Three horizontal potentiometers are also installed to capture the movements of the bottom flange at quarter points of the length of the girder, i.e. ¼, ½, ¾ of

girder length. One horizontal potentiometer is connected to the top flange at the mid-span section of the other girder which is farther to the loading points.

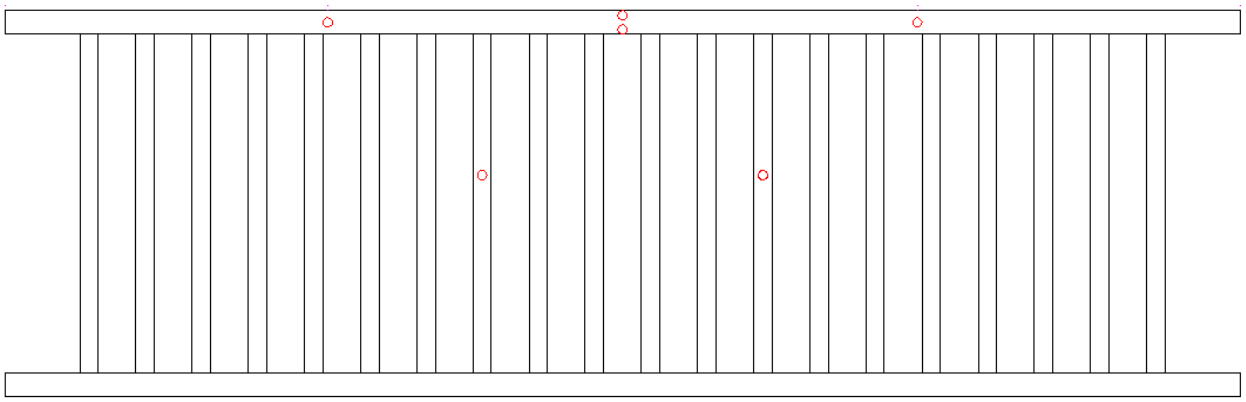

**Figure 4-30. Vertical Potentiometers in LTB Test (Unfractured Test).**

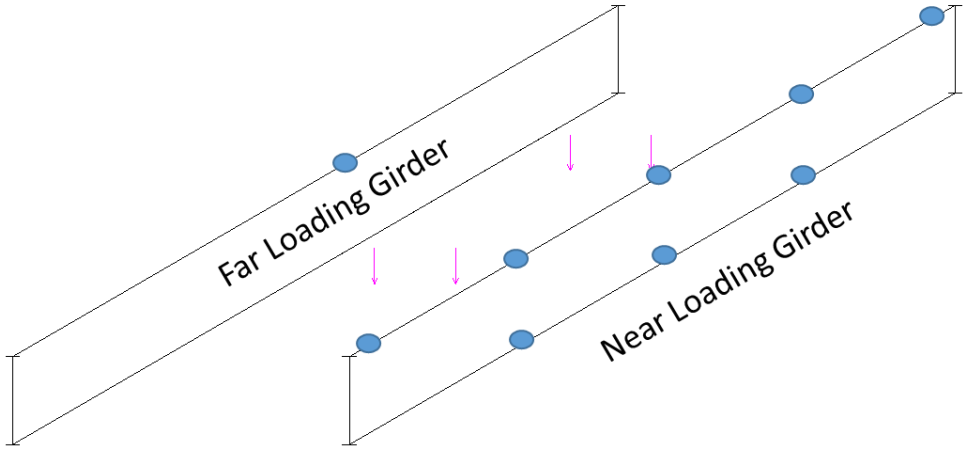


**Figure 4-31. Horizontal Potentiometers in LTB Test (Unfractured Test).**

#### 4.2.2.3.2 Fracture Test

In this stage of the experiment, the horizontal potentiometers were kept the same as in the LTB unfractured test above. However, one vertical potentiometer was added to the girder near the loading to record its vertical displacement and another potentiometer was used to measure the crack opening during the loading. One of the vertical potentiometer on the floor beam was removed due to the limitation on the number of potentiometer channels. The final setup of the potentiometers is shown in Figure 4-32 and Figure 4-33.

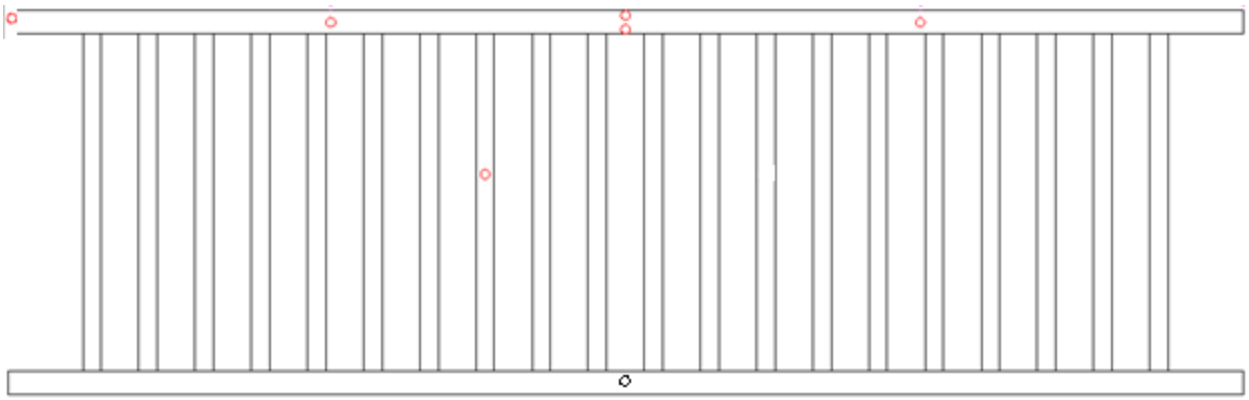

**Figure 4-32. Vertical Potentiometers in Fractured Test.**

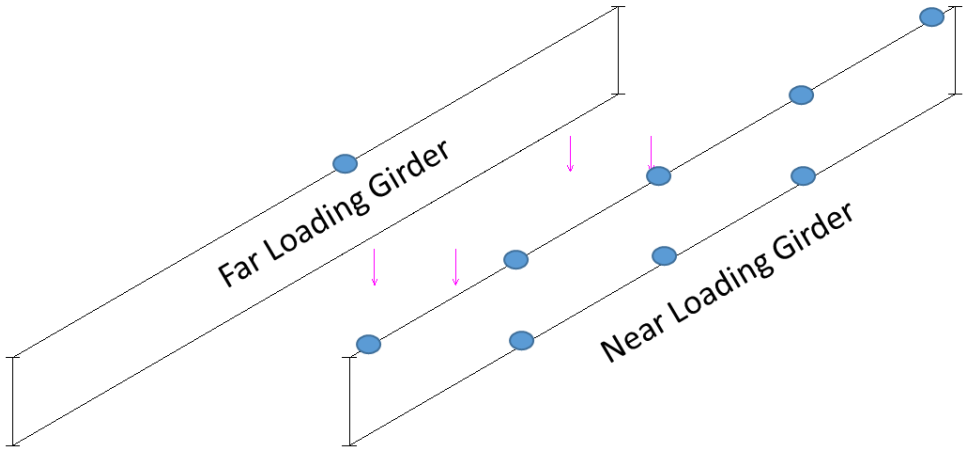


**Figure 4-33. Horizontal Potentiometers in Fractured Test.**

### 4.2.3 Test 2-A - LTB Capacity Evaluation

In this stage of the experiment, the lateral torsional buckling capacity of the two girder bridge with the built-up girders is evaluated. As explained before, the loads are applied through two point loads, one foot away from one of the girders. Figure 4-34 shows the test bridge before loading.

**Figure 4-34. Test Bridge Setup Before Loading**

Figure 4-35 shows the top flange of the girder before loading which has the horizontal potentiometers attached to it at its fifth points.

Figure 4-36 through Figure 4-46 depict the bridge, especially the top flange of the girder A, at different stages of loading.

**Figure 4-35. Instrumentation Installed on Top Flange of Plate Girder**

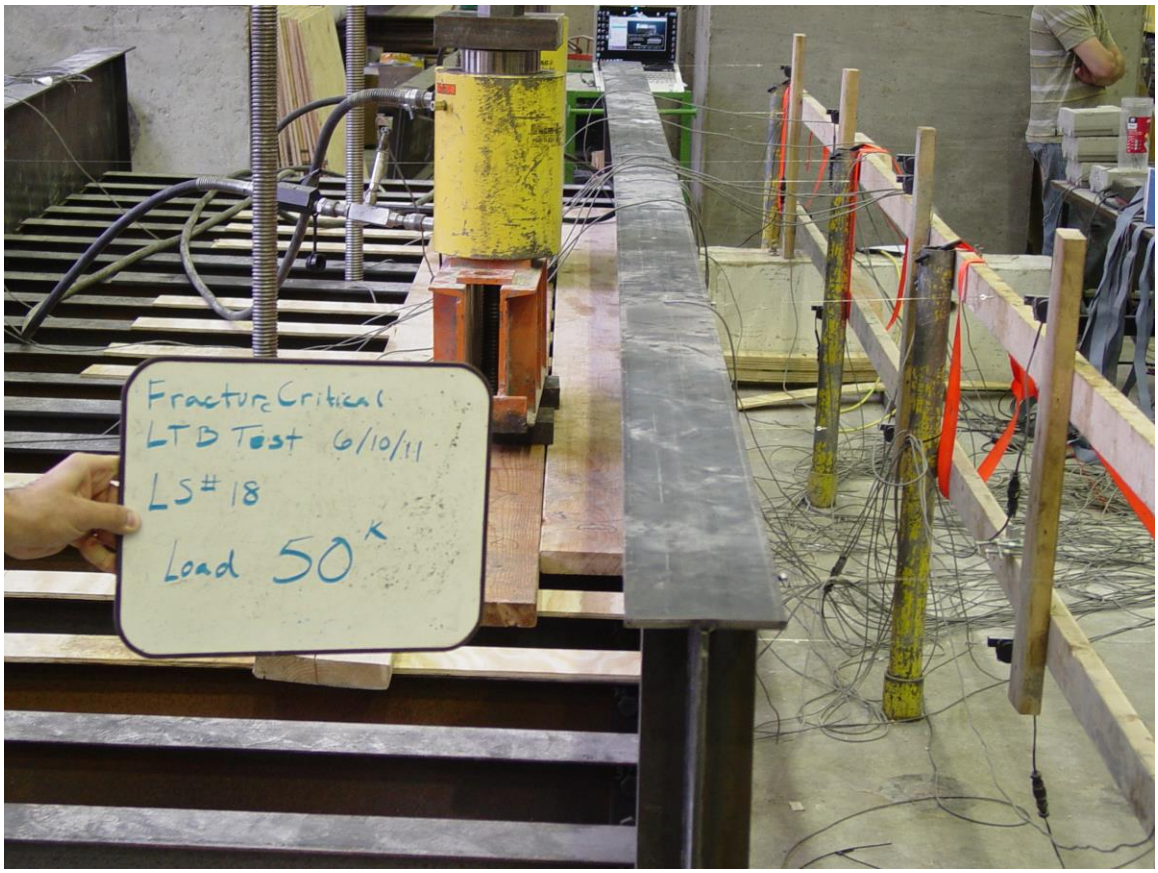


**Figure 4-36. Deformed Bridge Under 50 kips of Load**

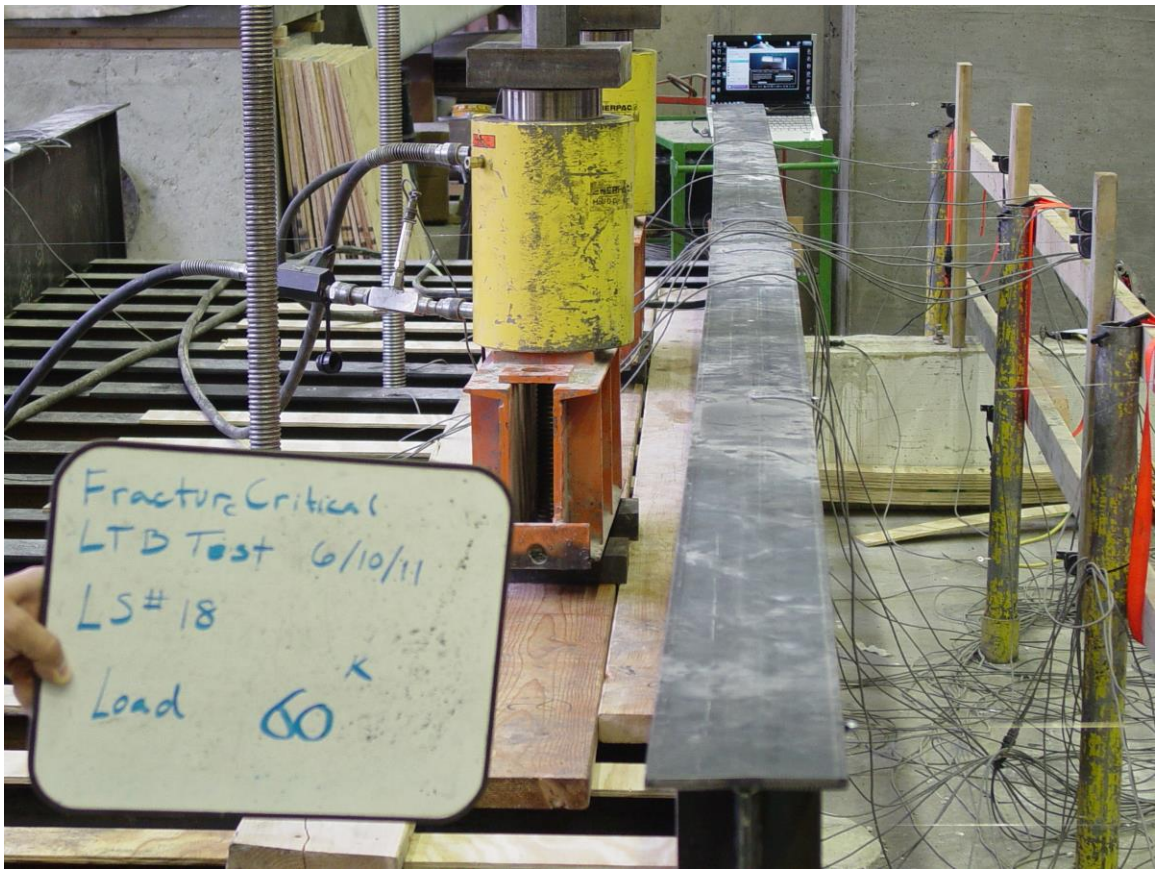


**Figure 4-37. Deformed Bridge Under 60 kips of Load**

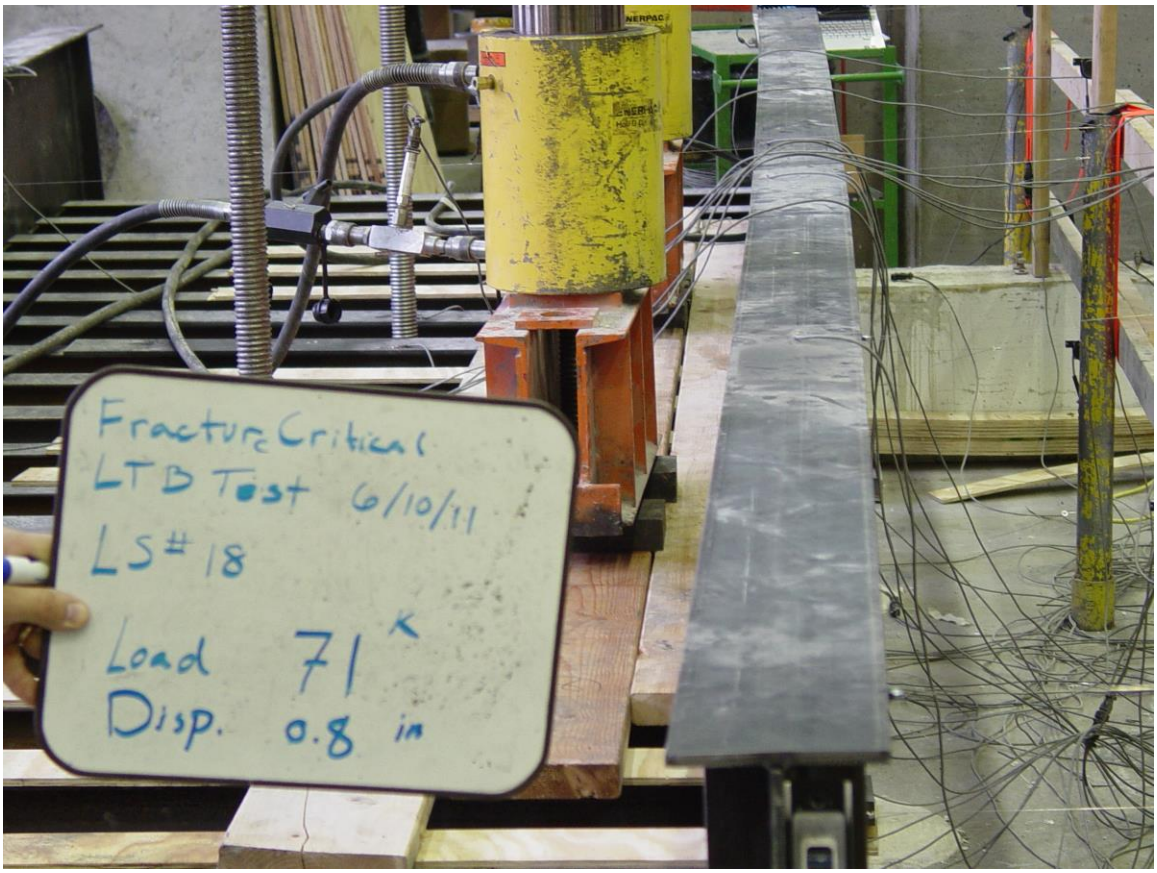


**Figure 4-38. Deformed Bridge Under 71 kips of Load**

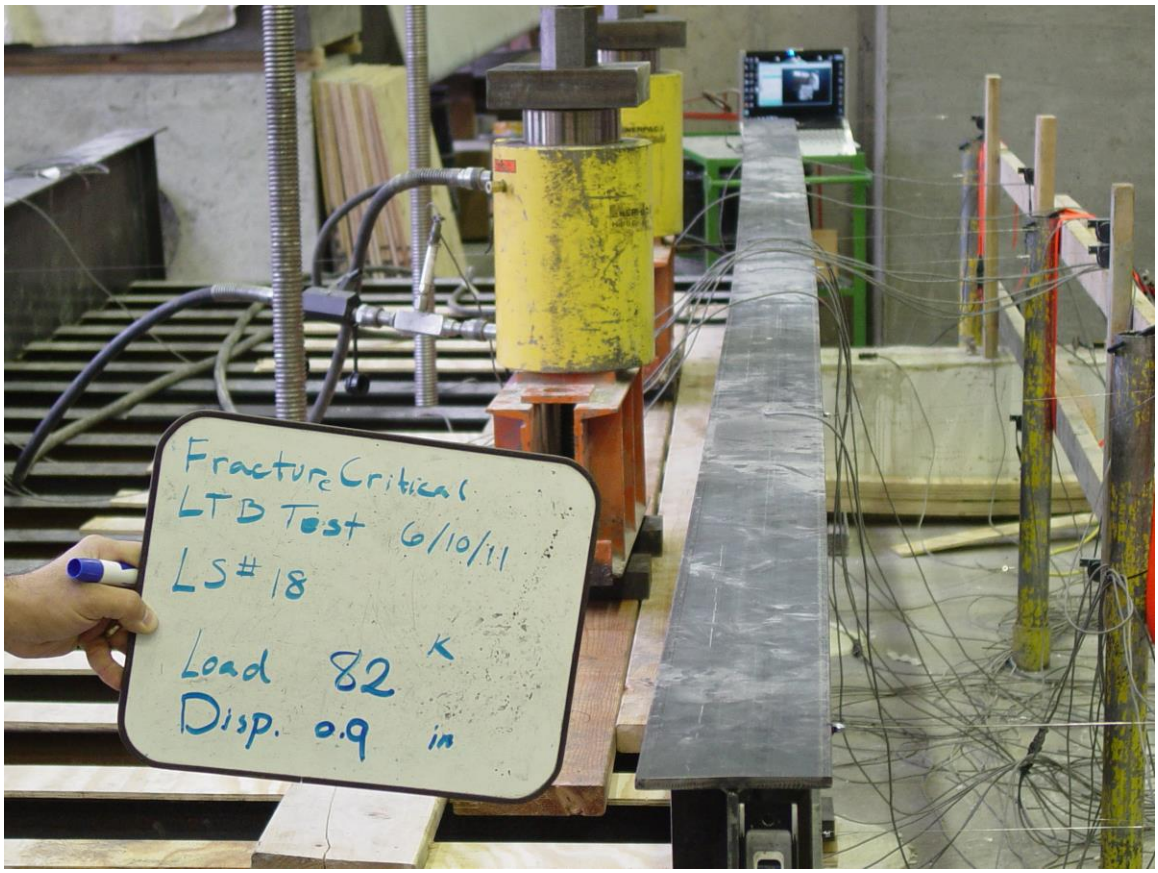


**Figure 4-39. Deformed Bridge Under 82 kips of Load**

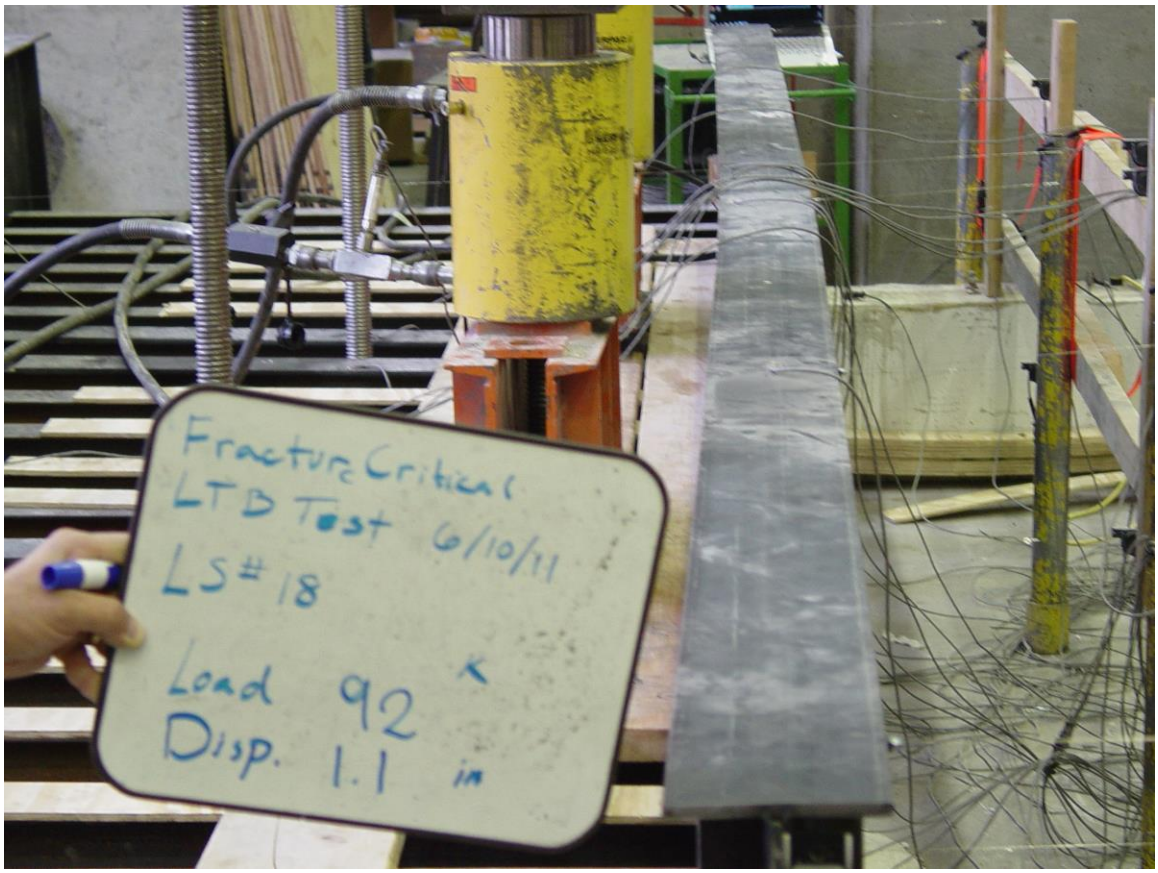


**Figure 4-40. Deformed Bridge Under 92 kips of Load**

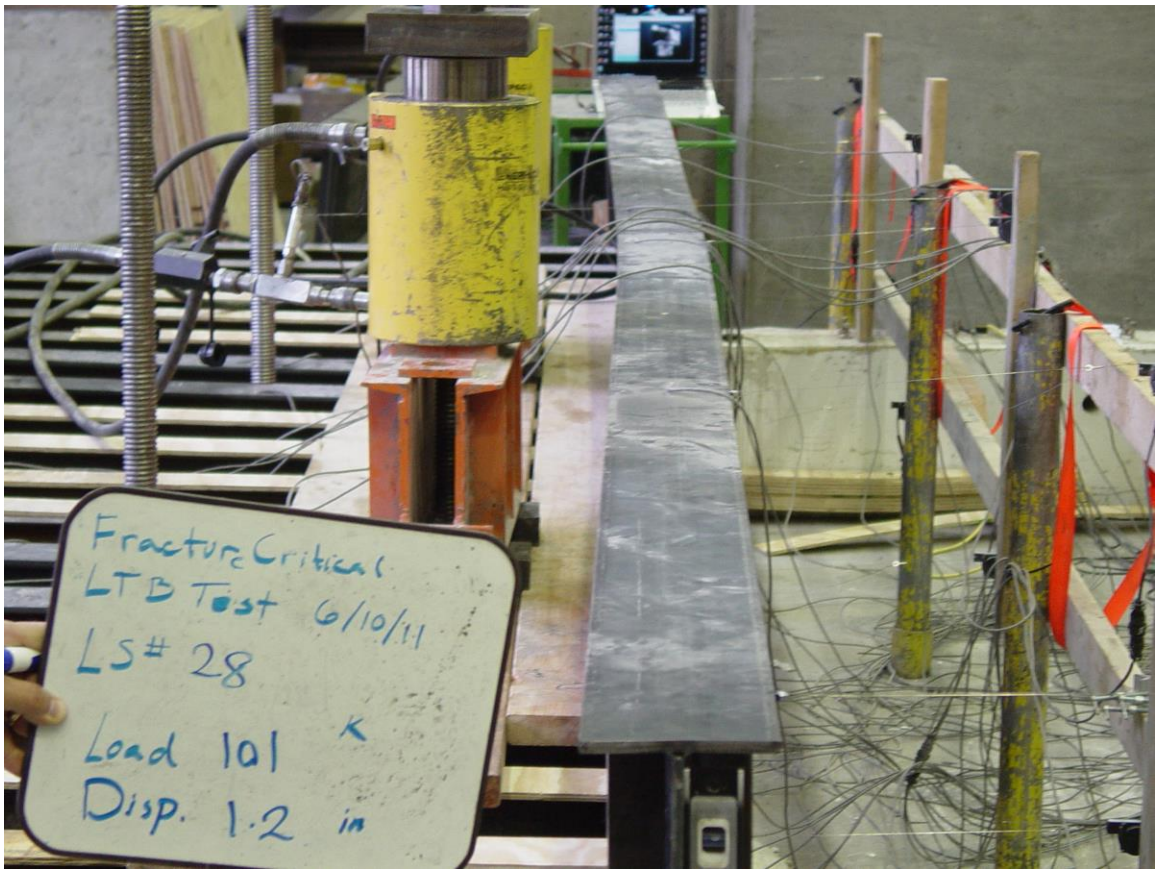


**Figure 4-41. Deformed Bridge Under 101 kips of Load**


**Figure 4-42. Deformed Bridge Under 106 kips of Load**

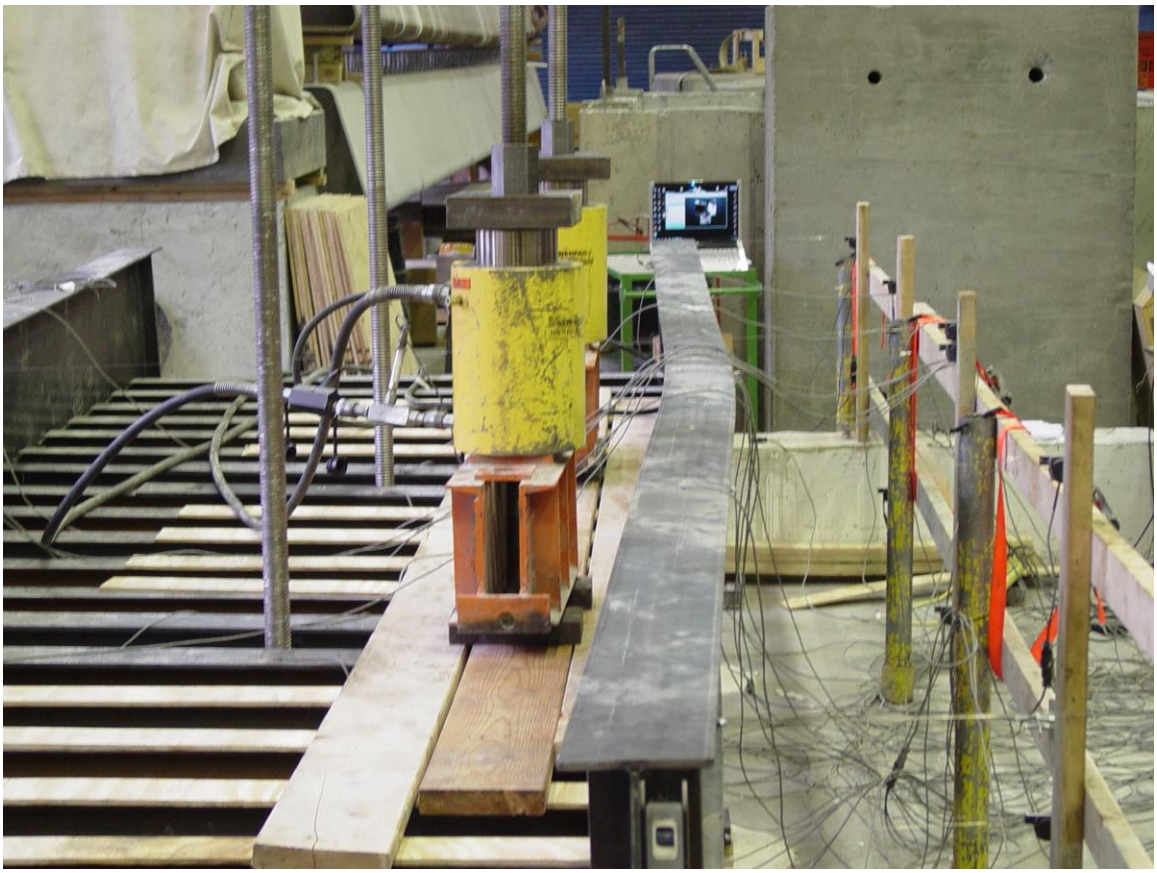

**Figure 4-43. Deformed Bridge Under 106 kips of Load**

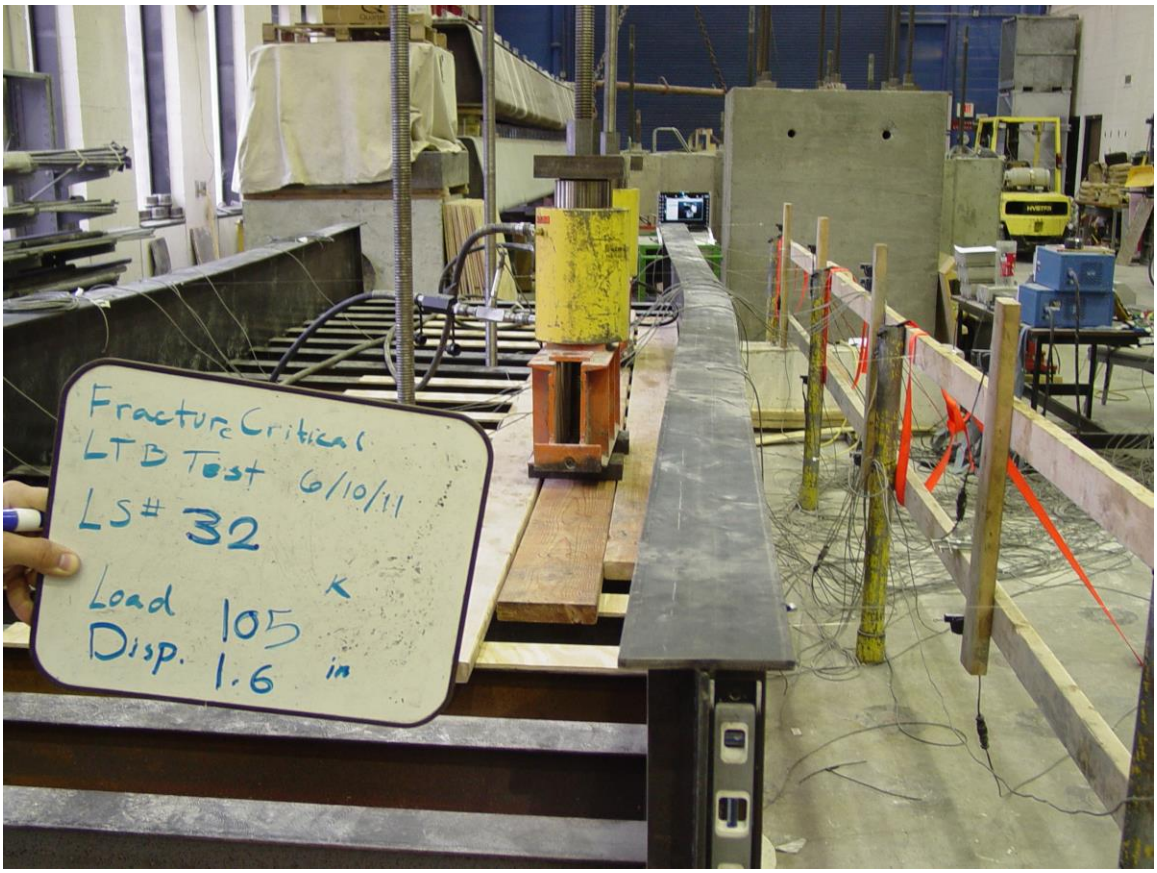


**Figure 4-44. Deformed Bridge Under 105 kips of Load**

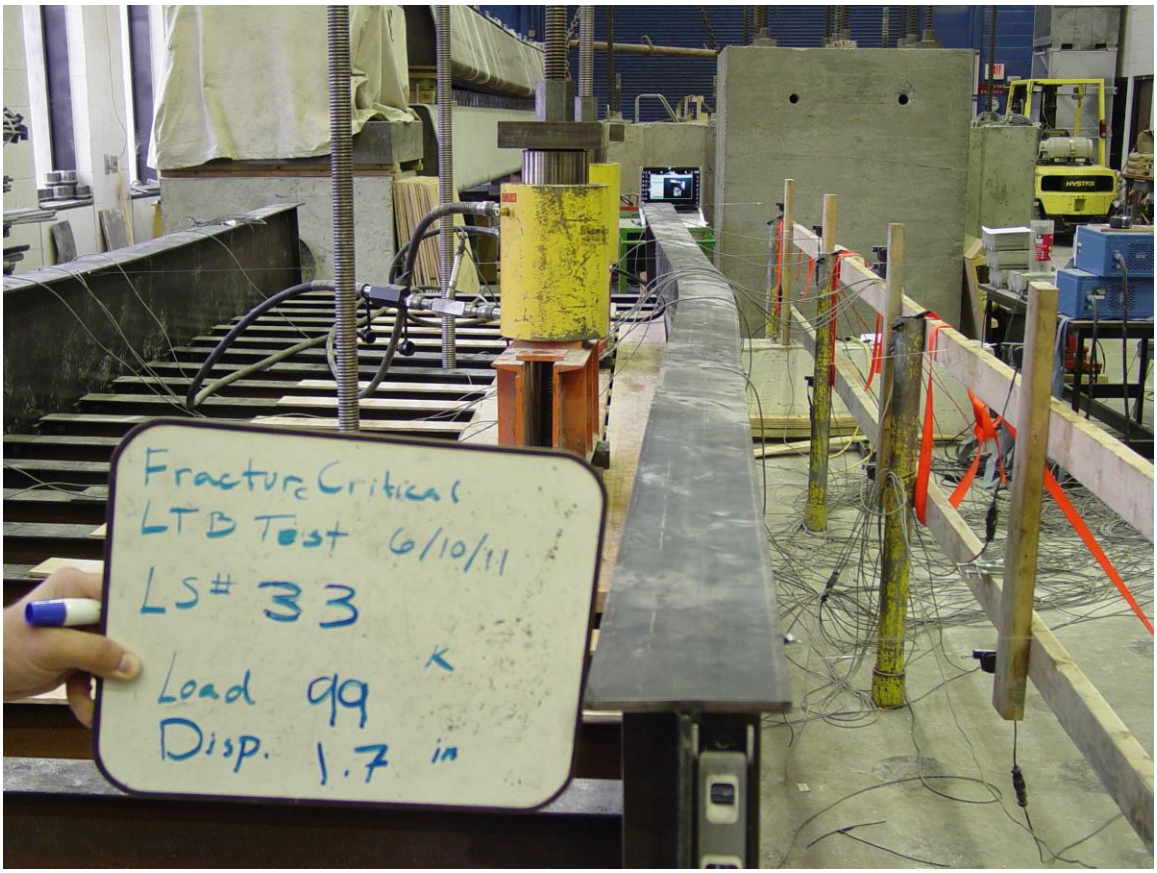


**Figure 4-45. Deformed Bridge Under 99 kips of Load**


**Figure 4-46. Plastic Deformation of Bridge after Load Removal**

Figure 4-47 illustrates the applied load versus the vertical deflection of the girder closer to the loading (Girder A) at mid-span. It is observed that a maximum load of 106 kips was carried by the bridge with a maximum vertical displacement of 1.7 inches. It is also observed that the girder experienced a plastic vertical deformation of about 0.45 inch at the mid-span of the loaded girder.

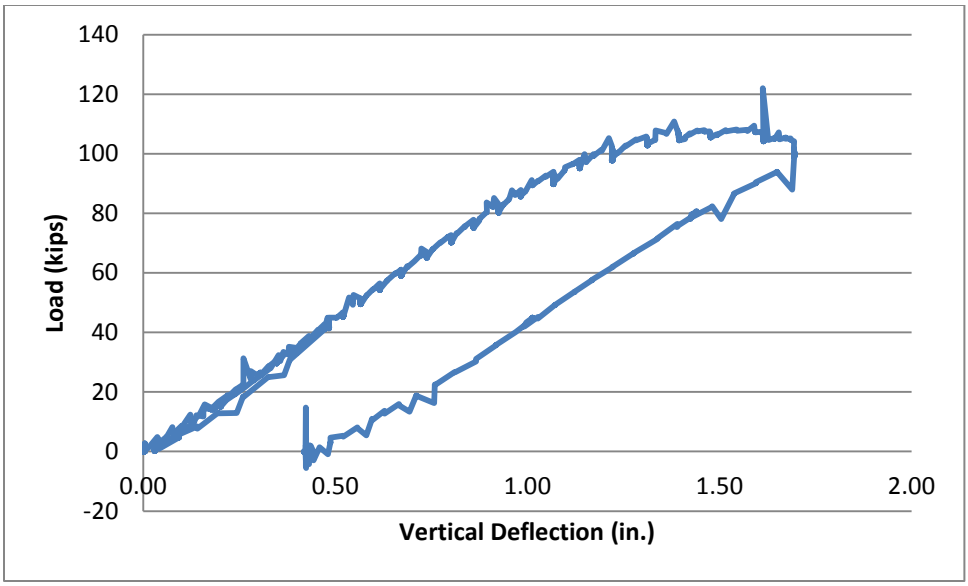


**Figure 4-47. Load vs. Vertical Deflection at Mid-span of Loaded Girder**

Load versus lateral displacement at mid span of the top flange of the girder near the loading is illustrated in Figure 4-48. Until 80 kip of applied load, lateral displacement of the top flange of the loaded girder was minimal. After that 80 kips of applied load, the lateral displacement increased drastically with a small increase in load.

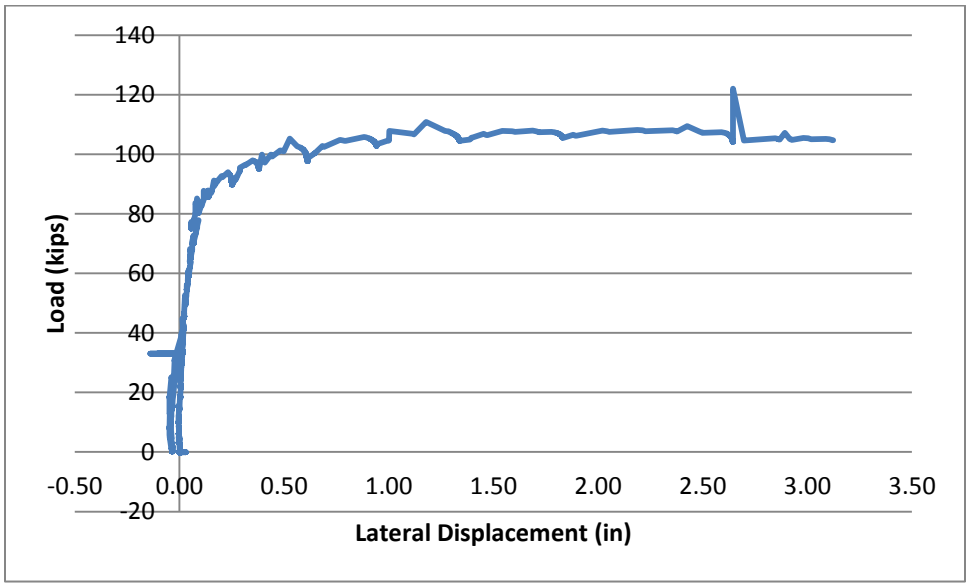


**Figure 4-48. Load vs. Lateral Displacement of Flanges Loaded Girder at Mid-span**

Lateral displacements are plotted versus the load at quarter points and at the ends in Figure 4-49 and Figure 4-50 respectively. As seen in these figures, the change in lateral displacement was minimal up to the point of 100 kip applied load then it increased drastically with a small increase in load. The maximum lateral displacement was observed in the top flange of Girder A (near the loading points). The lateral displacement at a distance of L/4 is slightly larger than that

at the distance of 3L/4. However, similar results were observed in these locations at the bottom flange.

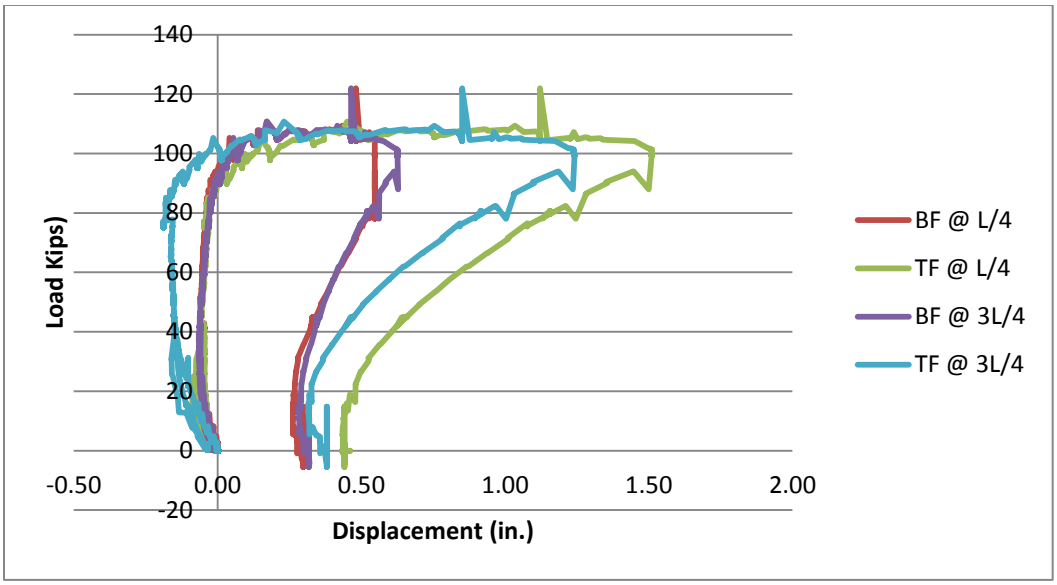


**Figure 4-49. Load vs. Lateral Displacement of Top Flange Loaded Girder at Quarter Length**

In contrast to the quarter points, the lateral displacements at the ends of Girder A were observed increased quickly at small loading level (up to 40 kips); then they increased more slowly as the load increased. However, the overall magnitude at the ends is much less than observed at midspan. The lateral displacement in one end was observed to be larger than that of the other end. Figure 4-51 illustrates rotation of the loaded girder at its ends.

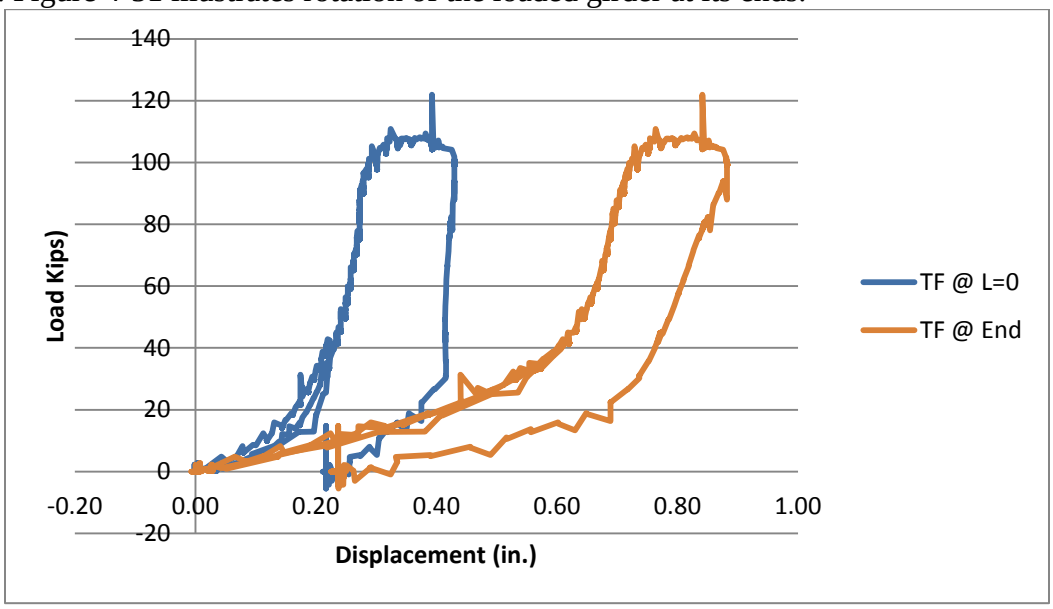


**Figure 4-50. Load vs. Lateral Displacement of Top Flange at Ends Loaded Girder**

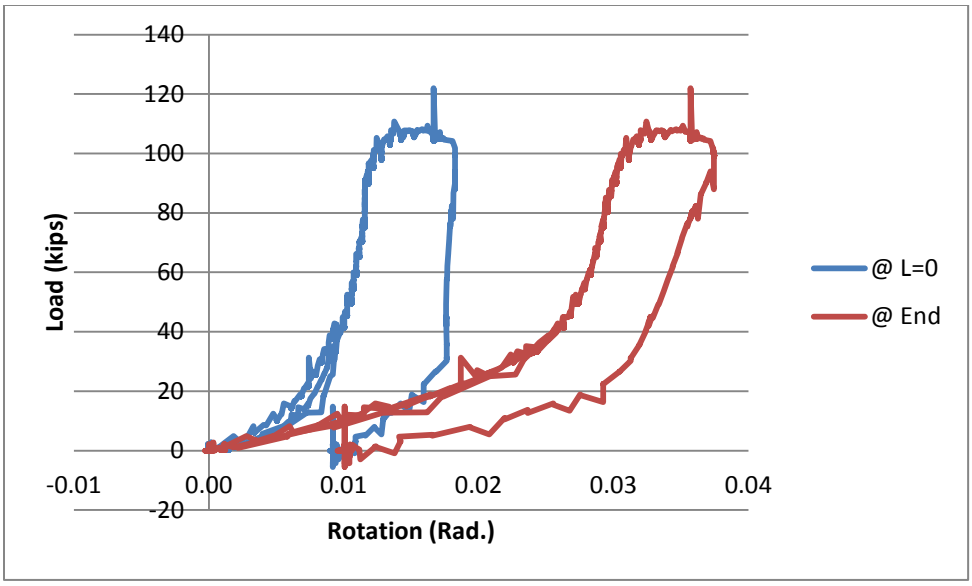


**Figure 4-51. Load vs. Rotation of Ends Loaded Girder**

Loading was halted once the plateau was reached indicating the lateral torsional strength of the system. The next step was to simulate fracture of one girder. Testing associated with this condition is described in the following section.

### 4.2.4 Cracking and Strengthening

In this stage of the experiment, the girder close to the loading point that experienced large plastic deformations due to high levels of loads during the LTB test was replaced with a new girder of the same size. Since the other girder was in the elastic range of the stress-strain curve, it was used again in this stage of the test.

In order to simulate a fractured bridge, the bottom flange of one of the girders was cut at the mid-span section. Then, using two one-inch diameter high strength rods, the girder bottom flange was strengthened over the middle half of its length. The material properties of the rods conformed to ASTM F1554 high strength steel. Figure 4-52 shows the girder in the cracked section and the attached crackmeter for crack opening measurements. Figure 4-53 depicts the strengthening rods under the bottom flange and the designed connection to connect them to the quarter points of the bottom flange length.

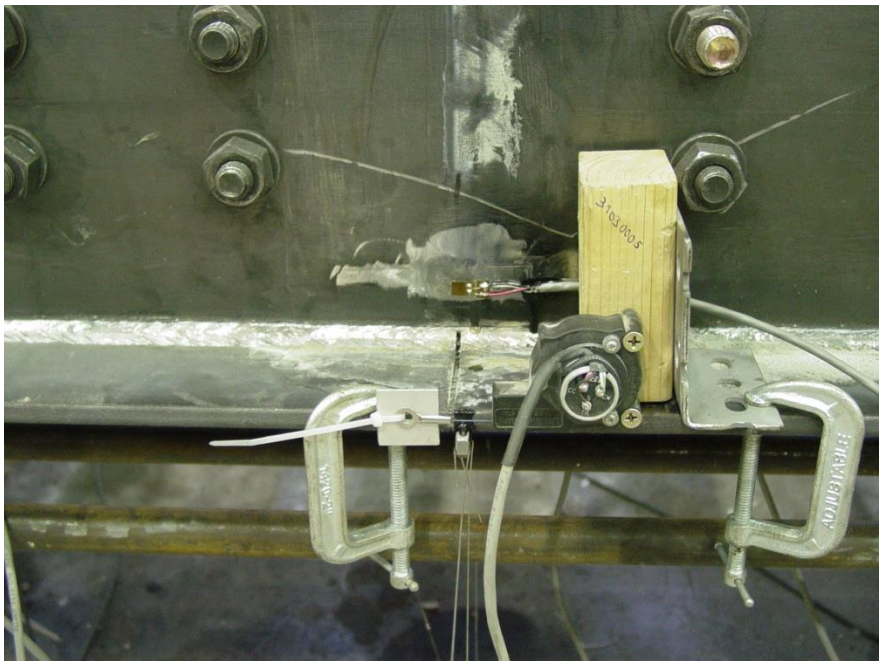

**Figure 4-52. Cracked Bottom Flange and the Crackmeter at the Girder Mid-span**

**Figure 4-53. Strengthening Rods and their Connection to Girder Bottom Flnage**

### 4.2.5 Loading of Cracked Bridge

In this section, the results of the experiment on the strengthened bridge are studied.

#### 4.2.5.1 Test 2-B - Cut Flange - Strengthened

Figure 4-54 shows the vertical deflection of the strengthened girder at mid-span versus the applied load to the bridge. It was observed that the cracked bridge with strengthening rods was able to carry about 108 kips of load before starting a plateau in the load-deflection curve. This load was even more than the load carried by the intact bridge, which can be explained by the larger effective depth of the girder with rods. Figure 4-55 shows the strengthened bridge after loading, which is displaying a lateral torsional buckling failure mode.

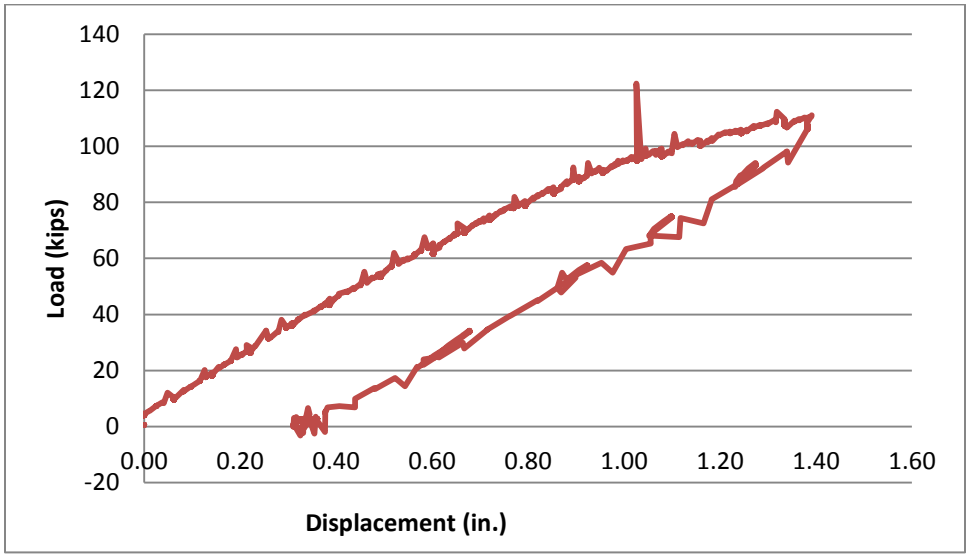


**Figure 4-54. Load vs. Vertical Deflection of Strengthened Girder**


**Figure 4-55. Loaded Strengthened Bridge**

#### *4.2.5.2 Test 2-C – Cut Flange*

In order to observe the behavior of the bridge without the strengthening rods, the rods were removed from the cracked girder and the data were zeroed out. The cracked bridge was loaded again. The results of the experiment showed that the cracked bridge was able to carry the loads up to 100 kips which was close to the capacity of the uncracked bridge indicating that the failure mode is lateral torsional buckling since it is independent of contribution from the bottom flange. The crack propagation into the web of the girder was just about ¼ inch, which is shown in Figure 4-56. Vertical deflection of the cracked girder is shown versus the applied load in Figure 4-57. It was also observed that the permanent vertical deflection of the cracked girder was about 0.5 inch which was close to the plastic deformation of the uncracked girder as seen in Figure 4-47.

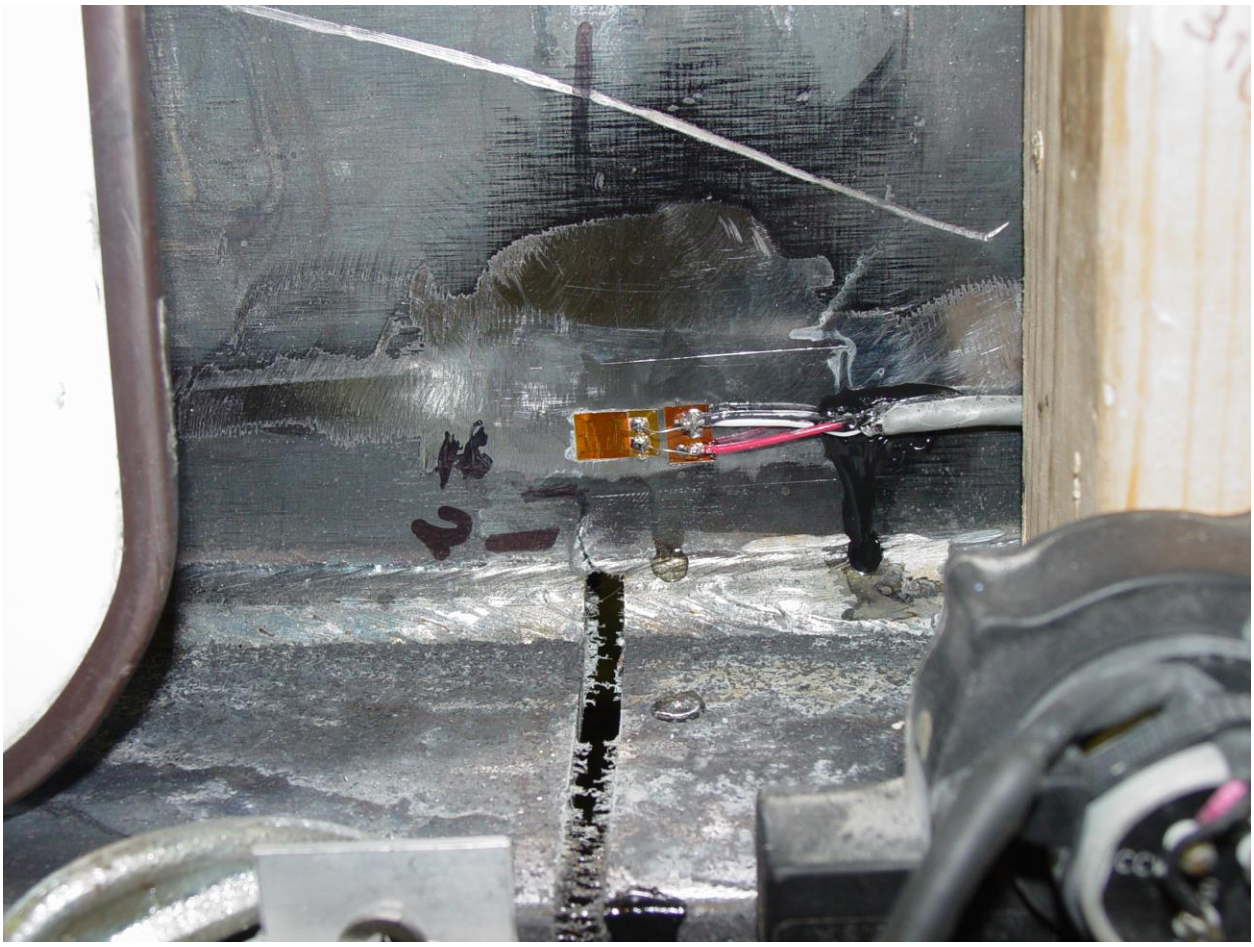

**Figure 4-56. ¼ inch Crack Propagation into the Girder Web**

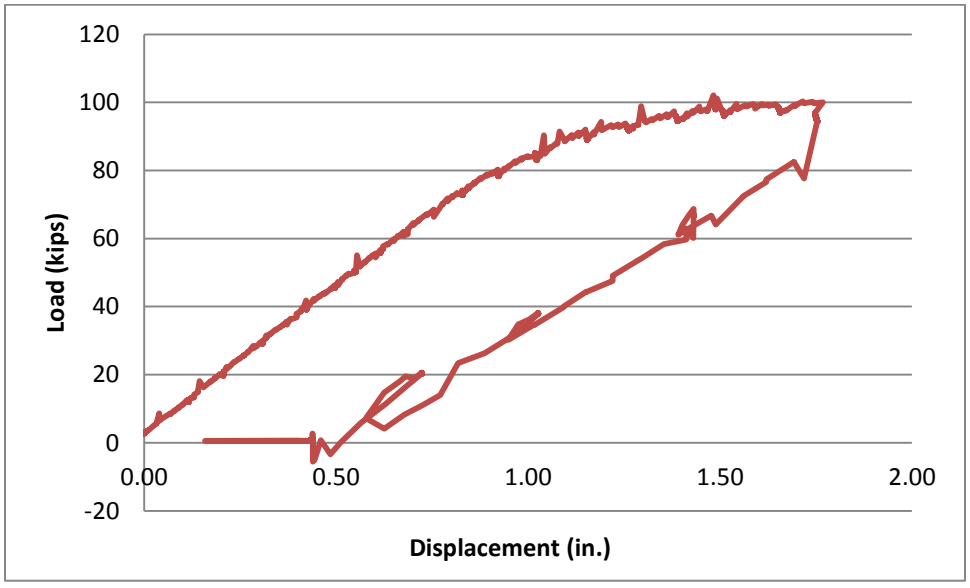


**Figure 4-57. Load vs. Vertical Deflection of Cracked Girder**

#### 4.2.5.3 Test 2-D – Web Cut 2.5 Inches

To continue observations of the cracked bridge behavior, the web of the pre-cracked girder was cut to a length of approximately 2.5 inches and the bridge was loaded again. Figure 4-58 illustrates the girder with the bottom flange and web cracked with the specified length. Figure 4-59 shows the load-deflection plot of the girder in this case. It was again noticed that the bridge showed almost elastic responses up to a load of approximately 80 kips. There was no noticeable crack propagation in the girder web in this case either.

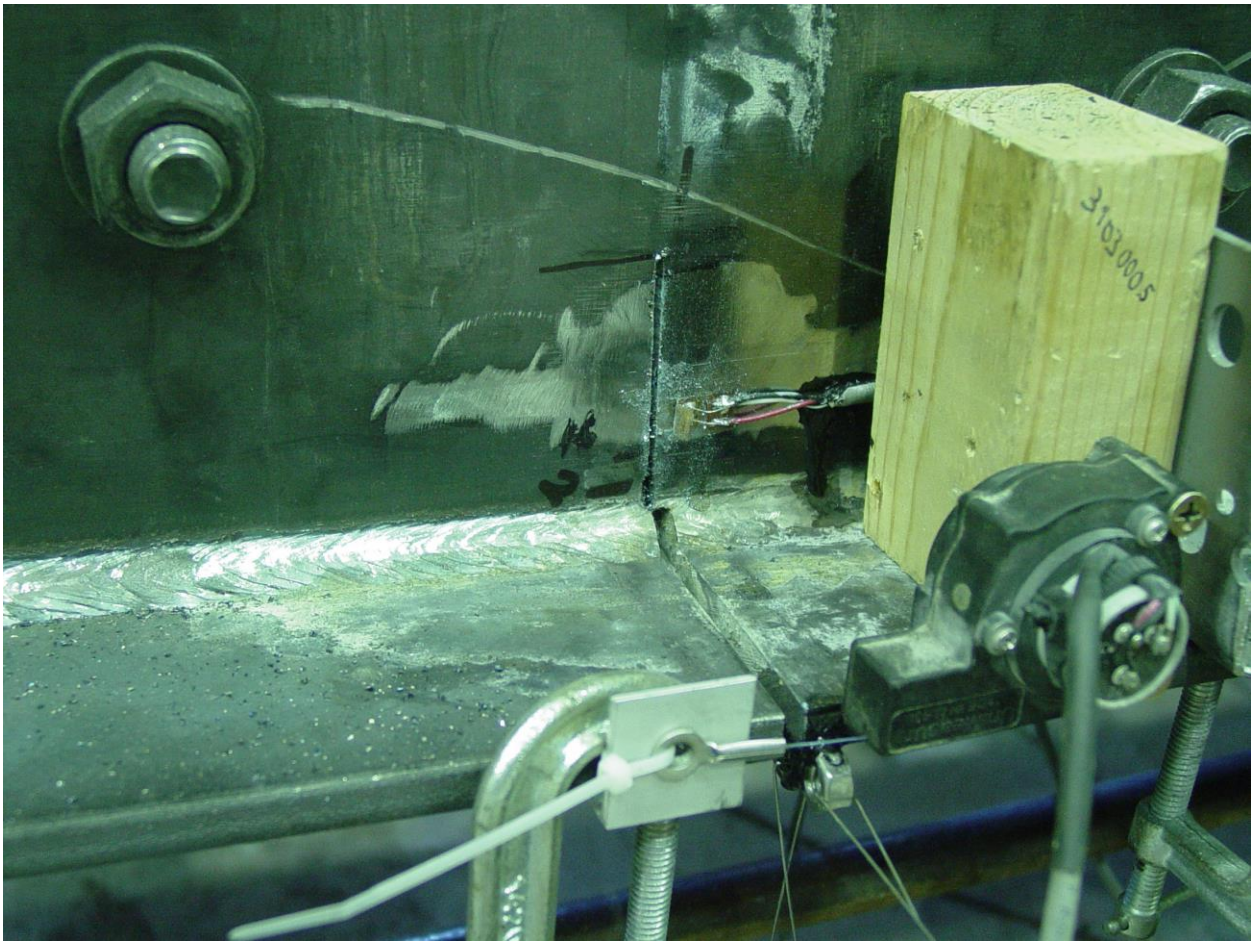

**Figure 4-58. Girder Web Cracked with the Length of 2.5 inches**

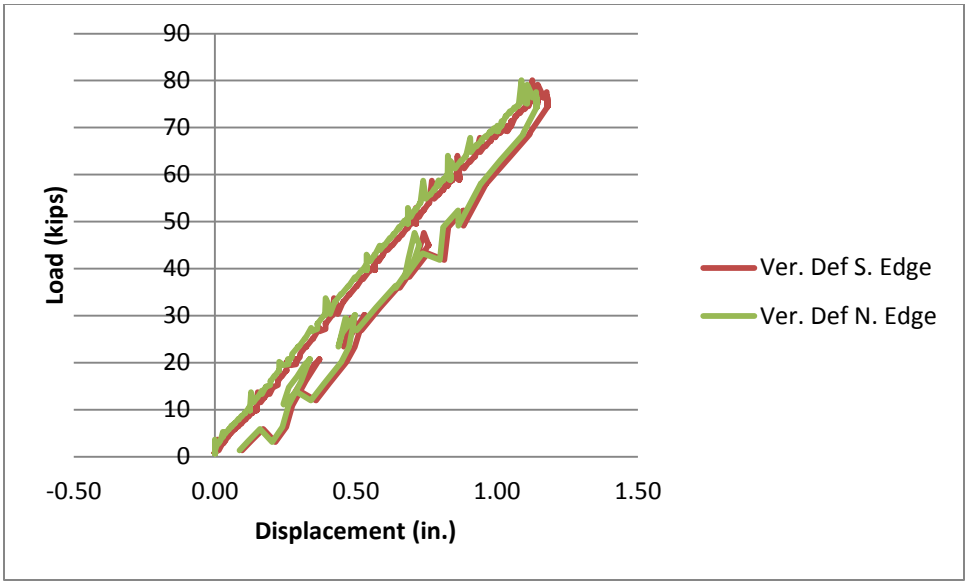


**Figure 4-59. Load vs. Vertical Deflection of 2.5" Web Cracked Girder**

#### *4.2.5.4 Test 2-E – Web Cut 10 Inches*

The crack was then extended manually in the web of the girder up to a length of approximately 10.5 inches and the bridge was loaded again. Figure 4-60 shows the crack made in the web of the girder. In this case, the load carrying capacity of the bridge dropped to a maximum of 48 kips. At this point, the crack started to propagate accompanied by load decrease. Figure 4-61 depicts the load-deflection curve of the bridge with the 10.5 inch crack. It is observed that the bridge deflected up to about 6 inches when the crack propagated and the load capacity dropped down to 33 kips. Figure 4-62 shows the picture of the propagated crack.

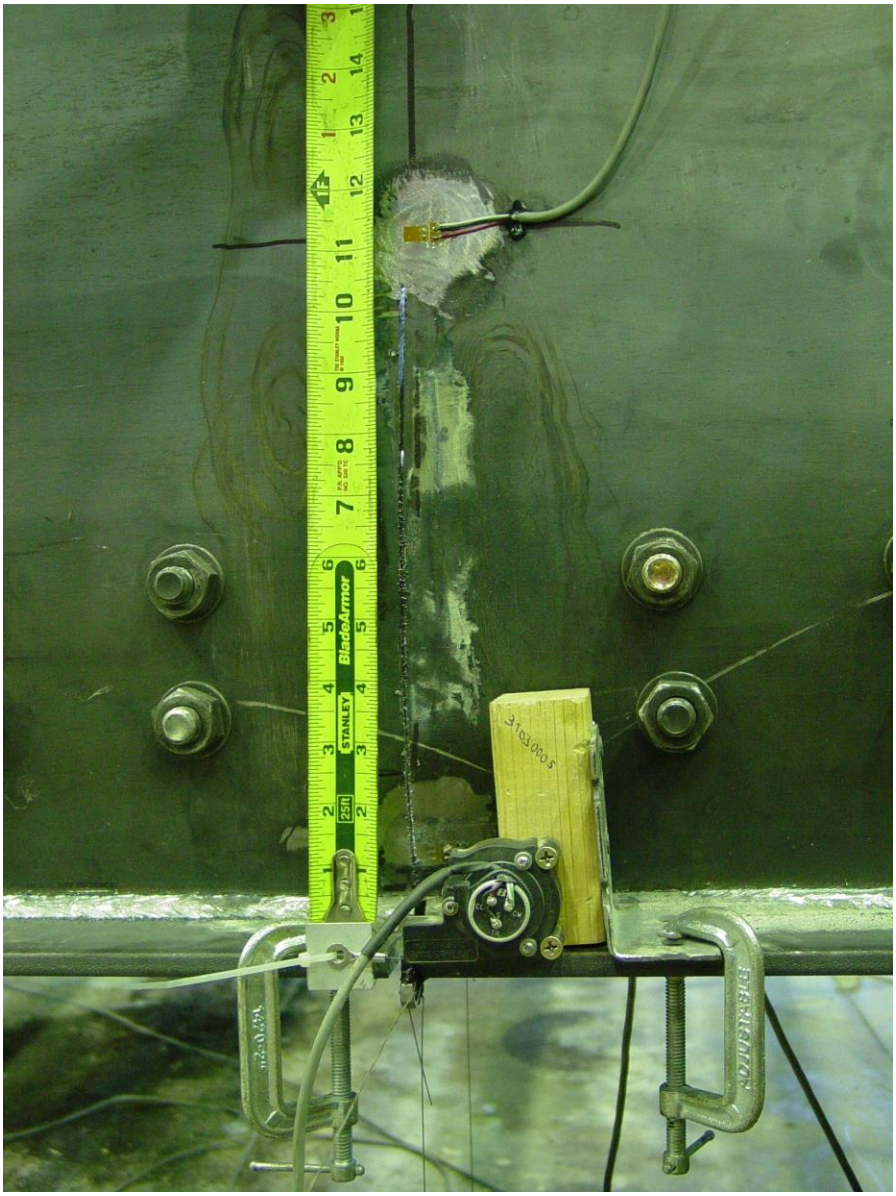


**Figure 4-60. Girder Web Cracked with the Length of 10.5 inches**

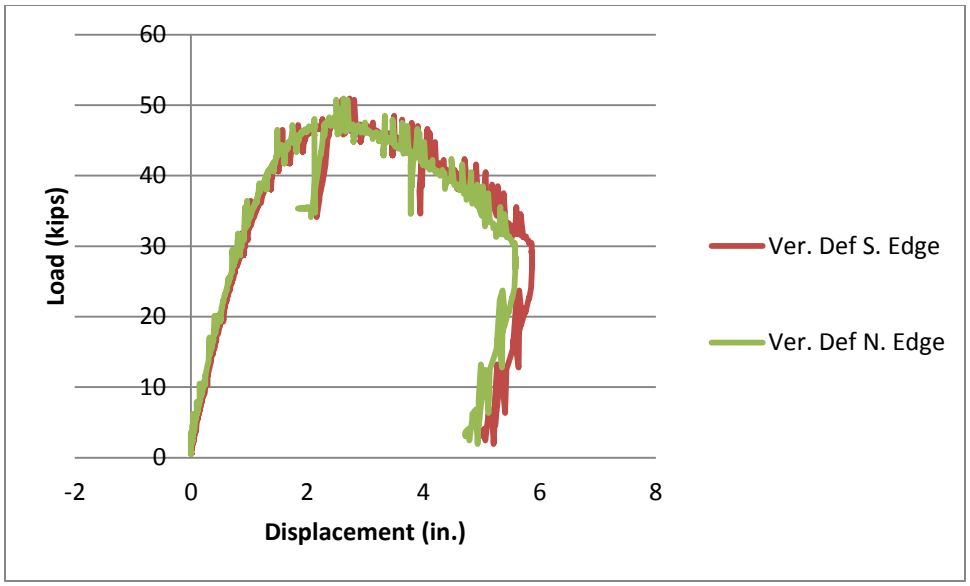


**Figure 4-61. Load vs. Vertical Deflection of 10.5" Web Cracked Girder**

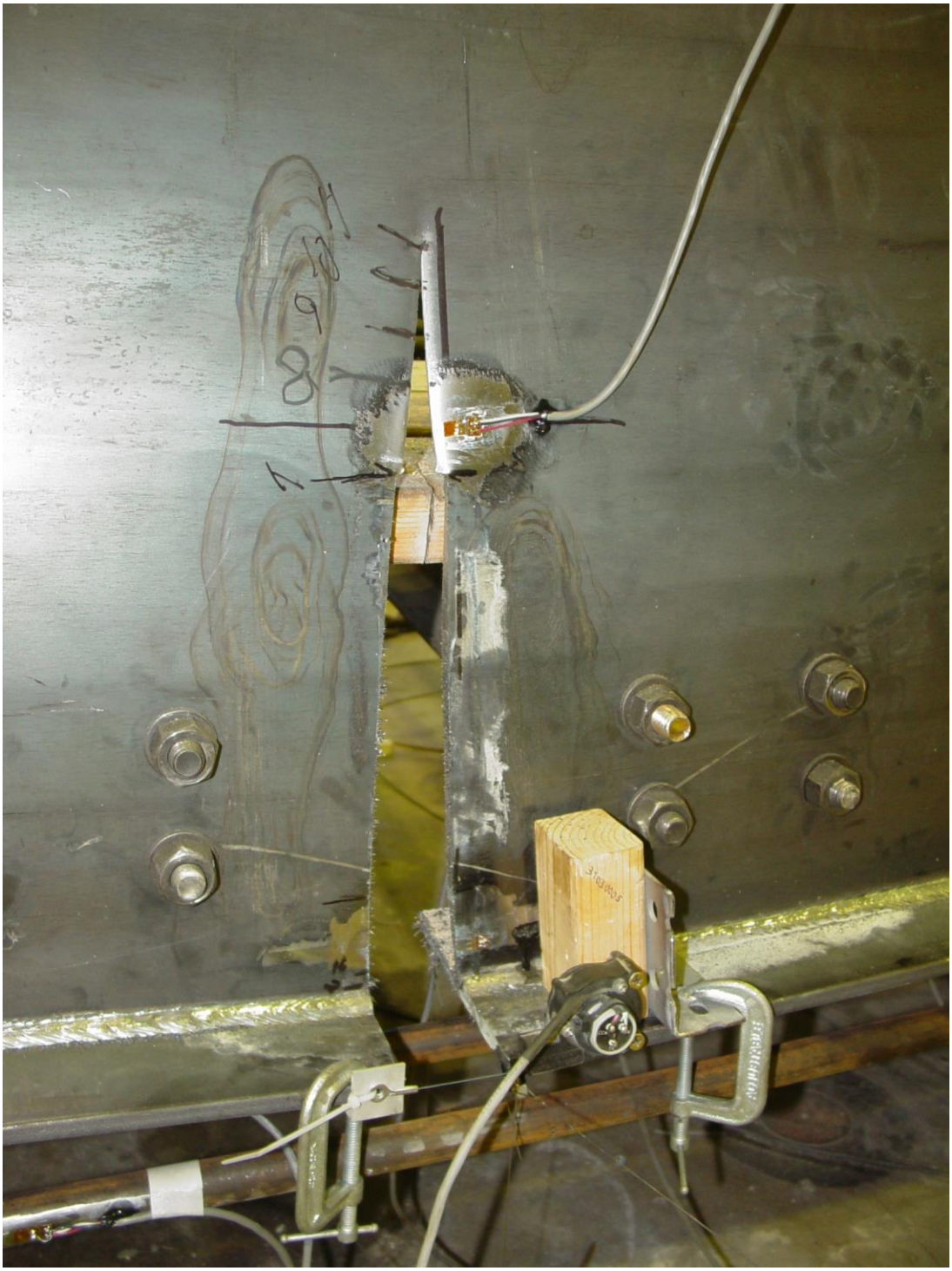

**Figure 4-62. Configuration of Propagated Crack**

### 4.2.6 Summary of Experiment 2

In the second experiment, a bridge with a built-up girder was chosen. The reason for not using hot rolled girders was to be able to perform the experiment on the maximum ratio that can be

found in practice for the height of the girder to height of the floor beams. In this experiment, the ratio was approximately 4.0. There were a total of five tests performed in Experiment 2.

In the first test, the uncracked bridge system carried a maximum load of 106 kips with a maximum vertical displacement of 1.7 inches. After unloading, the girder closer to the loading points (Girder A) experienced a permanent vertical deformation of approximately 0.45 inch at mid-span.

In the second test, the built-up girder system was cracked at the bottom flange of the girder near the loading points and then strengthened using two high-strength rods parallel to the bottom flange. This specimen was able to carry approximately 108 kips of load with 1.4 inch of displacement before starting a plateau in the load-deflection curve. This load was a little more than the load carried by the intact bridge, 106 kips. The permanent vertical displacement observed in this second test was approximately 0.32 inch, which occurred in the loaded girder.

In the third test, the strengthening rods were removed and the specimen with the cracked bottom flange was loaded again. The maximum load-carrying capacity of this specimen was observed to be approximately 100 kips.

In the fourth test, the crack in the bottom flange was extended up the web to a depth of 2.5 inch. The specimen was loaded up to 80 kips then unloaded. The load-displacement curve shows the specimen response was still linearly elastic.

In the last test, the crack was extended further in the web up to 10.5 inches. The load carrying capacity of this specimen dropped down to 48 kips. At this point, the initial crack started propagating further into the web. Due to this crack propagation, the capacity of the bridge decreased. At the time the test was stopped, the bridge specimen had 6 inches displacement under 33 kips of load.

# Chapter 5 Lateral-Torsional Buckling Capacity of Two-Girder Bridges

## 5.1 Yura Formulation

Taylor and Ojalvo (1996) developed Equation **5–1** for the critical moment of a doubly symmetric beam under uniform moment with continuous torsional bracing.

$$M_{cr} = \sqrt{M_o^2 + EI_y\overline{\beta_b}} \qquad \textbf{5–1}$$

Where $M_o$ = Buckling capacity of the unbraced beam (kip-in) whose equation was developed by Timoshenko and Gere (1961) as expressed below.

$$M_o = \frac{\pi}{L}\sqrt{EI_yGJ + E^2I_yC_w\frac{\pi^2}{L^2}}$$

$\overline{\beta_b}$ = Attached torsional brace stiffness (in-k/rad per in).

Equation **5–1** assumes no cross section distortion occurs in the beam. Later, this equation was expanded to account for the effect of cross section distortion, stiffeners, and other factors by introducing the concept of an equivalent continuous bracing stiffness, $\overline{\beta_T}$. For the case of discrete bracing, the equivalent continuous brace stiffness can be approximated by summing the total stiffness of individual braces along the length of the beam and dividing by the length ($\overline{\beta_T} = \frac{n\beta_T}{L}$) (Yura, 2001).

The total brace stiffness comes from a combination of factors and can be calculated by using the expression for springs in series (Yura, 2001) as follows:

$$\frac{1}{\beta_T} = \frac{1}{\beta_b} + \frac{1}{\beta_{sec}} + \frac{1}{\beta_g} \qquad \textbf{5–2}$$

Where $\beta_b$ = Stiffness of the attached brace
$\beta_{sec}$ = Cross section web stiffness
$\beta_g$ = Girder system in-plane stiffness

Descriptions of each term in Equation **5–2** are explained as follows:

$\beta_b$, the stiffness values of the various types of cross-frames are summarized in Yura (2001). The location on the girders at which the bracing system connects has significant effect on the stiffness of the brace, $\beta_b$ Figure 5-1 illustrates two types of bracing system and their equivalent stiffness ($\beta_b$).

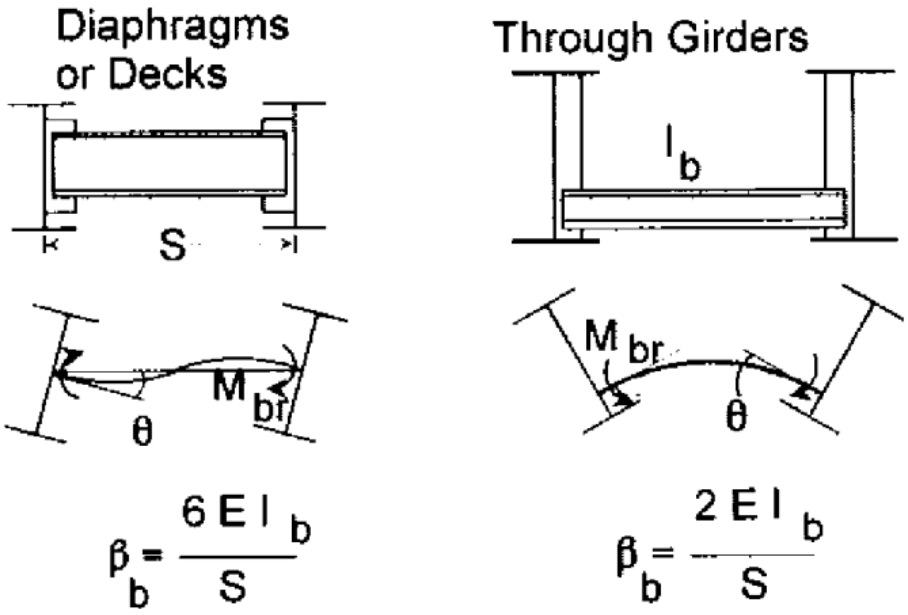


**Figure 5-1 Torsional bracing stiffness.**

The geometry of the brace connection is shown in Figure 5-2.

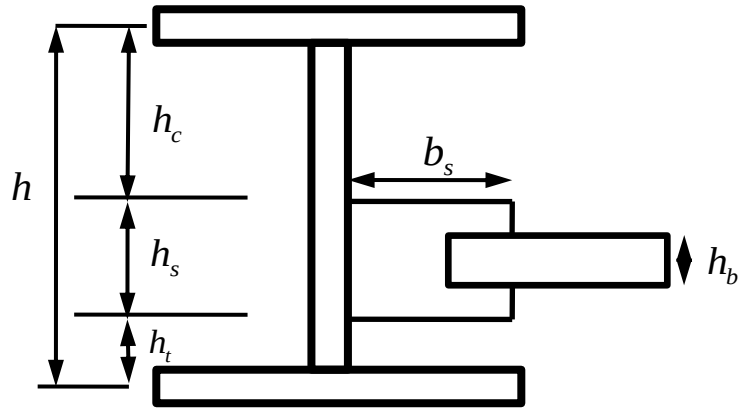


**Figure 5-2. Partially stiffened webs**

Where h = Depth of web of beam
$h_i$ = Depth of considered portion
N = Width of brace connection
$t_w$ = Thickness of web
$t_s$ = Thickness of stiffener
$b_s$ = Width of stiffener

For a single brace at mid-span in a twin girder system, the contribution of the in-plane girder flexibility to the brace system stiffness is expressed in Equation **5–3** . As the number of girders increases, the effect of girder stiffness will be less significant.

$$\beta_g = \frac{12S^2EI_x}{L^3} \qquad \textbf{5–3}$$

Where S = Girder Spacing
$I_x$ = Major axis moment of inertia of single girder
L = Girder Length

Cross section distortion is accounted for by considering the flexibility of the web. Equation **5–4** can be applied for both full depth and partial depth stiffeners. In case of full-depth stiffening, the term $h_i$ , will be taken equal to h.

$$\beta_i = \frac{3.3E}{h_i}\left(\frac{h}{h_i}\right)^2 ((N + 1.5h_i)\frac{t_w^3}{12} + \frac{t_s b_s^3}{12}) \qquad \textbf{5–4}$$

For the partial depth stiffening, the stiffness of various sections of the web can be evaluated separately using Equation **5–4** with $h_i = h_c, h_s,$ or $h_t$ and then combined as follows:

$$\frac{1}{\beta_{sec}} = \frac{1}{\beta_c} + \frac{1}{\beta_s} + \frac{1}{\beta_t} \qquad \textbf{5–5}$$

In addition to all of the above modifications, Yura (2001) also adjusted Equation **5–1** to account for effect of loading location and moment gradient factors as expressed below:

$$M_{cr} = \sqrt{C_{bu}^2 M_o^2 + \frac{C_{bb}^2 EI_y \overline{\beta_T}}{C_T}} \leq M_y \text{ or } M_{bp} \qquad \textbf{5–6}$$

Where $M_o$ = Buckling capacity of unbraced beam with uniform moment loading
$C_{bu}$ = Moment gradient factor for beam with no intermediate bracing
$C_{bb}$ = Moment gradient factor for beam with full bracing
$\overline{\beta_T}$ = Equivalent continuous torsional bracing system stiffness
$I_y$ = Minor axis moment of inertia of single girder
$C_T$ = 1.2 for top flange loading and 1.0 for centroid loading
$M_y$ = Yield moment of beam
$M_{bp}$ = Moment corresponding to buckling between brace points

## 5.2 Comparison of Yura Equation and FE Results

In order to evaluate the results of the formulation presented by Yura, the capacity of a sample bridge is evaluated using Yura's equations and also evaluated by means of finite element analysis. The geometry of the sample bridge and also the results are discussed in the following subsections.

### 5.2.1 Sample Bridge

For the two-girder bridge shown in Figure 5-3 with the following geometry and material properties, the moment capacity is calculated using both nonlinear finite element analysis and Yura formulation.

Girders: W16x40
Height of the connection of the floor beams to girders = 4.5” or 12”
Floor beam spacing: $S_{FB}$ = variable
Span length: $L$ = 252 in
Yield stress: $F_y$ = 53 ksi
Modulus of elasticity: $E$ = 29000 ksi
Poisson Ratio n = 0.3

**Figure 5-3. General Configuration of the Sample Bridge**

The results of Abaqus finite element analysis and the capacities calculated using Yura equation are presented in Figure 5-4 and Figure 5-5.

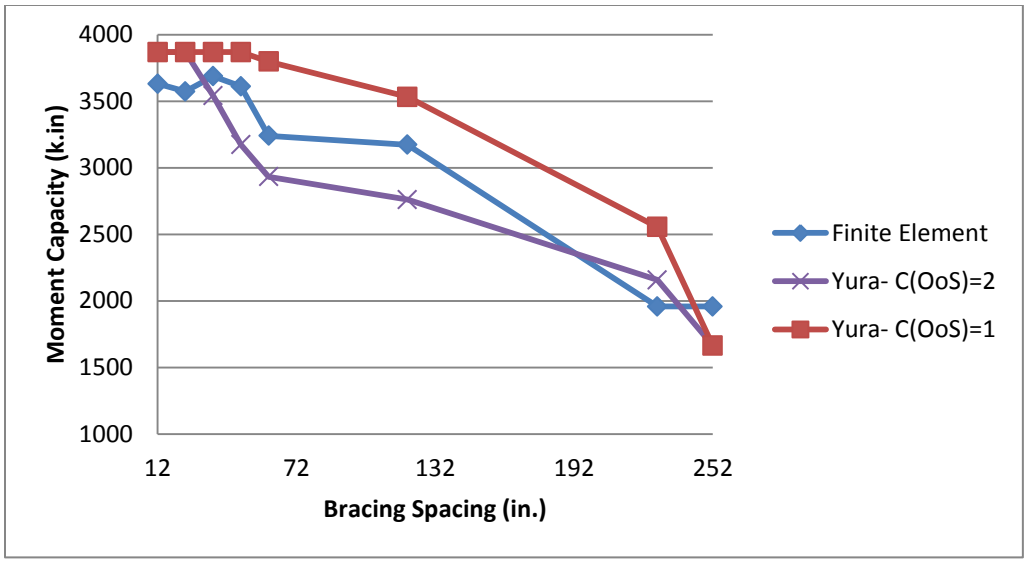


**Figure 5-4. Yura Equation vs. Finite Element Analysis- Connection Height= 4.5 in.**

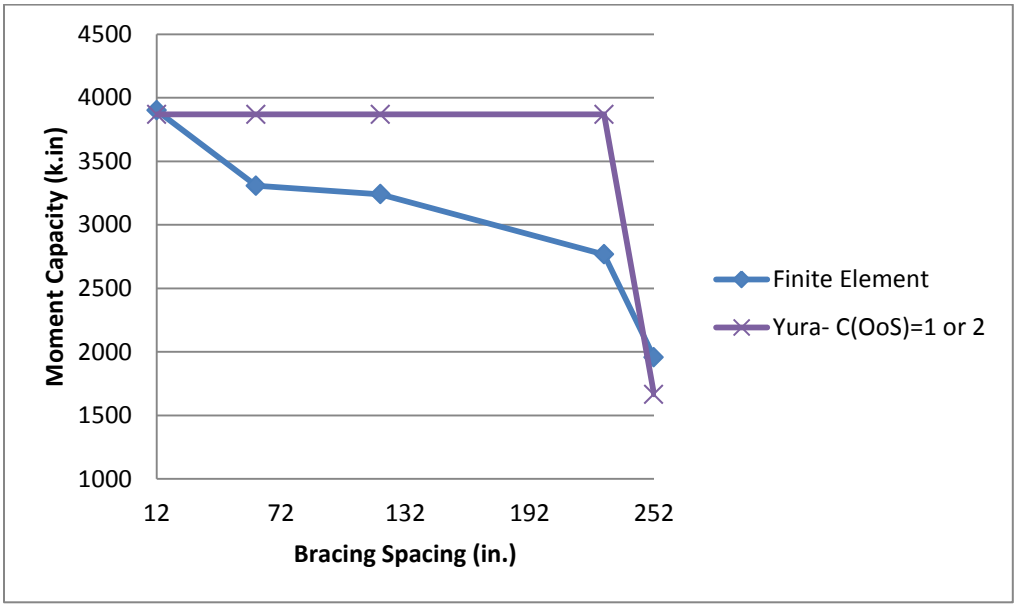


**Figure 5-5. Yura Equation vs. Finite Element Analysis- Connection Height= 12 in.**

For floor beam-to-girder connection height is equal to 4.5 inches, the Yura equation is evaluated for two different out-of-straightness factors, C(OoS), equal to 1 and 2. It is observed that for C(OoS) equal to 1, the formulation gives larger moments capacities than those of finite element analysis and for C(OoS) equal to 2, the formulation gives smaller moments capacities than those of finite element results.

For floor beam-to-girder connection height equal to 12 inches, the Yura equation yields larger moment capacities than finite element results. The equations result in moment capacities equal to the plastic moment for all floor beam spacings other than the case where the floor beams are placed only at the two ends of the main girders. For the floor beam spacing equal to 228 inches,

it is observed that finite element analysis results in a moment capacity of 2768 k.in while Yura formulation gives a capacity of 3869 k.in, which is 1.40 times larger than the finite element results.

Therefore, it is concluded that the Yura formulation can have a noticeable error in estimating the moment capacity of two girder bridges and there is a need for a more precise method of capacity evaluation for such bridges.

## 5.3 Capacity Based on AASHTO LRFD

The other source for evaluating the moment capacity of two girder bridges is the AASHTO LRFD Specifications, which requires fulfillment of Equation 5–7 for calculating the moment capacity.

$$f_{bu} + \frac{1}{3} f_l \leq \varphi_f F_{nc} \qquad \textbf{5–7}$$

Where:

$f_{bu}$ = Compression flange stress

$f_l$ = Flange lateral bending stress

$F_{nc}$ = Nominal flexural resistance of the flange

The specifications present the following equation for the nominal flexural resistance of the flange.

$$F_{nc} = F_{cr} = \frac{C_b R_b \pi^2 E}{\left(\frac{L_b}{r_t}\right)^2} \leq R_b R_h F_{yc} \qquad \text{For } L_b > L_r \qquad \textbf{5–8}$$

Where:

$C_b = 1.0$ = Moment gradient modifier

$R_h = 1.0$ = Hybrid factor

$F_{yc} = 50\ ksi$ = Compression flange yield stress

$L_b = 252\ in$ = Unbraced length

$r_t$ = Effective radius of gyration for lateral torsional buckling (in.)

$L_r$ = Limiting unbraced length to achieve the onset of nominal yielding

$R_b = 1.0$ = Web load shedding factor for rolled sections

The specifications give the following equation for the effective radius of gyration for lateral torsional buckling.

$$r_t = 1.0 \frac{b_{fc}}{\sqrt{12(1 + \frac{D_c t_w}{3 b_{fc} t_{fc}})}} \qquad \textbf{5–9}$$

Plugging the parameters for a W16x40 section, the effective radius of gyration is found to be 1.833 inches. Then, the value of $L_r$ can be calculated as follows:

$$L_r = \pi\, r_t \sqrt{\frac{E}{F_{yc}}} = 138.67\ in \qquad \textbf{5–10}$$

As the unbraced length of 252 in. is larger than $L_r$, the nominal flexural resistance of the flange will be equal to 15.14 ksi. Multiplying this flexural stress by the section modulus of the W16x40 section (S=64.7 $in^3$), results in a moment capacity equal to 979.7 k.in. Regarding the fact that in the laboratory experiment, the girders of the test bridge with such a configuration did not buckle under a load of 90 kips, which is corresponding to a moment of $90 * 0.7 * 0.5 * 90in. = 2835\ k.in$, it can be concluded that the AASHTO LRFD equations are very conservative for calculating the flexural capacity of two-girder bridges with closely spaced floor beams. Therefore, again it is concluded that a more accurate equation is needed to estimate the flexural capacity of two-girder bridges.

## 5.4 Recommending a New Equation for LTB Capacity

The flexural capacity of the main girders of a two-girder bridge is a function of the bridge geometry and material properties. The most important geometrical parameters in this problem are bridge span length, the height of the connection between the floor beams and the girders, floor beams spacing and girder cross sectional dimensions such as the depth of the girder.

The bending capacity of one of the main girders of such a structure is less than or equal to its plastic moment capacity. On the other hand, its bending capacity is greater than or equal to the capacity of an isolated girder under uniform moment. The later one has a closed form solution in the literature which can be found in reference (Timoshenko and Gere) as follows:

$$M_o = \frac{\pi}{L} \sqrt{E I_y G J + E^2 I_y C_w \frac{\pi^2}{L^2}} \qquad \textbf{5–11}$$

$M_o$is the critical moment of a girder with a uniform moment over its length (as derived by Timoshenko and Gere). For a two girder bridge, the maximum capacity is achieved if the girders are supported continuously by floor beams over their length. This maximum capacity is equal to plastic moment capacity $M_P$.

Based on the results of the conducted finite element analysis, it is observed that the LTB capacity of two-girder bridges can be calculated using the following equation:

$$M_{cr} = [C_{bb}M_P - \frac{(C_{bb}M_P - C_{bu}M_o)}{L} S_{FB}] * f_h \leq M_P \qquad \textbf{5–12}$$

which describes the moment capacity as a linear function of the floor beam spacing. The moment capacity is changing between the maximum moment capacity of $M_P$ and the minimum buckling moment capacity of $C_{bu}M_o$. The maximum capacity is corresponding to a theoretical floor beam spacing equal to zero for which the parameters $C_{bb}$ and $f_h$ are equal to unity. The minimum capacity of $C_{bu}M_o$ corresponds to the capacity of girders that are not supported by floor beams within their length for which the unsupported length of the girder is assumed to be equal to its length. In this case, the value of the parameter $C_{bu}$ is a function of the loading configuration.

The parameter $f_h$is the height factor as described below:

$$f_h = \left(\frac{1}{2} - \frac{R}{2}\right)\left(\frac{S_{FB}}{L}\right) + (2R - 2)\left(\frac{H_C}{H_G}\right)\left(\frac{S_{FB}}{L}\right) + 1 \qquad \textbf{5–13}$$

in which

$$R = \frac{\alpha C_{bb}M_P + (1 - \alpha)C_{bu}M_o}{C_{bu}M_o} \qquad \textbf{5–14}$$

In the above equations $\frac{H_C}{H_G}$ is the ratio of the height of the connection of floor beam to the height of girder. This ratio is found to be between 0.25 and 0.75 in the bridges in inventory. The recommended function for $f_h$ returns a value of one for minimum $\frac{H_C}{H_G}$ values equal to 0.25, independent of the values of the parameters $S_{FB}$, $L$ and $R$. But, for maximum $\frac{H_C}{H_G}$ values equal to 0.75, it returns a value of one for $S_{FB}$ equal to zero and a value equal to the parameter $R$ for unsupported length equal to the length of the girder, i.e. $S_{FB} = L$.

### 5.4.1 Definition of the parameters

The parameters used in section 5.4 are defined as follows:

$M_{cr}$: Moment capacity of the girder

$C_{bb}$: Moment gradient factor for the segment of braced girder under consideration. It can be calculated based on AASHTO equations for $C_b$. For practical geometries the $C_{bb}$ factor is either 1.0 or very close to 1.0.

$C_{bu}$: Moment gradient factor for the unbraced girder. It can be calculated based on AASHTO equations for $C_b$.

$M_P$: Plastic moment capacity of the girder equal to plastic section modulus times the yield stress $F_y$.

$L$: Total length of the girder.

$M_o$: Critical moment of a girder with a uniform moment over its length without any intermediate support calculated using the following equation:

$$M_o = \frac{\pi}{L}\sqrt{EI_yGJ + E^2I_yC_w\frac{\pi^2}{L^2}}$$

where in the above equation $M_o$ is the buckling moment of the unbraced girder, $L$ is the unbraced length of the compression flange, $E$ is Young's modulus, $I_y$ is the moment of inertia of the girder about the weak axis, $G=E/2(1+n)$ is the shear modulus of elasticity, $J$ is the torsional constant and $C_w = \frac{I_y d^2}{4}$ is warping constant in which $d$ is the distance between the flange centroids.

$S_{FB}$: Distance between the floor beams.

$f_h$: Height factor

$H_C$: Height of the connection of the floor beam to girder.

$H_G$: Height of the girder.

$\alpha$: A constant equal to 0.1

### 5.4.2 Example 1

For the two-girder bridge shown in the following picture

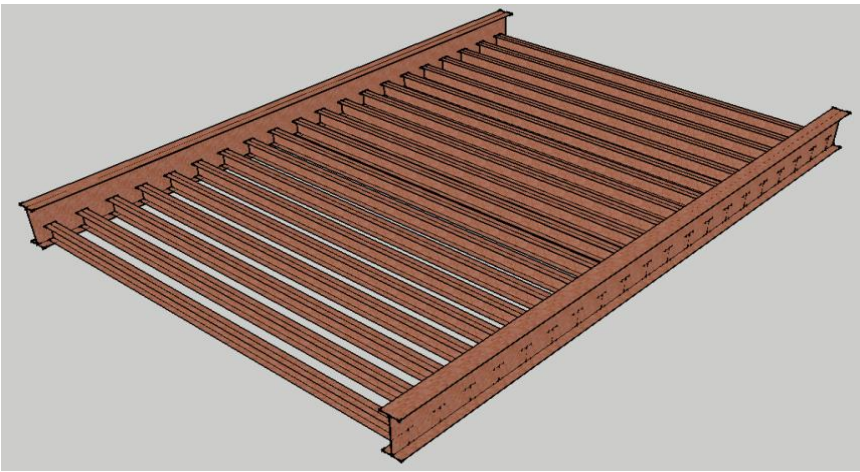

**Figure 5-6. Type 1 Two-Girder Bridge**

The moment capacity of the girder is calculated based on the assumptions stated below:

Girders: W16x40
Height of the connection of the floor beams to girders = 4.5”
$F_y$ = 53 ksi
$S_{FB}$ = 12 in
$L$ = 252 in
$E$ = 29000 ksi
Poisson Ratio = 0.3

**Solution:**

For a W16x40 section, the following constants can be found from engineering tables:
Z= 73 $in^3$ (plastic section modulus of the girder)
Iy = 28.9 $in^4$
J = 0.794 $in^4$
Cw = 1730 $in^6$

Using the above equations, we will have:

Mp = Z . Fy = 3869 k.in
G = 29000 / 2/ (1+0.3) = 11154 ksi

Using the equation for $M_o$, it can be calculated as follows:

$M_o$ = 1472 k.in
$C_{bb}$ = 1.0 (because of approximately uniform moment between the braces)
$C_{bu}$=1.13 (based on AASHTO equation)
$\alpha$ = 0.1

Plugging the above values into the equation for R, this factor is calculated as:

$R$ =1.13

$H_c$ = 4.5 in

$H_g$ = 16 in

$f_h$ = 1.0

So using the equation for $M_{cr}$ the flexural capacity will be:

$M_{cr}$ = 3766 k.in

### 5.4.3 Example 2

For the two-girder bridge shown in the following picture

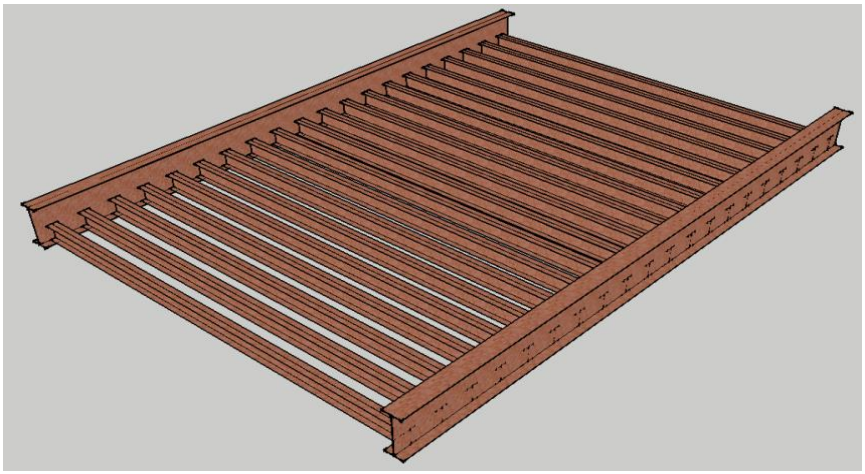

**Figure 5-7. Type 1 Two-Girder Bridge**

The moment capacity of the girder is calculated based on the assumptions stated below:

Girder: W16x40

Height of the connection of the floor beams to girders = 4.5”

Fy = 53 ksi

$S_{FB}$ = 60 in

L = 252 in

E = 29000 ksi

Poisson Ratio = 0.3

**Solution:**

For a W16x40 section, the following constants can be found from engineering tables:

Z= 73 $in^3$ (plastic section modulus of the girder)

Iy = 28.9 $in^4$

J = 0.794 $in^4$

Cw = 1730 $in^6$

Using the above equations, we will have:

Mp = Z . Fy = 3869 k.in
G = 29000 / 2/ (1+0.3) = 11154 ksi

Using the equation for Mo we will have:

Mo = 1472 k.in
Cbb = 1.0 (because of approximately uniform moment between the braces)
Cbu=1.13 (based on AASHTO equation)
$\alpha$ = 0.1

Plugging the above values into the equation for R, this factor is calculated as:

R=1.13
Hc = 4.5 in
Hg = 16 in
Fh = 1.0

So using the equation for Mcr the flexural capacity will be:

Mcr = 3351 k.in

The following two pictures show the result of the above formulation compared to that of Yura equation and also the finite element results. Also shown is the curve for a new recommended equation that is described in the next section.

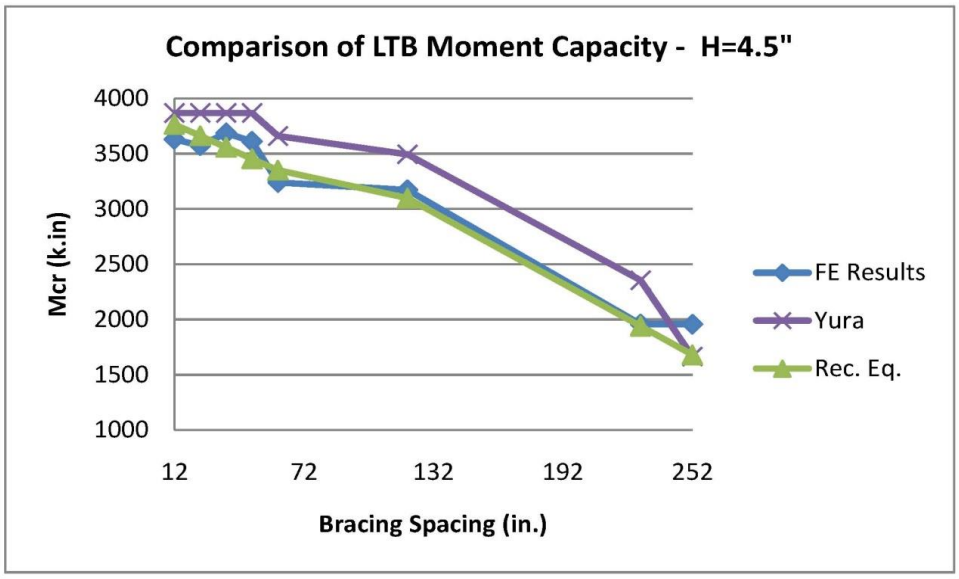


**Figure 5-8. Comparison of FEA Results, Yura Formulation and the Recommended Equation (for Hc=4.5")**

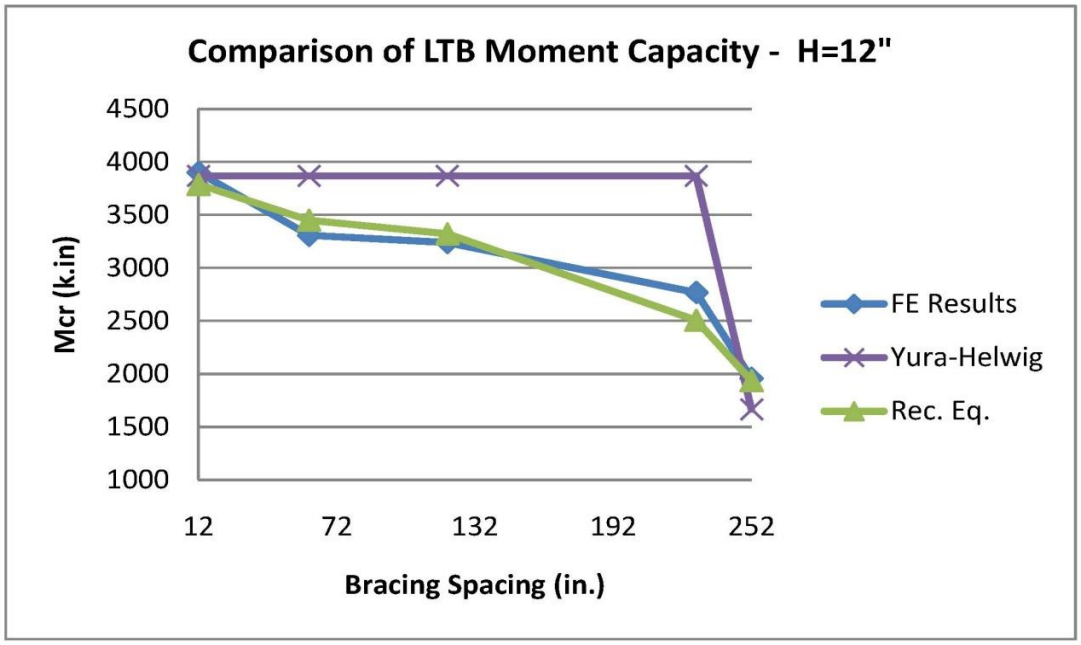


**Figure 5-9. Comparison of FEA Results, Yura Formulation and the Recommended Equation (for Hc=12")**

## 5.5 Summary

The new equation for calculating the LTB capacity of a two-girder bridge is proposed as follows:

$$M_{cr} = [C_{bb}M_P - \frac{(C_{bb}M_P - C_{bu}M_o)}{L} S_{FB}] * f_h \leq M_P$$

This equation presents moment capacity as a linear function of the floor beam spacing. The moment capacity varies between a maximum possible moment capacity of $M_P$ and the minimum buckling moment capacity of $C_{bu}M_o$.

The parameter $f_h$is the height factor as described below:

$$f_h = \left(\frac{1}{2} - \frac{R}{2}\right)\left(\frac{S_{FB}}{L}\right) + (2R - 2)\left(\frac{H_C}{H_G}\right)\left(\frac{S_{FB}}{L}\right) + 1$$

in which

$$R = \frac{\alpha C_{bb}M_P + (1 - \alpha)C_{bu}M_o}{C_{bu}M_o}$$

The comparison between this recommended equation and Yura's equation and ASSHTO equations shows that the recommended equation provides a better estimation of lateral torsional buckling capacity of the two-girder bridge systems as shown in Figure 5-8 and Figure 5-9.

# Chapter 6 Redundancy Analysis of Two I-girder Bridges

In this section, redundancy of the studied two-girder bridges is analyzed based on recommendations of NCHRP Report #406.

## 6.1 Redundancy Analysis # 1

### 6.1.1 Bridge Configuration

The same bridge system that tested in Experiment 1 is employed to carry out the redundancy analysis. . The deck is supported by W6x9 floor beams that are connected to the bridge main girders. The girders have W16x40 hot-rolled steel sections. The span length of the bridge is 21 feet and the distance between the main girders is 73 inches. The length of the floor beams is 72 inches. Four point loads are eccentrically applied to the bridge to provide the maximum effects in one of the girders. Figure 6-1 and Figure 6-2 show the bridge cross section and longitudinal view.

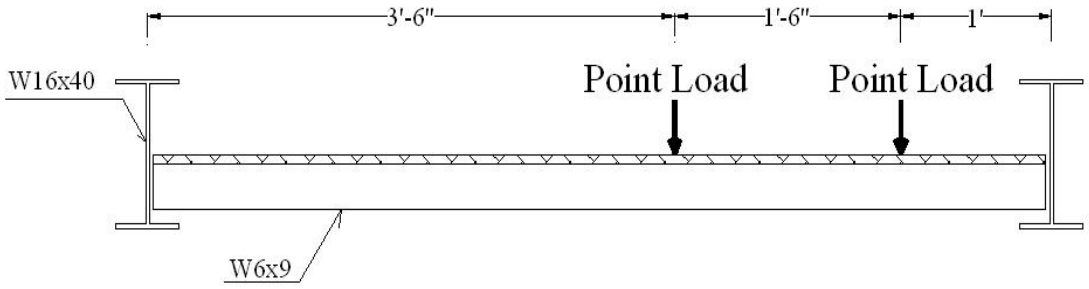


**Figure 6-1. Cross Section of the Test Bridge Specimen**

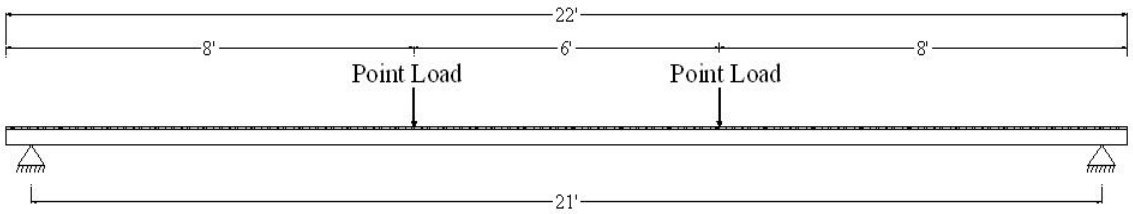


**Figure 6-2. Elevation View of the Test Bridge Specimen**

### 6.1.2 Redundancy Analysis Limit States Definition

In order to perform a redundancy analysis for the bridge, the capacity of the bridge in the following four limit states should be evaluated:

1- **Member Failure**, which is a check of individual member safety using elastic analysis
2- **Ultimate Limit State**, which is defined as the ultimate capacity of the bridge system or the formation of a collapse mechanism
3- **Functionality Limit State**, which is defined as the capacity of the structure to resist a live load displacement in a main longitudinal member equal to the span length/100
4- **Damage Condition Limit State**, which is defined as the ultimate capacity of the bridge system after removal or cracking of one load carrying component from the structure model.

Therefore, the first task is to calculate the load carrying capacity of the bridge girders and so that of the bridge structural system.

$P_{max} = ?$

or

$M_{max} = ?$

So, in the following section the flexural capacity of the bridge girders are evaluated.

### 6.1.3 Bridge Flexural Capacity

The yield stress of steel for W16x40 hot rolled girders based on a set of tension tests is determined which is equal to 51 ksi.

$F_y = 51ksi$

The section properties of W16x40 I-girders are as follows:

$I = 518\ in^4$
$Z_x = 78\ in^3$
$S_{xc} = \frac{I}{c_c} = \frac{518}{8} = 64.75\ in^3$
$J = 0.794\ in^4$

First, the moment capacity of one of the girders of the bridge based on the provisions of AASHTO LRFD Chapter 6 is calculated.

The section proportions are check as follows:

$\frac{b_f}{2t_f} = \frac{7}{2\times0.505} = 6.93 < 12$ OK

$\frac{D}{b_f} = \frac{16}{7} = 2.28 < 6$ OK

$\frac{t_f}{t_w} = \frac{0.505}{0.305} = 1.66 > 1.1$ OK

$0.1 < \frac{I_{yc}}{I_{yt}} = 1.0 < 10$ OK

$\frac{D}{t_w} = \frac{16}{0.305} = 52.5 < 150$ OK

Therefore, the section passes all proportionality checks.

Based on the AASHTO LRFD Specifications, the factored stress in the girders, $f_{bu}$ , should be less than the reduced resistance, $\phi_f F_{nc}$:

$$f_{bu} < \phi_f F_{nc} \qquad \phi_f = 1.0 \qquad F_y = 51ksi$$

in which the resistance of the girder is the minimum of local buckling (LB) and lateral torsional buckling (LTB) resistances:

$$F_{nc} = \min\left(F_{nc,LB}, F_{nc,LTB}\right)$$

Now, the strength of the girder for local buckling and lateral torsional buckling is evaluated.

The local buckling resistance of the compression flange shall be taken as $F_{nc,LB} = R_b R_h F_{yc}$ provided that $\lambda_f < \lambda_{pf}$.

$$\lambda_f = \frac{b_f}{2t_f} = 6.93$$

$$\lambda_{pf} = 0.38\sqrt{\frac{E}{F_y}} = 0.38\sqrt{\frac{29000}{51}} = 9.06$$

Therefore $\lambda_f < \lambda_{pf}$ and

$$F_{nc,LB} = R_b R_h F_{yc}$$

As the web and flanges of the girder are of the same material (it is not hybrid), the hybrid section factor is equal to one:

$R_h = 1.0$

Web load-shedding factor: $R_b$ =?

$$\frac{2D_c}{t_w} = \frac{2\left(\frac{16-2\times0.505}{2}\right)}{0.305} = 49.1 \; < \; \lambda_{rw} = 5.7\sqrt{\frac{E}{F_{yc}}} = 5.7\sqrt{\frac{29000}{51}} = 135.9$$

where $D_c$ is the depth of the web in compression.

Hence

$$R_b = 1.0$$

Therefore

$$F_{nc,LB} = 1.0 \times 1.0 \times 51 = 51ksi$$

Now, the lateral torsional bucking (LTB) capacity of the girders should be calculated. First, the LTB capacity is calculated based on Chapter 6 of AASHTO LRFD Specifications.

$F_{nc,LTB} = ?$

$L_{span} = 21' \rightarrow L_b = 21' = 252"$ unbraced length of the compression flange

$$L_p = 1.0 r_t \sqrt{\frac{E}{F_{yc}}}$$

Chapter 6 provisions:

$$r_t = \frac{b_{fc}}{\sqrt{12\left(1 + \frac{1}{3}\frac{D_c t_w}{b_{fc} t_{fc}}\right)}} = \frac{7}{\sqrt{12\left(1 + \frac{1}{3} \times \frac{7.495 \times 0.305}{7 \times 0.505}\right)}}$$

$$r_t = 1.83"$$

$$L_p = 1.0 \times 1.83 \sqrt{\frac{29000}{51}} = 43.6"$$

As $L_b = 252" > L_p = 43.6"$, the $L_r$ factor should be calculated.

$$L_r = \pi r_t \sqrt{\frac{E}{F_y}}$$

$$F_{yr} = \min\left(0.7F_{yc}, F_{yw}\right) \geq 0.5F_{yc} = \min(0.7 \times 51, 51) \geq 0.5 \times 51 = 35.7ksi > 25.5ksi$$

$$L_r = \pi \times 1.83 \times \sqrt{\frac{29000}{35.7}} = 163.9" < L_b = 252"$$

Therefore, the LTB capacity is obtained using the Euler elastic buckling equation for the compression flange:

$$F_{nc,LTB} = F_{cr} \leq R_b R_h F_{yc} = 51ksi$$

$$F_{cr} = \frac{C_b R_b \pi^2 E}{\left(\frac{L_b}{r_t}\right)^2}$$

The moment gradient factor, $C_b$, is equal to unity for simply supported beams:

$$f_2 = 0 \quad \rightarrow \quad C_b = 1.0$$

And the Euler equation gives:

$$F_{cr} = \frac{1.0 \times 1.0 \times \pi^2 \times 29000}{\left(\frac{252}{1.83}\right)^2} = 15.1ksi$$

Therefore, the LTB capacity of the girder is:

$$F_{nc,LTB} = 15.1\ ksi \leq R_b R_h F_{yc} = 51 ksi$$

The flexural capacity of the girder would be the minimum of the LB and LTB capacities:

$$F_{nc} = \min(15.1, 51) = 15.1\ ksi$$

The maximum flexural stress in the girders can be equal to $\phi_f F_{nc}$ which is equal to:

$$f_{bu,max} = \phi_f F_{nc} = 1.0 \times 15.1 = 15.1 ksi$$

The moment corresponding to this level of stress will be:

$$M_{max} = f_{bu,max} S = 15.1 \times 64.7 = 977.0\ K - in$$

in which $S = 64.7\ in^3$ is the section modulus of the section.

The load P which creates such a moment is a function of loading configuration is calculated using equilibrium of floor beams and main girder as illustrated in Figure 6-3 and Figure 6-4.

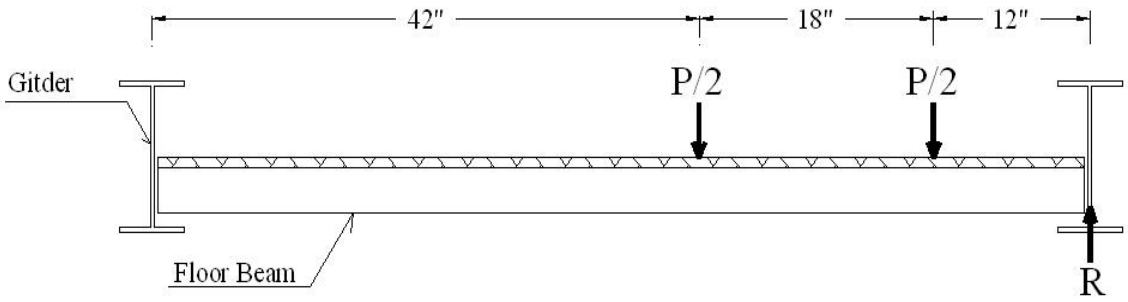


**Figure 6-3. Floor Beam Equilibrating Reaction Force**

$$R = \frac{42}{72}\left(\frac{P}{2}\right) + \frac{60}{72}\left(\frac{P}{2}\right) = 0.708P$$

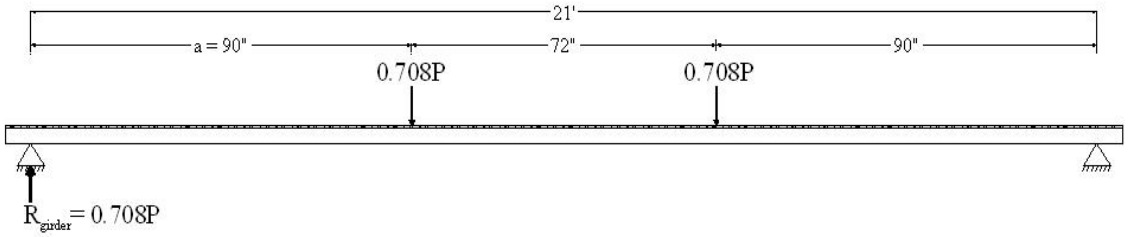


**Figure 6-4. Main Girder Equilibrating Reaction Force**

$$M_{max} = 0.708P \times a$$

$$P = \frac{M_{max}}{0.708a}$$

$$Load\ Capacity = 2P$$

$$Load\ Capacity = \frac{2}{0.708}\left(\frac{M_{max}}{a}\right) = \frac{2}{0.708}\left(\frac{977.0}{90}\right) = 30.7\ kips$$
$$\ll \sim 100\ capacity\ observed\ in\ experiment$$

As can be seen, the capacity calculated based on the provisions of AASHTO LRFD is much lower that the capacity of the bridge which is observed in the experiment. Therefore, the flexural capacity of the bridge girders is re-calculated based on the provisions of Appendix-A of AASHTO and also the AISC Steel Design Manual.

Based on the recommendations of Appendix-A of AASHTO LRFD the limiting unbraced length $L_r$ is calculated using the following equation:

$$L_r = 1.95\, r_t \frac{E}{F_{yr}}\sqrt{\frac{J}{S_{xc}\, h}} \cdot \sqrt{1 + \sqrt{1 + 6.76\left(\frac{F_{yr}}{E} \cdot \frac{S_{xc} h}{J}\right)^2}}$$

Entering the following values for the parameters, the limiting unbraced length is calculated:

$$J = 0.794 in^4$$
$$S_{xc} = \frac{I}{c_c} = \frac{518}{8} = 64.75 in^3$$
$$h = 16\text{"- } 0.505\text{"} = 15.5\text{"}$$
$$F_{yr} = 35.7\ ksi$$

$$L_r = 1.95 \times 1.83 \times \frac{29000}{35.7}\sqrt{\frac{0.794}{64.75 \times 15.5}} \cdot \sqrt{1 + \sqrt{1 + 6.76\left(\frac{35.7}{29000} \times \frac{64.75 \times 15.5}{0.794}\right)^2}}$$

$$L_r = 185.3\text{"} < L_b = 252\text{"}$$

Therefore the flexural resistance based on lateral torsional buckling shall be taken as:

$$M_{nc,LTB} = F_{cr} S_{xc} \leq R_{pc} M_{yc}$$

$$F_{cr} = \frac{C_b \pi^2 E}{\left(\frac{L_b}{r_t}\right)^2}\sqrt{1 + 0.078 \cdot \frac{J}{S_{xc} h}\left(\frac{L_b}{r_t}\right)^2}$$

$$= \frac{\pi^2 C_b \times 29000}{\left(\frac{252}{1.83}\right)^2}\sqrt{1 + 0.078 \times \frac{0.794}{64.75 \times 15.5}\left(\frac{252}{1.83}\right)^2}$$

$$F_{cr} = 22.2 C_b\ \ ksi$$

The flexural resistance is limited to $R_{pc} M_{yc}$ in which the web plastification factor for compression flange of compact sections $R_{pc}$ is calculated as:

$$R_{pc} = \frac{M_p}{M_{yc}} = \frac{Z_x}{S_{xc}}$$

$$Z_x = 73\ in^3$$

$$R_{pc} = \frac{73}{64.75} = 1.13$$

$$M_{nc,LTB} = F_{cr}S_{xc} \leq R_{pc}M_{yc} = 1.13 \times 51 \times 64.75 = 3732\ \ k.in \qquad \checkmark$$

Based on AISC 2008, for flexural capacity calculations, first the compactness of the sections should be checked:

$$\frac{b_f}{t_f} = \frac{\frac{7}{2}}{0.505} = 6.93 < 0.38\sqrt{\frac{E}{F_y}} = 9.06 \quad OK$$

$$\frac{h}{t_w} = \frac{16}{0.305} = 52.5 < 3.76\sqrt{\frac{E}{F_y}} = 89.7 \quad OK$$

Hence, the section is compact. Now the unbraced length should be checked with the limiting length:

$$L_r = 1.95 r_{ts}\frac{E}{0.7F_y}\sqrt{\frac{Jc}{S_x h}} \times \sqrt{1 + \sqrt{1 + 6.76\left(\frac{0.7F_y}{E} \times \frac{S_x h}{Jc}\right)^2}}$$

For doubly symmetric members, $c = 1.0$ and therefore, the equation for $L_r$ in AISC will be the same as that of Appendix-A of AASHTO LRFD. So:

$$L_r = 185.3" < \ L_b = 252"$$

And

$$\Longrightarrow M_n = F_{cr}S_x = 22.2C_b\ S_x\ (k.in)$$

So, the flexural capacity based on both AASHTO Appendix-A and AISC is equal to $22.2C_b\ S_x$. Now, the moment gradient factor $C_b$ is calculated based on both of the codes.

Based on AASHTO LRFD, as the moment at the end of the unbraced length is equal to zero, the moment gradient factor will be equal to zero:

$$C_b = 1.0 \quad (M_2 = 0) \qquad\qquad AASHTO\ LRFD$$

And based on AISC manual the moment gradient factor is a function of the value of moment at the quarter point of the girder length:

$$C_b = \frac{12.5M_{max}}{2.5M_{max} + 3M_A + 4M_B + 3M_c}R_m \leq 3.0$$

Where $R_m$ is equal to 1.0 for doubly symmetric members.

$$L = 252" \ \ and \quad \frac{L}{4} = 63"$$

$$M_A = M_C = P \times 63" = 63P$$

$$M_{max} = M_B = 90P$$

$$C_b = \frac{12.5 \times 90P}{(2.5 \times 90 + 3 \times 63 + 4 \times 90 + 3 \times 63)P} = 1.168 \qquad AISC$$

Therefore, the LTB capacity based on Appendix-A and AISC will be:

$$M_{nc,LTB} = F_{cr} S_{xc} = 22.2 C_b \, S_x$$

$$\begin{cases} M_{nc,LTB} = 22.2 \times 1.0 \times 64.75 = 1437 \leq 3732 \ (k.in) & \text{AASHTO LRFD App-A} \\ M_{nc,LTB} = 22.2 \times 1.168 \times 64.75 = 1679 \ (k.in) & \text{AISC} \end{cases}$$

And the maximum girder reaction can be found as:

$$M_u = \phi M_n, \quad \phi = 1.0, \quad So: \ M_u = M_n$$

$$M_u = R_{girder} a = 90" \times R_{girder} = M_n \implies R_{girder} = \frac{M_n}{90"}$$

Therefore:

$$\begin{cases} R_{girder,max} = \frac{1437}{90} = 15.97 \ kips & \text{AASHTO LRFD App-A} \\ R_{girder,max} = \frac{1697}{90} = 18.86 \ kips & \text{AISC} \end{cases}$$

The total load on the bridge is calculated as follows:

$$Max \ Load = 2R_{girder,max}/0.708$$

where 0.708 is the distribution factor for the girder closer to loading.

$$\begin{cases} Max \ Load = 45.1 \ kips & \text{AASHTO LRFD App-A} \\ Max \ Load = 53.3 \ kips & \text{AISC} \end{cases}$$

### 6.1.4 Redundancy Analysis

For redundancy analysis of the bridge, first the flexural capacity of the bridge is needed. Based on the previous calculations and AISC recommendations, the moment capacity of the W16x40 girder is chosen equal to 1679 k.in. The four limit state factors are evaluated for the bridge as follows:

#### *6.1.4.1 Member Failure ($LF_1$)*

Member failure limit state is a check of individual member safety using elastic analysis or the capacity of the structure to resist its first member failure.

$$LF_1 = \frac{R - D}{L} \leftarrow Linear \ elastic \ analysis$$

$$M_R = 1679 \ kip - in$$

A linear elastic model of the bridge is made in SAP2000.

Dead Weight:

Girder: W16x40 $A = 11.8in^2$ , $L = 252in$

$W_1 = 40lb/ft$

20 floor Beams: W6x9 $L = 6ft = 72in$

$$W_2 = \frac{9lb}{ft}$$

$$W_2 = 9\frac{lb}{ft} \times 3ft = 0.027kip$$

$$W_D = W_1 + W_2 = 0.040 + 0.027 = 0.067\ k/ft$$

$$M_D = \frac{W_D L^2}{8} = \frac{0.067 \times 21^2}{8} = 3.69\ \ kip.ft = 44.3\ \ k.in$$

Live Load:

Four point loads of 5 kip are applied to the bridge and the moment due to that load in the girder closer to the loading is calculated:

$$M_{LL} = (5k + 5k) \times 0.708 \times 90" = 637.2 \quad (k.in)$$

$$LF_1 = \frac{1679 - 44.3}{637.2} = 2.57$$

### *6.1.4.2 Ultimate Limit State ($LF_u$)*

Ultimate limit state is defined as the ultimate capacity of the bridge system or the load required for the formation of a collapse mechanism in the bridge system. For this purpose, a nonlinear finite element model is built in Abaqus and four point loads equal to 5 kips are applied to the bridge with the same configuration as the one used for Member Failure limit state. This loading represents the live load effect on the scaled specimen. Figure 6-5 shows the load-deflection curves resulting from nonlinear finite element analysis of the bridge using ABAQUS and also the laboratory experiment.

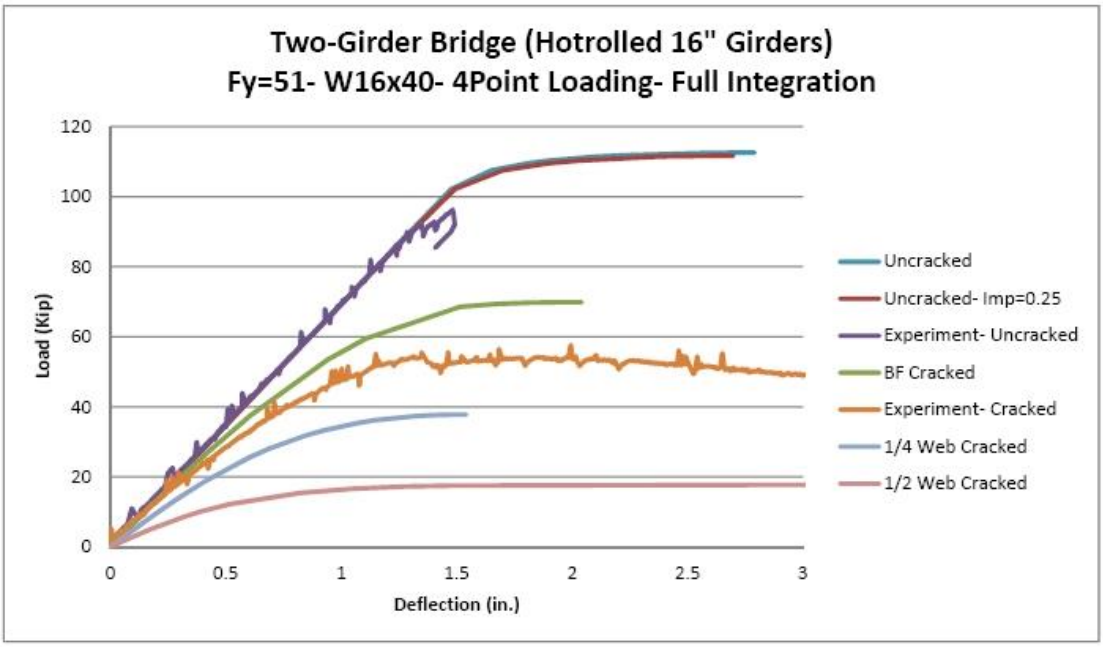


**Figure 6-5. Experimental and Analytical Load-Deflection Curves**

The obtained ultimate load carrying capacity of the bridge is equal to 112.6 kips. Therefore, the Ultimate Limit State Factor ($LF_u$) will be equal to:

$$LF_u = \frac{112.6}{4 \times 5\ kips} = 5.63$$

Hence:

$$R_u = \frac{LF_u}{LF_1} = \frac{5.63}{2.57} = 2.19 > 1.30 \qquad \text{O.K.}$$

So the capacity of the bridge in its ultimate limit state is satisfactory.

### 6.1.4.3 Functionality Limit State ($LF_f$)

Functionality limit state is defined as the capacity of the structure to resist a live load displacement in a main longitudinal member equal to the span length/100.

$$LF_f = \frac{Load\ Capacity\ corresponding\ to \frac{L}{100}\ deflection}{4 \times 5\ kips}$$

And the criterion for this limit state is:

$$R_f = \frac{LF_f}{LF_1} = \frac{LF_f}{2.57} \geq 1.10$$

Table 6-1 shows the capacity and the redundancy factors of the bridge with different damage levels in this limit state.

**Table 6-1. Ultimate Capacity and Load Factors in Functionality Limit State**

| | Live Load Capacity @ L/100 | $LF_f$ | $R_f$ |
|---|---|---|---|
| Bottom Flange Cracked | 69.8 | 3.49 | 1.36 |
| ¼ of Web Cracked | 37.8 | 1.89 | 0.74 |
| ½ of Web Cracked | 17.6 | 0.88 | 0.34 |

It is shown that the two girder bridge does not satisfy the functionality limit state provided that ¼ and ½ of its web are cracked.

#### *6.1.4.4 Damage Condition Limit State ($LF_d$)*

Damage condition limit state is defined as the ultimate capacity of the bridge system after removal or cracking of one load carrying component from the structure model.

$$LF_d = \frac{Ultimate\ Load\ Capacity\ of\ Damaged\ Bridge}{4 \times 5\ kips}$$

The limiting value for this limit state is defined as follows:

$$R_d = \frac{LF_d}{LF_1} = \frac{LF_d}{2.57} \geq 0.50$$

Table 6-2 shows the capacity and the redundancy factors of the bridge with different damage levels in this limit state.

**Table 6-2. Ultimate Capacity and Load Factors in Damage Limit State**

| | Ultimate Live Load Capacity | $LF_d$ | $R_d$ |
|---|---|---|---|
| Bottom Flange Cracked | 69.8 | 3.49 | 1.36 |
| ¼ of Web Cracked | 37.8 | 1.89 | 0.74 |
| ½ of Web Cracked | 18.0 | 0.90 | 0.35 |

It is shown that the two girder bridge does not satisfy the damage condition limit state if one half of its web is cracked.

Overall, this bridge satisfies redundancy requirements for the damage condition limit state for the cases of bottom flange cracked and ¼ depth of web cracked. For the ultimate limit state and functionality limit state, the bridge is shown redundant for the bottom flange cracked condition only. However, when the web is cracked (both ¼ and ½ depth of web) the functionality limit state is not satisfied. The specimen also does not satisfy the damage limit state when 1/2 of the web depth cracked. The reserve ratios, R, for each limit state are summarized in Table 6-3.

**Table 6-3. Summary of reserve ratios of the specimen in Experiment 1.**

| Damage Condition | Ultimate Limit State (1.3) | Functional Limit State (1.1) | Damage Limit State (0.5) |
|---|---|---|---|
| Undamaged Structure | 2.19 | N/A | N/A |
| Bottom Flange Cracked | N/A | 1.36 | 1.36 |
| ¼ of Web Cracked | N/A | 0.74 | 0.74 |
| ½ of Web Cracked | N/A | 0.34 | 0.35 |

Note: The number in ( ) is the minimum reserve ratio based on NCHRP Report 406 for which the structure is classified as a redundant one.

## 6.2 Redundancy Analysis # 2

### 6.2.1 Bridge Configuration

This redundancy analysis is carried out on the same bridge system that tested in Experiment 2. The deck is supported by W6x9 floor beams that are connected to the bridge main girders. The plate girders have 6"x3/8 flanges and 23"x5/16 webs. The span length of the bridge is 21 feet and the distance between the main girders is 73 inches. The length of the floor beams is 72 inches. Two point loads are eccentrically applied to the bridge to provide the maximum effects in one of the girders. Figure 6-6 and Figure 6-7 show the bridge cross section and longitudinal view.

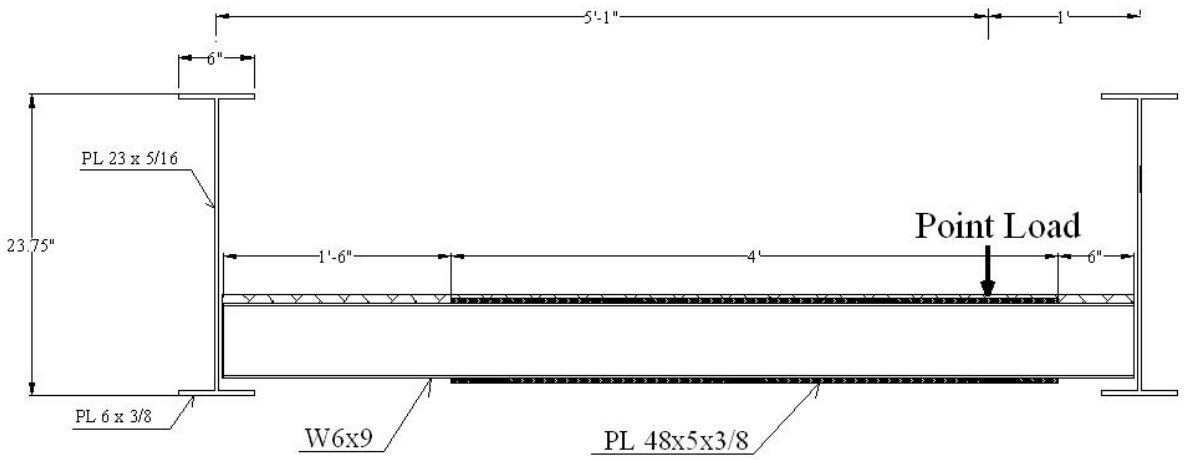


**Figure 6-6. Cross Section of the Test Bridge Specimen**

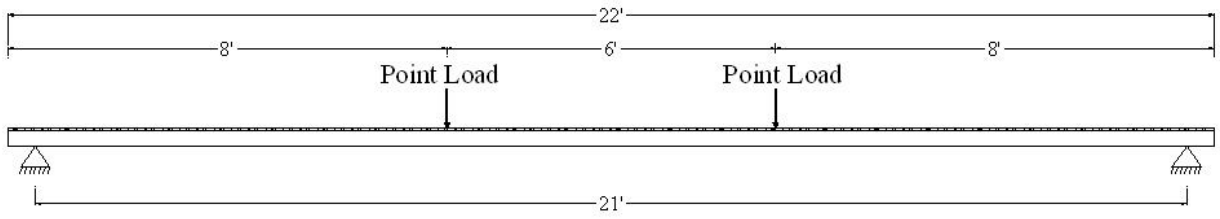


**Figure 6-7. Elevation View of the Test Bridge Specimen**

### 6.2.2 Redundancy Analysis Limit States Definition

In order to perform a redundancy analysis for the bridge, the capacity of the bridge in the following four limit states should be evaluated:

1- **Member Failure**, which is a check of individual member safety using elastic analysis
2- **Ultimate Limit State**, which is defined as the ultimate capacity of the bridge system or the formation of a collapse mechanism
3- **Functionality Limit State**, which is defined as the capacity of the structure to resist a live load displacement in a main longitudinal member equal to the span length/100
4- **Damage Condition Limit State**, which is defined as the ultimate capacity of the bridge system after removal or cracking of one load carrying component from the structure model.

Therefore, the first task is to calculate the load carrying capacity of the bridge girders and so that of the bridge structural system.

$$P_{max} = ?$$

or

$$M_{max} = ?$$

So, in the following section the flexural capacity of the bridge girders are evaluated.

### 6.2.3 Bridge Flexural Capacity

The yield stress of steel for webs and flanges of the plate girders based on a set of tension tests is determined which is equal to 54 ksi.

$$F_y = 54ksi$$

The section properties of plate I-girders are as follows:

$$I = 931.6\ in^4$$
$$Z_x = 93.92\ in^3$$

$$S_{xc} = \frac{I}{c_c} = \frac{931.6}{\frac{23}{2} + \frac{3}{8}} = 78.45\ in^3$$

$$J = 0.4366\ in^4$$

First, the moment capacity of one of the girders of the bridge based on the provisions of AASHTO LRFD Chapter 6 is calculated.

The section proportions are check as follows:

$\frac{b_f}{2t_f} = \frac{6}{2\times\frac{3}{8}} = 8 < 12$ OK

$\frac{D}{b_f} = \frac{23.75}{6} = 3.96 < 6$ OK

$\frac{t_f}{t_w} = \frac{3/8}{5/16} = 1.2 > 1.1$ OK

$0.1 < \frac{I_{yc}}{I_{yt}} = 1.0 < 10$ OK

$\frac{D}{t_w} = \frac{23}{5/16} = 73.6 < 150$ OK

Therefore, the section passes all proportionality checks.

Based on the AASHTO LRFD Specifications, the factored stress in the girders, $f_{bu}$ , should be less than the reduced resistance, $\phi_f F_{nc}$:

$$f_{bu} < \phi_f F_{nc} \qquad \phi_f = 1.0 \qquad F_y = 54ksi$$

in which the resistance of the girder is the minimum of local buckling (LB) and lateral torsional buckling (LTB) resistances:

$$F_{nc} = \min\left(F_{nc,LB}, F_{nc,LTB}\right)$$

Now, the strength of the girder for local buckling and lateral torsional buckling is evaluated.

The local buckling resistance of the compression flange shall be taken as $F_{nc,LB} = R_b R_h F_{yc}$ provided that $\lambda_f < \lambda_{pf}$.

$$\lambda_f = \frac{b_f}{2t_f} = 8$$

$$\lambda_{pf} = 0.38\sqrt{\frac{E}{F_y}} = 0.38\sqrt{\frac{29000}{54}} = 8.8$$

Therefore $\lambda_f < \lambda_{pf}$ and

$$F_{nc,LB} = R_b R_h F_{yc}$$

As the web and flanges of the girder are of the same material (it is not hybrid), the hybrid section factor is equal to one:

$$R_h = 1.0$$

Web load-shedding factor: $R_b$ =?

$$\frac{2D_c}{t_w} = \frac{2\left(\frac{23}{2}\right)}{5/16} = 73.6 \; < \; \lambda_{rw} = 5.7\sqrt{\frac{E}{F_{yc}}} = 5.7\sqrt{\frac{29000}{54}} = 132$$

where $D_c$ is the depth of the web in compression.

Hence

$$R_b = 1.0$$

Therefore

$$F_{nc,LB} = 1.0 \times 1.0 \times 54 = 54ksi$$

Now, the lateral torsional bucking (LTB) capacity of the girders should be calculated. First, the LTB capacity is calculated based on Chapter 6 of AASHTO LRFD Specifications.

$F_{nc,LTB}$ =?

$L_{span} = 21' \rightarrow L_b = 21' = 252"$ unbraced length of the compression flange

$$L_p = 1.0r_t\sqrt{\frac{E}{F_{yc}}}$$

Chapter 6 provisions:

$$r_t = \frac{b_{fc}}{\sqrt{12\left(1 + \frac{1}{3}\frac{D_c t_w}{b_{fc}t_{fc}}\right)}} = \frac{7}{\sqrt{12\left(1 + \frac{1}{3} \times \frac{23/2 \times 5/16}{6 \times 3/8}\right)}}$$

$$r_t = 1.40"$$

$$L_p = 1.0 \times 1.40\sqrt{\frac{29000}{54}} = 32.4"$$

As $L_b = 252" > L_p = 32.4"$, the $L_r$ factor should be calculated.

$$L_r = \pi r_t\sqrt{\frac{E}{F_y}}$$

$$F_{yr} = \min\left(0.7F_{yc}, F_{yw}\right) \geq 0.5F_{yc} = \min(0.7 \times 54, 54) \geq 0.5 \times 54 = 37.8ksi > 27\ ksi$$

$$L_r = \pi \times 1.40 \times \sqrt{\frac{29000}{37.8}} = 121.8" < L_b = 252"$$

Therefore, the LTB capacity is obtained using the Euler elastic buckling equation for the compression flange:

$$F_{nc,LTB} = F_{cr} \leq R_b R_h F_{yc} = 54ksi$$

$$F_{cr} = \frac{C_b R_b \pi^2 E}{\left(\frac{L_b}{r_t}\right)^2}$$

The moment gradient factor, $C_b$, is equal to unity for simply supported beams:

$$f_2 = 0 \quad \rightarrow \quad C_b = 1.0$$

And the Euler equation gives:

$$F_{cr} = \frac{1.0 \times 1.0 \times \pi^2 \times 29000}{\left(\frac{252}{1.40}\right)^2} = 8.83\ ksi$$

Therefore, the LTB capacity of the girder is:

$$F_{nc,LTB} = 8.83\ ksi \leq R_b R_h F_{yc} = 54\ ksi$$

The flexural capacity of the girder would be the minimum of the LB and LTB capacities:

$$F_{nc} = \min(8.83, 54) = 8.83\ ksi$$

The maximum flexural stress in the girders can be equal to $\phi_f F_{nc}$ which is equal to:

$$f_{bu,max} = \phi_f F_{nc} = 1.0 \times 8.83 = 8.83\ ksi$$

The moment corresponding to this level of stress will be:

$$M_{max} = f_{bu,max} S = 15.1 \times \frac{931.6}{11.875} = 692.7\ k.in$$

in which $S = \frac{931.6}{11.875}\ in^3$ is the section modulus of the section.

The load P which creates such a moment is a function of loading configuration is calculated using equilibrium of floor beams and main girder as illustrated in Figure 6-8 and Figure 6-9.

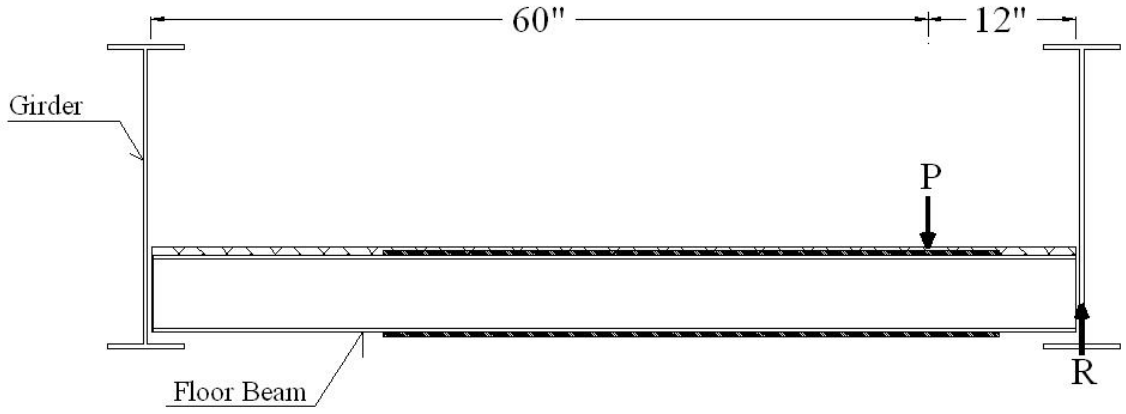


**Figure 6-8. Floor Beam Equilibrating Reaction Force**

$$R = \frac{60}{72}(P) = 0.833P$$

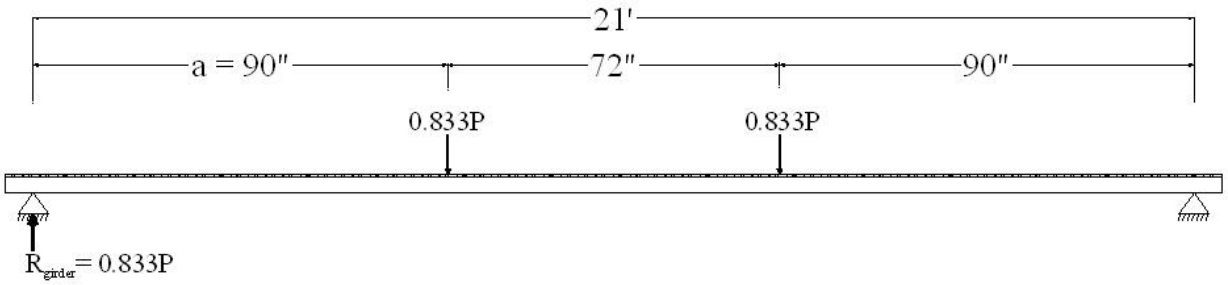


**Figure 6-9. Main Girder Equilibrating Reaction Force**

$$M_{max} = 0.833P \times a$$
$$P = \frac{M_{max}}{0.833a}$$
$$Load\ Capacity = 2P$$
$$Load\ Capacity = \frac{2}{0.833}\left(\frac{M_{max}}{a}\right) = \frac{2}{0.833}\left(\frac{692.7}{90}\right) = 18.5\ kips$$
$$\ll \sim 100\ capacity\ observed\ in\ experiment$$

As can be seen, the capacity calculated based on the provisions of AASHTO LRFD is much lower that the capacity of the bridge which is observed in the experiment. Therefore, the flexural capacity of the bridge girders is re-calculated based on the provisions of Appendix-A of AASHTO and also the AISC Steel Design Manual.

Based on the recommendations of Appendix-A of AASHTO LRFD the limiting unbraced length $L_r$ is calculated using the following equation:

$$L_r = 1.95\, r_t \frac{E}{F_{yr}} \sqrt{\frac{J}{S_{xc}\, h}} \cdot \sqrt{1 + \sqrt{1 + 6.76\left(\frac{F_{yr}}{E} \cdot \frac{S_{xc} h}{J}\right)^2}}$$

Entering the following values for the parameters, the limiting unbraced length is calculated:

$$J = 0.4366 in^4$$
$$S_{xc} = \frac{I}{c_c} = 78.45 in^3$$
$$h = 23" + 3/8 = 23.375"$$
$$F_{yr} = 37.8\ ksi$$

$$L_r = 1.95 \times 1.40 \times \frac{29000}{37.8}\sqrt{\frac{0.4366}{78.45 \times 23.375}} \cdot \sqrt{1+\sqrt{1+6.76\left(\frac{37.8}{29000}\times\frac{78.45\times 23.375}{0.4366}\right)^2}}$$

$$L_r = 126.2" < L_b = 252"$$

Therefore the flexural resistance based on lateral torsional buckling shall be taken as:

$$M_{nc,LTB} = F_{cr}S_{xc} \le R_{pc}M_{yc}$$

$$F_{cr} = \frac{C_b\pi^2 E}{\left(\frac{L_b}{r_t}\right)^2}\sqrt{1+0.078\cdot\frac{J}{S_{xc}h}\left(\frac{L_b}{r_t}\right)^2}$$

$$= \frac{\pi^2 C_b \times 29000}{\left(\frac{252}{1.40}\right)^2}\sqrt{1+0.078\times\frac{0.4366}{78.45\times 23.375}\left(\frac{252}{1.40}\right)^2}$$

$$F_{cr} = 11.18 \times C_b \ \ ksi$$

The flexural resistance is limited to $R_{pc}M_{yc}$ in which the web plastification factor for compression flange of compact sections $R_{pc}$ is calculated as:

$$R_{pc} = \frac{M_p}{M_{yc}} = \frac{Z_x}{S_{xc}}$$

$$Z_x = 93.92\ in^3$$

$$R_{pc} = \frac{93.92}{78.45} = 1.197$$

$$M_{nc,LTB} = F_{cr}S_{xc} \le R_{pc}M_{yc} = 1.197 \times 54 \times 78.45 = 5071\ \ k.in \qquad \checkmark$$

Based on AISC 2008, for flexural capacity calculations, first the compactness of the sections should be checked:

$$\frac{b_f}{t_f} = \frac{\frac{6}{2}}{3/8} = 8 < 0.38\sqrt{\frac{E}{F_y}} = 8.8 \quad OK$$

$$\frac{h}{t_w} = \frac{23}{5/16} = 73.6 < 3.76\sqrt{\frac{E}{F_y}} = 87.1 \quad OK$$

Hence, the section is compact. Now the unbraced length should be checked with the limiting length:

$$L_r = 1.95 r_{ts} \frac{E}{0.7F_y}\sqrt{\frac{Jc}{S_x h}} \times \sqrt{1+\sqrt{1+6.76\left(\frac{0.7F_y}{E}\times\frac{S_x h}{Jc}\right)^2}}$$

For doubly symmetric members, $c = 1.0$ and the equation for $L_r$ would be the same as Appendix-A of AASHTO LRFD:

$$L_r = 126.2" < L_b = 252"$$

And

$$\Longrightarrow M_n = F_{cr} S_x = 11.18 C_b\, S_x\ (k.in)$$

So, the flexural capacity based on both AASHTO Appendix-A and AISC is equal to $11.18 C_b\, S_x$. Now, the moment gradient factor $C_b$ is calculated based on both of the codes.

Based on AASHTO LRFD, as the moment at the end of the unbraced length is equal to zero, the moment gradient factor will be equal to zero:

$$C_b = 1.0 \quad (M_2 = 0) \qquad\qquad AASHTO\ LRFD$$

And based on AISC manual the moment gradient factor is a function of the value of moment at the quarter point of the girder length:

$$C_b = \frac{12.5 M_{max}}{2.5M_{max} + 3M_A + 4M_B + 3M_c} R_m \le 3.0$$

Where $R_m$ is equal to 1.0 for doubly symmetric members.

$$L = 252" \quad and \quad \frac{L}{4} = 63"$$
$$M_A = M_C = P \times 63" = 63P$$
$$M_{max} = M_B = 90P$$
$$C_b = \frac{12.5 \times 90P}{(2.5\times 90 + 3\times 63 + 4\times 90 + 3\times 63)P} = 1.168 \qquad AISC$$

Therefore, the LTB capacity based on Appendix-A and AISC will be:

$$M_{nc,LTB} = F_{cr} S_{xc} = 11.18 C_b\, S_x$$

$$\begin{cases} M_{nc,LTB} = 11.18 \times 1.0 \times 78.45 = 877 \le 5071\ (k.in) & \text{AASHTO LRFD App-A} \\ M_{nc,LTB} = 11.18 \times 1.168 \times 78.45 = 1025\ (k.in) & \text{AISC} \end{cases}$$

And the maximum girder reaction can be found as:

$$M_u = \phi M_n, \quad \phi = 1.0, \quad So:\ M_u = M_n$$
$$M_u = R_{girder} a = 90" \times R_{girder} = M_n \quad \Longrightarrow \quad R_{girder} = \frac{M_n}{90"}$$

Therefore:

$$\begin{cases} R_{girder,max} = \frac{877}{90} = 9.74\ kips & \text{AASHTO LRFD App-A} \\ R_{girder,max} = \frac{1025}{90} = 11.39\ kips & \text{AISC} \end{cases}$$

The total load on the bridge is calculated as follows:

$$Max\ Load = 2R_{girder,max}/0.833$$

where 0.833 is the distribution factor for the girder closer to loading.

$$\begin{cases} Max\ Load = 23.4\ kips & \text{AASHTO LRFD App-A} \\ Max\ Load = 27.3\ kips & \text{AISC} \end{cases}$$

### 6.2.4 Redundancy Analysis

For redundancy analysis of the bridge, first the flexural capacity of the bridge is needed. Based on the previous calculations and AISC recommendations, the moment capacity of the plate girder is chosen equal to 1025 k.in. The four limit state factors are evaluated for the bridge as follows:

#### *6.2.4.1 Member Failure ($LF_1$)*

Member failure limit state is a check of individual member safety using elastic analysis or the capacity of the structure to resist its first member failure.

$$LF_1 = \frac{R - D}{L} \quad \leftarrow \quad Linear\ elastic\ analysis$$
$$M_R = 1025\ kip - in$$

A linear elastic model of the bridge is made in SAP2000.

<u>Dead Weight:</u>

Girder: $A = 11.6875\ in^2$ , $L = 252in$

$$W_1 = 11.6875 \times 2.836 \times 10^{-4} = 0.003315\frac{k}{in} = 0.03977\ k/ft$$

20 floor Beams: W6x9 $L = 6ft = 72in$

$$W_2 = \frac{9lb}{ft}$$
$$W_2 = 9\frac{lb}{ft} \times 3ft = 0.027\ kip$$
$$W_D = W_1 + W_2 = 0.06677\ k/ft$$
$$M_D = \frac{W_D L^2}{8} = \frac{0.06677 \times 21^2}{8} = 3.68\ \ kip.ft = 44.2\ \ k.in$$

<u>Live Load:</u>

Two point loads of 10 kip are applied to the bridge and the moment due to that load in the girder closer to the loading is calculated:

$$M_{LL} = (10k) \times 0.833 \times 90" = 749.7 \quad (k.in)$$

$$LF_1 = \frac{1025 - 44.2}{749.7} = 1.31$$

#### 6.2.4.2 Ultimate Limit State ($LF_u$)

Ultimate limit state factor is defined as the ultimate capacity of the bridge system or the load required for the formation of a collapse mechanism in the bridge system. For this purpose a nonlinear finite element model is built in Abaqus and two point loads equal to 10 kips are applied to the bridge with the same configuration as the one used for Member Failure limit state. Figure 6-10 shows the load-deflection curves resulting from nonlinear finite element analysis of the bridge using ABAQUS and also the laboratory experiment.

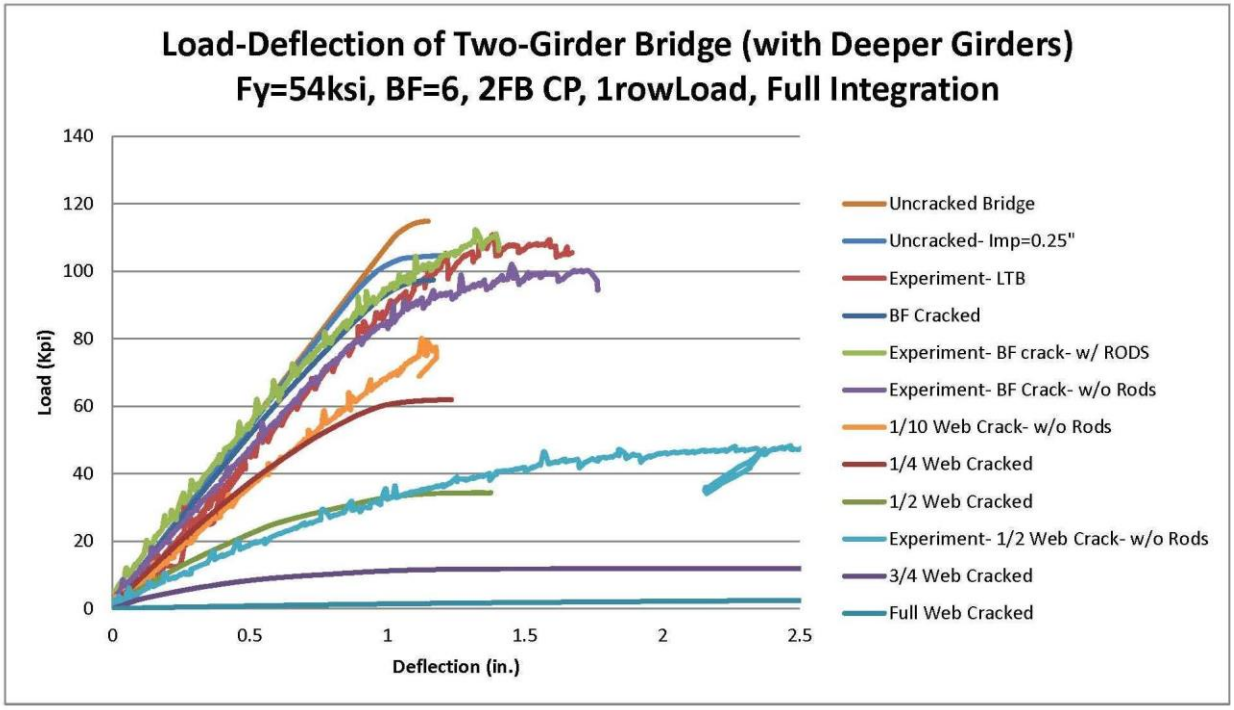


**Figure 6-10. Experimental and Analytical Load-Deflection Curves**

The obtained ultimate load carrying capacity of the bridge is equal to 112 kips. Therefore, the Ultimate Limit State Factor ($LF_u$) will be equal to:

$$LF_u = \frac{112}{2 \times 10\ kips} = 5.6$$

Hence:

$$R_u = \frac{LF_u}{LF_1} = \frac{5.6}{1.31} = 4.27 > 1.30 \qquad \text{O.K.}$$

So, the capacity of the bridge in its ultimate limit state is satisfactory.

#### 6.2.4.3 Damage Condition Limit State ($LF_d$)

Damage condition limit state is defined as the ultimate capacity of the bridge system after removal or cracking of one load carrying component from the structure model.

$$LF_d = \frac{Ultimate\ Load\ Capacity\ of\ Damaged\ Bridge}{2 \times 10\ kips}$$

The limiting value for this limit state is defined as follows:

$$R_d = \frac{LF_d}{LF_1} = \frac{LF_d}{1.31} \geq 0.50$$

Table 6-4 shows the capacity and the redundancy factors of the bridge with different damage levels in this limit state.

**Table 6-4. Ultimate Capacity and Load Factors in Damage Limit State**

| | Ultimate Load Capacity | $LF_d$ | $R_d$ |
|---|---|---|---|
| Bottom Flange Cracked | 94.59 | 4.73 | 3.61 |
| ¼ of Web Cracked | 59.18 | 2.96 | 2.26 |
| ½ of Web Cracked | 31.59 | 1.58 | 1.21 |
| ¾ of Web Cracked | 16.54 k | 0.827 | 0.63 |

It is shown that the two girder bridge satisfies all the damage condition limit state in all of the considered damage levels.

#### 6.2.4.4 Functionality Limit State ($LF_f$)

Functionality limit state is defined as the capacity of the structure to resist a live load displacement in a main longitudinal member equal to the span length/100.

$$LF_f = \frac{Load\ Capacity\ corresponding\ to\ \frac{L}{100}\ deflection}{2 \times 10\ kips}$$

And the criterion for this limit state is:

$$R_f = \frac{LF_f}{LF_1} = \frac{LF_f}{1.31} \geq 1.10$$

As observed in Figure 6-10 the deflections of the bridge at ultimate capacity for bottom flange, ¼ and ½ of web cracking were less than the span over 100 criterion. Therefore, it can be concluded that the capacity of the bridge at L/100 deflection is more than the maximum obtained capacities. Based on this conclusion, Table 6-5 shows the capacity obtained from nonlinear finite element analysis and the redundancy factors of the bridge with different damage levels in this limit state.

**Table 6-5. Load Capacity and Load Factors in Functionality Limit State**

| | Live Load Capacity @ L/100 | $LF_f$ | $R_f$ |
|---|---|---|---|
| Bottom Flange Cracked | > 94.59 k | > 4.73 | > 3.61 |
| ¼ of Web Cracked | > 59.18 k | > 2.96 | > 2.26 |
| ½ of Web Cracked | > 31.59 k | >1.58 | >1.21 |
| ¾ of Web Cracked | 9.03 k | 0.45 | 0.34 |

It is shown that the two girder bridge does not satisfy the functionality limit state provided that three quarter of its web is cracked.

Overall, this bridge with built-up girders is classified as redundant for all of the cases except when the web is cracked by ¾ of its depth.

**Table 6-6. Summary of reserve ratios of the specimen in Experiment 1.**

| Damage Condition | Ultimate Limit State (1.3) | Functional Limit State (1.1) | Damage Limit State (0.5) |
|---|---|---|---|
| Undamaged Structure | 4.27 | N/A | N/A |
| Bottom Flange Cracked | N/A | 3.61 | 3.61 |
| ¼ of Web Cracked | N/A | 2.26 | 2.26 |
| ½ of Web Cracked | N/A | 1.21 | 1.21 |
| ¾ of Web Cracked | N/A | 0.63 | 0.34 |

Note: The number in ( ) is the minimum reserve ratio based on NCHRP Report 406 for which the structure is classified as a redundant one.

# Chapter 7 Conclusions

The primary objective of this research was to understand the behavior of two-girder steel bridges and to quantify their redundancy level. This can be achieved by investigating and identifying the factors which control whether a two-girder will survive a girder fracture without collapse. Once identified, these factors may be used in the evaluation of existing in-service bridges to reclassify their redundancy level as "non-fracture critical" and decide whether a mandatory hands-on inspection is necessary every two years. These factors may also be used in the design of new bridges so that future steel two-girder bridges are no longer classified as fracture-critical.

To this end, a series of scale model tests were conducted. The model contained two main longitudinal supporting girders with transverse floor beams. Loading was applied at mid-span and offset from the centerline. In the first model, the bridge had rolled girders and two separate tests were performed. The first test was to evaluate the lateral torsional buckling capacity of the intact bridge. The bridge in its undamaged condition was loaded up to the point at which the lateral and torsional displacement of girders was observed to begin accelerating, or incipient buckling. This occurred at 92 kips of load corresponding to 1.36 inches of vertical displacement in the bottom flange. Strain gauge data showed that a majority of the specimen did not yield except for the top flange of the girder (near the loading point) at mid-span.

In the second test, the bottom flange of the girder closer to the loading point (Girder A) was cut at the mid-span section to simulate fracture. Under load, the behavior of the specimen was linear up to 51 kips of load, when its stiffness began to decrease. The maximum load carrying capacity of this cracked bridge was reached at 54 kips with 1.37 inches of vertical displacement. After reaching the maximum capacity the crack propagated up through the web which led to a drop in load capacity of the specimen. The test was stopped when the load capacity had dropped to 21 kips with a 6.8 inch displacement.

Non-linear finite element analysis was used to evaluate the redundancy of the test specimen following the procedures given by NCHRP report 406. The redundancy analysis for the first model bridge showed the bridge was redundant for the cases of undamaged and bottom flange cracked. Nevertheless, when a quarter of the web was cracked, the bridge did not satisfy the functional limit state. And when a half of the web was cracked the bridge did not satisfy both functional limit state and damage limit state.

In the second model, a bridge with a built-up girder was used to provide a taller specimen. This provided the maximum ratio found in practice for the height of the girder to the height of the floor beams. In this experiment, the ratio was approximately 4.0. There were a total of five tests performed in on the second model. In the first test, the uncracked bridge system carried a maximum load of 106 kips with a maximum vertical displacement of 1.7 inches. After

unloading, the girder closer to the loading point (Girder A) experienced a permanent vertical deformation of approximately 0.45 inch at mid-span.

In the second test, the built-up girder system was cut at the bottom flange of the girder near the loading points and then strengthened using two high-strength rods parallel to the bottom flange. This specimen was able to carry approximately 108 kips of load with 1.4 inch of displacement before starting a plateau in the load-deflection curve. This load was a little more than the load carried by the intact bridge, 106 kips. The permanent vertical displacement observed in this second test was approximately 0.32 inch, which occurred in the loaded girder.

In the third test, the strengthening rods were removed and the specimen with the cracked bottom flange was loaded again. The maximum load-carrying capacity of this specimen was observed to be approximately 100 kips.

In the fourth test, the crack in the bottom flange was extended up the web to a depth of 2.5 inch. The specimen was loaded up to 80 kips then unloaded. The load-displacement curve shows the specimen response was still linearly elastic.

In the last test, the crack was extended further in the web up to 10.5 inches. The maximum load carrying capacity of this specimen was observed dropping down to 48 kips. At this point, the initial crack started propagating further into the web. Due to this crack propagation, the capacity of the bridge decreased. At the time the test was stopped, the bridge specimen had 6 inches displacement under 33 kips of load.

The second bridge model 2 showed a higher level of redundancy than the first due to a larger cross section of girders. Even when the web was cracked up to half of its depth, the bridge was still proved redundant. Once the crack was extended up to three quarters of the web, the bridge wasn't redundant anymore since it didn't satisfy functional and damage limit states.

In this research, a new equation to estimate the lateral torsional buckling capacity of two-girder bridges was proposed. This equation presents moment capacity as a linear function of the floor beam spacing and varies between the maximum moment capacity of $M_P$ and the minimum buckling moment capacity of $C_{bu}M_o$. The equation was validated by means of finite element analysis and was also compared with Yura's equation and the traditional equation based on AASHTO LRFD Specification. The comparison showed that the proposed equation provided better agreement with the finite element analysis results than the other two methods.

The primary conclusions that can be drawn from this research are:

- Depending on the level of damage, certain two-girder steel bridge systems can be considered redundant.
- In specimen 2 (with larger ration of girder height to floor beam height), the strength of the specimen with a fracture of the bottom flange only was similar to the strength of the undamaged specimen and the crack did not propagate under increasing load.

- As bottom flange in one girder was cracked, the capacity of specimen 1 reduced significantly while the capacity reduction in specimen 2 was minimal. It implies that larger ratio of girder height to floor beam height in specimen 2 helps to improve the redundancy of the system once the crack occurs.
- As the artificial fracture (cut) extended into the web, the resulting strength of the specimens reduced. However, crack propagation was minimal when the maximum load carrying capacity of the specimen was reached. It was not until the cut in the web was extended to mid-depth that crack propagation occurred once the maximum load was reached.
- Additional work is required to develop fracture mechanic or fatigue based procedures to relate traffic volume to inspection cycle.

# Chapter 8 References


American Association of State Highway Transportation Officials. (2010). *AAHSTO LRFD Bridge Design Specifications.* Washington, D.C.

Barnard, T., Hovell, C.G., Sutton, J. P., Mouras, J.M., Neuman, B.J., Samaras, V.A., Kim, J., William, E.B, Frank, K.H. (2010). "Modeling the Response of Fracture Critical Steel Box-Girder Bridges," Report FHWA/TX-10/9-5498-1, Center for Transportation Research, University of Texas at Austin, Austin, TX.

Connor, R.J., Dexter, R., and Mahmoud, H. (2005). "Inspection and Management of Bridges with Fracture-Critical Details," *National Cooperative Highway Research Program Synthesis 354.* Transportation Research Board, National Academy Press, Washington, D.C.

Goshn, M. (2010). "Redundancy and robustness of highway bridge superstructures and substructures." *Structure and Infrastructure Engineering*. 6.1-2: 257-278.

Goshn, M. and Moses, F. (1998). "Redundancy in Highway Bridge Superstructures." NCHRP Report 406, TRB, National Research Council, Washington, D.C.

HNTB-Milwaukee Transportation Center "A Study of the Marquette Interchange HPS Twin Box Girder Structures." Report WI-1060-05-1222, HNTB and Milwaukee Transportation Center, Milwaukee, WI.

Kachlakev, D., Miller, T., and Yim, S. (2001). "Finite Element Modeling of Reinforced Concrete Structures Strengthened with FRP Laminates." Final Report, Oregon, USA.

Taylor, A. C. and Ojalvo, M. (1966). "Torsional Restraint of Lateral Buckling." Journal of the Structural Division, ASCE, ST2, 115-129.

Timoshenko, S.P., and Gere, J.M. (1961). "Theory of Elastic Stability." McGraw-Hill, New York.

Yura, J.A. (2001). "Fundamental of Beam Bracing." Engineering Journal, AISC, 38(1), 11-26.